2023-05

Stapp Car Crash Journal, Vol. 67 (November 2023), pp. 112-170

Frontal-Crash Occupant Protection in the Rear Seat: Submarining and Abdomen/Pelvis Response in Midsized Male Surrogates

Allison J. Guettler, Samuel T. Bianco, Devon L. Albert, David M. Boyle, Andrew R. Kemper, and Warren N. Hardy

Virginia Tech, Center for Injury Biomechanics

ABSTRACT – Frontal-crash sled tests were conducted to assess submarining protection and abdominal injury risk for midsized male occupants in the rear seat of modern vehicles. Twelve sled tests were conducted in four rear-seat vehicle-bucks with twelve post-mortem human surrogates (PMHS). Select kinematic responses and submarining incidence were compared to previously observed performance of the Hybrid III 50th-percentile male and THOR-50M ATDs (Anthropomorphic Test Devices) in matched sled tests conducted as part of a previous study. Abdominal pressure was measured in the PMHS near each ASIS (Anterior Superior Iliac Spine), in the inferior vena cava, and in the abdominal aorta. Damage to the abdomen, pelvis, and lumbar spine of the PMHS was also identified. In total, five PMHS underwent submarining. Four PMHS, none of which submarined, sustained pelvis fractures and represented the heaviest of the PMHS tested. Submarining of the PMHS occurred in two out of four vehicles. In the matched tests, the Hybrid III never underwent submarining while the THOR-50M submarined in three out of four vehicles. Submarining occurred in vehicles having both conventional and advanced (pretensioner and load limiter) restraints. The dominant factors associated with submarining were related to seat pan geometry. While the THOR-50M was not always an accurate tool for predicting submarining in the PMHS, the Hybrid III could not predict submarining at all. The results of this study identify substantive gaps in frontal-crash occupant protection in the rear seat for midsized males and elucidates the need for additional research for rear-seat occupant protection for all occupants.

KEYWORDS – PMHS, ATD, Submarining, Abdominal Injury

INTRODUCTION

As advancements in passive safety technology in the front seat have outpaced those in the rear seat, the safety benefit of the rear seat for some restrained passengers has decreased. Specifically, as features like pretensioners, load limiters, and airbags have become mandatory in the front seat, it has become safer than the rear seat for older occupants in frontal crashes (Bilston et al. 2010; Kent et al. 2007; Kuppa et al. 2005; Smith and Cummings 2006; Tatem and Gabler 2019). While adults tend to make up a small portion of rear-seated occupants (Tatem and Gabler 2019; Trowbridge and Kent 2009), they make up a disproportionately high percentage of fatalities of restrained rear-seated occupants in frontal crashes (Tatem and Gabler 2019). Additionally, more adults are expected to ride in the rear seat due to use of ride-sharing services and autonomous vehicles. In fact, in both conventional seating arrangements and potential face-to-face configurations in autonomous vehicles, occupants are likely to select the rear seat for its perceived safety benefits (Nie et al. 2020).

Address correspondence to Allison Guettler
Electronic mail: aguett@vt.edu

Of particular concern for rear seat occupants is abdominal injuries. Of all belted occupants, occupants in the rear seat have the highest risk of abdominal injury, which occurs at lower crash severities than in front row occupants (Frampton et al. 2012; Lamielle et al. 2006). Additionally, belt-only restraints have been found to be least effective at reducing abdominal injury when compared to advanced restraints or restraints paired with other safety features like airbags or anti-submarining features (Frampton et al. 2012).

Abdominal injuries related to direct belt loading to the abdomen are often to the hollow organs (Elhagediab and Rouhana 1998; Klinich et al. 2010; Lamielle et al. 2006; Lee and Yang 2002) and are often related to submarining, during which the lap belt slips off the pelvis and onto the abdomen. Kinematics that can initiate submarining include excessive downward motion of the pelvis coupled with rearward rotation of the torso and excessive forward excursion of the pelvis, leading to posterior rotation of the pelvis (Adomeit 1977; Adomeit and Heger 1975). Many studies have focused specifically on the pelvis and lap belt kinematics required to initiate submarining. Frequently, the lap belt angle, pelvis angle, and the relative angle between the two have been thought to be important factors in predicting submarining (Adomeit and Heger 1975; Horsch and Hering 1989; Leung et al. 1982; Luet et al. 2012; Nilson and Håland 1995; Rouhana et al. 1989; Uriot et al. 2015b). Adomeit and Heger (1975) identified an ideal minimum lap belt angle of 45-50 degrees from horizontal to prevent submarining kinematics and to reduce undesired torso rotation. Similarly, MacLaughlin et al. (1989) found that a lap belt angle of 45 degrees was a transition point, below which the tendency for submarining increased. Rouhana et al. (1989) found that 28 degrees of rearward pelvis rotation was required for the Hybrid III to submarine. Several studies identified a critical angle between the belt and pelvis where the tangent of the relative angle must be larger than the coefficient of friction between the belt and pelvis to produce belt slip (Horsch and Hering 1989; Leung et al. 1982; Nilson and Håland 1995). One of these studies determined that lifting of the buckle by the shoulder belt reduced the critical angle (Horsch and Hering 1989) and Leung et al. (1982) determined that the angle of the belt in the X-Y planar projection was critical for assessing restraint characteristics for submarining risk. These studies highlight the complex nature of submarining and an occupant's interaction with the lap belt.

A 2015 study conducted frontal crash sled tests with post mortem human surrogates (PMHS) in both front and rear seat configurations (Uriot et al. 2015a). Tests were conducted with a change in velocity (ΔV) of approximately 50 kph with a semi-rigid seat with separate lap and shoulder belts. In the rear seat condition, which included belt anchor locations similar to a rear seat, all four PMHS demonstrated submarining. However, each PMHS also sustained a unilateral iliac wing fracture, which was difficult to isolate from the submarining event. No injuries to the bowels or mesentery were noted. A series of studies conducted a total of 8 PMHS sled tests with a rear seat buck resembling a 2004 sedan (Michaelson et al. 2008; Forman, et al. 2009a; Forman, et al. 2009b). They compared standard 3-point belts to advanced restraints with a pretensioner and force limiter. In general, the advanced restraints reduced submarining in approximate midsized males, but had no effect on larger males. No abdominal damage was found during post-test autopsy. In these studies both restraint type and geometry affected the submarining response of the PMHS.

Submarining risk can also be a factor of surrogate type. One study compared submarining in the Hybrid II and Hybrid III 50th-percentile male ATDs (Anthropomorphic Test Devices) and 50th-percentile male PMHS during frontal-crash sled tests (Luet et al. 2012). The study used three test configurations varying the test severity, seat pan angle, and initial belt angle to create conditions more or less conducive to submarining. While the Hybrid III did not submarine during the loading phase of any test, the Hybrid II submarined at rates similar to the PMHS. Later, similar tests were run to compare the submarining responses of the Hybrid II, Hybrid III, and THOR-NT (Test device for Human Occupant Restraint – New Technology) ATDs to PMHS (Uriot et al. 2015). In these tests the Hybrid III failed to predict submarining and while the Hybrid II and THOR-NT both submarined, the THOR-NT was most-similar to the PMHS. In a rear-seat study that varied pulse severity and impact direction, the THOR-NT almost always submarined while the Hybrid III 5th-percentile female submarined some of the time and the Hybrid III 95th-percentile male never submarined indicating that the THOR-NT was more likely to submarine than Hybrid III ATDs of varying sizes (Hu et al. 2015). These studies demonstrate that submarining response varies by ATD and ATD size, and that the effectiveness of an ATD in predicting submarining in a PMHS might also vary by test condition.

In anticipation of increased rear seat use due to ride sharing and future novel seating compartments, Bianco et al. (2022) and Guettler et al. (2022) conducted frontal sled tests to assess rear-seat protection for midsized male occupants. Sled tests were conducted with the Hybrid III and THOR-50M ATDs in seven rear-seat vehicle bucks, each with three frontal crash pulse conditions. The bucks were made from modern vehicles that had a wide range of seat and restraint characteristics including conventional and advanced restraints (conventional three-point belts with pretensioners and load limiters). The front seats were removed from the vehicle bucks to allow for the evaluation of the rear seat in isolation, particularly for the application of novel seating compartments. Guettler et al. assessed submarining of the Hybrid III and THOR-50M ATDs in the rear seat tests. Throughout the study of 24 sled tests, the Hybrid III never underwent submarining while the THOR submarined to varying degrees in 16 tests. However, without PMHS responses for comparison, no determinations as to which ATD had the most biofidelic response could be made.

To allow for meaningful interpretation of the ATD data from Bianco et al. (2022) and Guettler et al. (2022), PMHS response data from the same test conditions are necessary. Frontal crash sled tests were conducted with midsized male PMHS in a subset of the vehicles and test conditions from the ATD study. The objectives of this study are to identify and characterize submarining in the PMHS, compare PMHS submarining to the submarining responses of the Hybrid III 50th-percentile male and THOR-50M ATDs, identify factors that might increase the likelihood of PMHS submarining, and to identify associated damage to the abdomen, pelvis, and lumbar spine.

METHODS

Twelve frontal crash sled tests were conducted using twelve PMHS. Three tests were conducted in each of four rear-seat vehicle bucks. The bucks were selected out of seven used in previous studies (Bianco et al. 2022; Guettler et al. 2022). Tests were conducted with high-speed vehicle-specific crash pulses (NCAP85, ΔV≈56 kph). The submarining responses of the PMHS were compared to the responses of the Hybrid III and THOR ATDs in matched NCAP85 tests from Guettler et al. (2022). Damage to the abdomen, lumbar spine, and pelvis of the PMHS were also assessed.

Test Conditions

Four modern-vehicle bucks were selected from Bianco et al. (2022) and Guettler et al. (2022) for PMHS testing (Table 1). The selected vehicles included two compact sport utility vehicles (CUVs, vehicles V13 and V14) and two midsize sedans (vehicles V15 and V19), and represented the bottom, top, and middle two performers from the ATD tests, respectively. The performance of each vehicle was rated based on ATD injury risk values and submarining results. An exemplar buck and test setup are shown in Figure 1. Buck development is described in detail by Bianco et al. (2022). One of each vehicle type had conventional restraints and one of each type had advanced restraints in the rear seat (Table 1). The advanced restraints were 3-point belts with a pretensioner and load limiter at the retractor (shoulder) whereas the conventional restraints were basic 3-point belts with a retractor at the shoulder. The restraints and seat cushions used in the study were original equipment parts and were replaced after each test.

TABLE 1. Vehicle information for the bucks in the ATD study conducted by Bianco et al. and Guettler et al. (2022). Vehicles selected for the PMHS study are highlighted.

Buck	Model Year	Vehicle Type	Seat Type	Restraint Type
V1	2018	CUV	Suspended	Advanced
V6	2017	Minivan	Pedestal	Conventional
V10	2018	SUV	Basket	Conventional
V13	2017	CUV	Rigid	Conventional
V14	2018	CUV	Rigid	Advanced
V15	2018	Sedan	Rigid	Conventional
V19	2018	Sedan	Rigid	Advanced

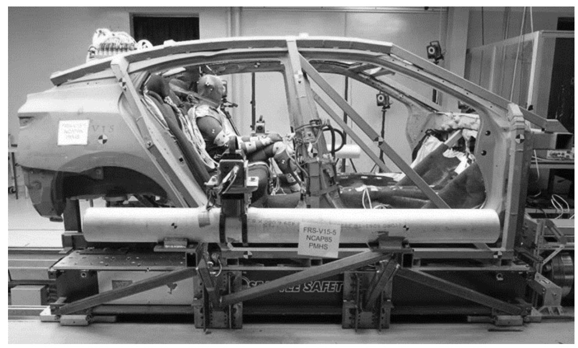

FIGURE 1. Final setup for a PMHS test in vehicle V15.

During the vehicle selection process, basic characterizations of the seat pans were done to capture important geometries and features like anti-submarining bars and seat pan angles. Additionally, estimated seat cushion stiffness was measured using varying weights and a FAROArm (FARO, Lake Mary, FL) to approximate deflection.

Tests were conducted using a 1.4 MN ServoSled (Seattle Safety LLC, Kent, WA) with the bucks bolted to the sled deck. All PMHS tests were conducted using the vehicle-specific "NCAP85" pulse for each buck. The NCAP85 pulses were created by scaling each vehicle's NCAP pulse (full frontal rigid barrier test) to 85% of its full magnitude. Scaling was done to remove rebound effects from the NCAP test (producing a ΔV of 56 kph) and to ensure that the ServoSled could produce the pulses. The NCAP85 pulse was selected from the ATD study because it produced higher ATD injury risks than either of the 32 kph pulse conditions. For tests with vehicles that had advanced restraints, pretensioners were set to fire 10 ms after the beginning of the sled pulse.

Each test was conducted with the PMHS seated in the rear left outboard seat for direct comparison to the THOR-50M in the ATD sled tests (Bianco et al.

2022; Guettler et al. 2022). One NCAP85 test from the ATD testing with each of these vehicles was selected for comparison to PMHS responses. The PMHS test matrix with matched ATD test IDs are listed in Table 2. Because the Hybrid III did not submarine in any vehicle in Guettler et al., only data for the THOR is included for comparison to the PMHS tests.

TABLE 2. Test matrix for the PMHS tests with PMHS characteristics and matched ATD test IDs.

Buck	Test No.	Surrogate	Sex	Age	Stature (cm)	Mass (kg)
V13	4	SM129	M	79	178	63
	5	SM155	M	65	168	85
	6	SM161	M	83	175	81
	2	THOR				
V14	5	SM156	M	68	188	89
	6	SM157	M	59	173	68
	7	SM160	M	74	178	79
	4	THOR				
V15	5	SM152	M	63	180	81
	6	SM153	M	51	168	64
	7	SM165	M	51	175	89
	4	THOR				
V19	5	SM154	M	74	178	89
	6	SM095	M	74	170	64
	7	SM159	M	29	163	73
	4	THOR				

Specimen Preparation

The PMHS were obtained from informed-consent programs. Selection criteria included male PMHS, with stature ranging from 166.5 to 184.0 cm, mass from 66.4 to 89.9 kg, and BMI ranging from 20 to 30 kg/m2. Prior to PMHS selection, anatomical donors went through serological analysis for viral risks as well as medical imaging such as plain film x-ray or computed tomography (CT) scans. Inspection of medical imaging identified fractures, skeletal abnormalities, and osteophytes between vertebrae, which could exclude a PMHS from the study. All PMHS were frozen until 48 hours before specimen preparation and refrigerated overnight throughout preparation.

Twelve PMHS were selected for use in this study. The average age, stature, and mass of the specimens were 64 +/- 15 years old, 175 +/- 7 cm, and 77 +/- 10 kg, respectively. General information about the PMHS is provided in Table 2.

Pelvis kinematics were recorded using a 6DOF (six degree of freedom) motion block clamped to the left ilium (bolted for test V15-5). The pelvis block was instrumented with 3 single-axis accelerometers (Endevco 7264c-2k, PCB Piezotronics of North Carolina, Inc., Halifax, NC) and 3 angular rate sensors (ARS) (DTS Pro 18k, Diversified Technical Systems, Inc., Seal Beach, CA). A tilt sensor was installed on the right ilium for determination of pelvis angle during positioning, and was removed just before the test. Sacrum kinematics were recorded with a 6DOF sensor (DTS 6DX Pro), mounted dorsally to the sacrum. The aluminum mount for the sacrum 6DOF block was rigidly fixed to the sacrum with screws driven through the pedicles.

Intravascular pressure transducers (Mikro-Tip® SPR-350S, Millar, Houston, TX) were installed in the abdominal aorta proximal to the bifurcation and the inferior vena cava near the liver via the femoral arteries and veins. To install the pressure transducers, the tips were removed from two foley catheters and perfusion tubing was connected to each catheter. The perfusion tubing included a T-fitting which allowed for introduction of perfusion fluid and the Millar pressure transducer. The catheters were installed in the femoral artery and vein on opposite sides of the body, and the unused vessel in each thigh was then ligated. For example, if the right femoral vein and left femoral artery were used, the right femoral artery and left femoral vein were ligated. Prior to the positioning of the pressure transducers, they were inserted beyond their intended position to ensure the vessels were patent. Before a test, the catheter balloons were inflated which, along with vessel ligation, limited backflow of perfusion fluid into the lower extremities and ensured fluid went into the abdominal vasculature. Two additional Millar pressure transducers were installed in the subcutaneous tissue adjacent and medial to the right and left ASIS. Incisions were made in the skin on the lateral abdomen, and the pressure transducers were guided into the subcutaneous adipose tissue. When the transducers were in the desired location, they were stitched into place. X-ray images showing the locations of the pressure transducers and motion blocks in the coronal plane are in Figure 2.

The PMHS were dressed in a full-body spandex suit before being fitted with cotton t-shirts and shorts. The shoes used for the PMHS tests were the same as those used for the ATD tests. The perfusion tubing was connected to an onboard perfusion system, which was used to perfuse the abdomen with normal saline for 5-10 seconds before and during each test.

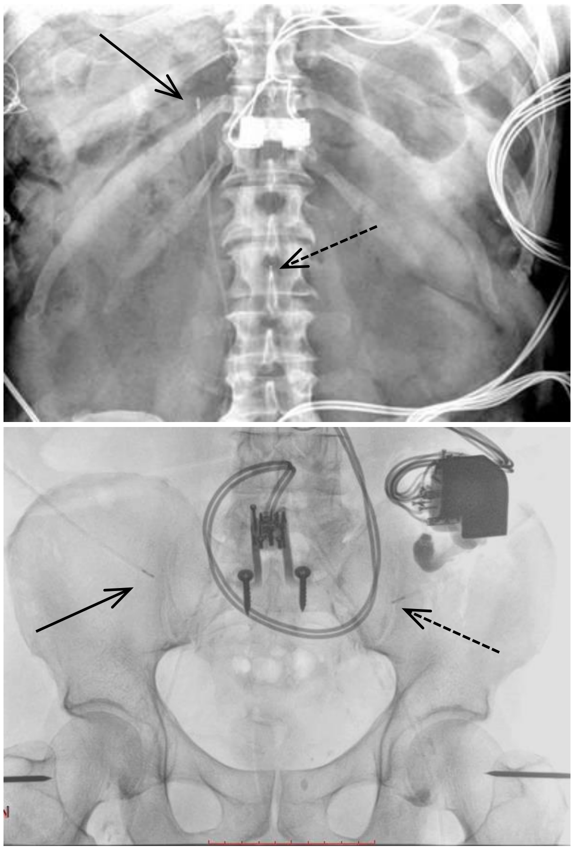

FIGURE 2. Locations of pressure transducers in the inferior vena cava (top, solid arrow) and aorta (top, dashed arrow), and at the left ASIS (bottom, dashed arrow) and right ASIS (bottom, solid arrow). Additionally, locations of the sacrum and ilium instrumentation mounts can be seen in the right image.

Positioning

In each buck, the head restraint was set to the highest position and the centerline of the seat was determined using the center of the head restraint and the centerline of the seat cushion between the right and left thigh bolsters of the left outboard seating position. First, the PMHS were centered in the seat with the pelvis pushed as far rearward as possible and the torso resting against the seatback. Adjustments were made to the fore-aft position of the pelvis to set the pelvis angle to the target of 29 degrees relative to horizontal. The pelvis angle was determined using a tilt sensor mounted to the right ilium near the tubercle of the iliac crest. The tilt sensor was calibrated to determine the angle between the plane defined by the pubic symphysis and right and left ASIS and the horizontal plane (with respect to the vehicle coordinate system). The target angle was selected to match that of the THOR-50M pelvis in the ATD tests. Next, the head was positioned using a marionetting technique to keep the Frankfort plane horizontal and the head and neck in a "natural" position for a seated occupant while leaving the torso against the seat back. The feet were positioned so that the knee angle was 100 +/- 5 degrees and the knees were 225 mm apart. The hands were placed on the anterior thigh so that the arms were 40 degrees from vertical. After each positioning step the pelvis angle was checked to ensure it had not rotated and that the superior aspect of the posterior pelvis remained in contact with the seatback. Finally, the belt was routed so that the shoulder strap crossed over the mid-sternum and the lap belt was overlapping both ASIS as much as specimen geometry allowed. Seat belt load cells were installed on the outboard lap belt (Anchor), inboard shoulder belt (Buckle), and outboard shoulder belt (Retractor). An example of the final positioning of a PMHS is provided in Figure 3. Prior to each test the tape used in the marionetting procedure was cut across the partial width so that it would break free at the start of the test.

Data Acquisition and Analysis

Transducer data were recorded on two onboard data acquisition systems, the DTS G5 and TDAS Pro (Diversified Technical Systems, Inc., Seal Beach, CA). Data were sampled using a rate of 20,000 samples per second (sps). Five high-speed video cameras (Phantom, V9.1, Vision research Inc., Wayne, NJ) provided right, left, and frontal onboard views, and overhead and lateral offboard views. Video was captured using 1,250 frames per second (fps). A Vicon motion capture system (Vicon Motion systems, Oxford, UK) with 16 MX T-20 cameras was used to quantify 3D kinematics of the PMHS using 1,000 fps. All data acquisition systems were triggered by an offboard DTS TDAS Pro, which received the trigger from the sled system. During data processing, time zero for all data (transducer, video, and Vicon) was set to the onset of sled acceleration, which typically occurred 80 ms post-trigger.

The global coordinate system was defined according to the SAE J211 standard (Society of Automotive Engineers, 2014) such that the X-axis is parallel to the longitudinal axis of the vehicle and is positive from posterior to anterior (back to front), the Y-axis is positive from left to right, and the Z-axis is positive downward (superior to inferior). The local coordinate systems of each instrumentation array were also defined according to SAE J211, which sets the same axes as the global system when the surrogate is standing. Filtering was performed to match the data filtering for the ATD tests (Guettler et al. 2022) and followed SAE J211.

The PMHS motion block data were rotated to align with anatomical conventions using the directionality

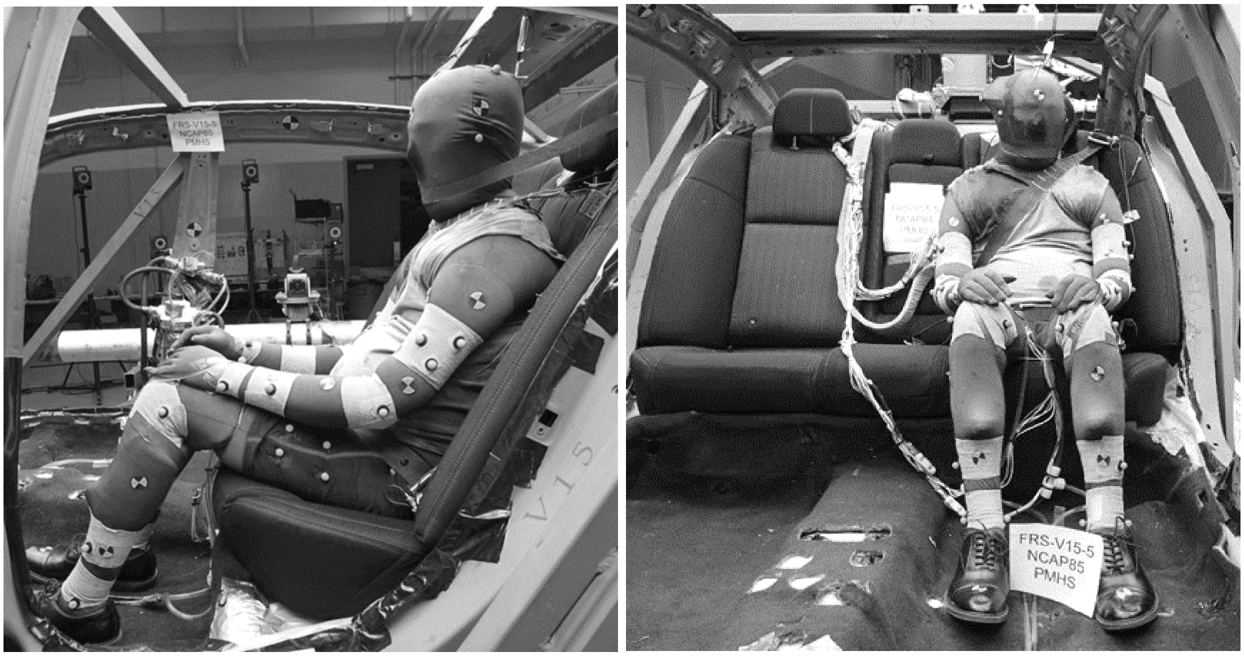

FIGURE 3. Final positioning for test V15-5 (SM152).

specified by SAE J211. To define the body-fixed basis for each motion block, pre-test CT scans were segmented using 3DSlicer (Open Source, (Fedorov et al. 2012)). Points were selected to develop the 3D anatomical coordinate system for each bone or body segment. Data were transformed from the motion block coordinate system to the scanner system, and then to the anatomical system. The coordinate system for the pelvis is defined by Padgaonkar (Padgaonkar et al. 1978), where the Y-Z plane is defined by the left and right ASIS and the superior edge of the pubic symphysis. The origin of the coordinate system is the midpoint between the right and left ASIS. The X-axis is normal to the defined plane pointing anteriorly, the Y-axis is along the ASIS line, pointing right, and the Z-axis points downward in the plane.

Post-test photographs, high-speed video, belt loads, abdominal pressures, and resultant pelvis acceleration were used to identify and characterize submarining. As with the ATD study, unilateral encroachment of the lap belt on the abdomen was categorized as minor submarining, bilateral encroachment with moderate abdominal loading was moderate submarining, and bilateral encroachment of the lap belt with substantial abdominal loading and departure of the pelvis from the seat cushion was considered severe (Guettler et al. 2022).

Post-test autopsies were performed on each PMHS to identify any damage from the tests. Autopsy information related to the pelvis, abdominal viscera, and lumbar spine was synthesized within the context of submarining.

Relative seat belt angle was calculated throughout each test for the PMHS and THOR-50M. For the PMHS, pelvis rotation was calculated by integrating the transformed Y-axis angular speed data from the pelvis instrumentation block. If the pelvis data were compromised, the sacrum data were used as a proxy, which occurred in two cases. The initial pelvis angle as measured from the tilt sensor was used as the baseline angle for the pelvis. The Vicon motion capture system was used to determine pelvis rotation in the THOR-50M with four to five retroreflective markers adhered directly to the pelvis flesh with double sided tape. Belt angle was determined throughout the PMHS and matched ATD tests by motion tracking of the lap belt in the onboard high-speed video. Angle definitions for this analysis are provided in Figure 4. The Vicon data were filtered using Channel Frequency Class (CFC) 60 and the lap belt angles and PMHS pelvis rotation data were filtered using CFC 180.

Pelvis angles were defined so that rotations follow J211. As shown in Figure 4, rotation of the pelvis/belt angle is positive in the clockwise direction. The pelvis angle as shown is negative, and would be zero when horizontal. The belt angle is positive as drawn and would also be zero when horizontal. Changes in both the pelvis and belt angle are positive for clockwise rotation. The relative belt angle is defined as the difference between the belt angle and the X-axis of the pelvis so that it is positive as the pelvis rotates rearward relative to the belt. For reference, when the belt is routed directly rearward from the pelvis, the relative belt angle is 0 degrees. As the relative angle increases, the angle between the belt and pelvis gets steeper, and is more positive.

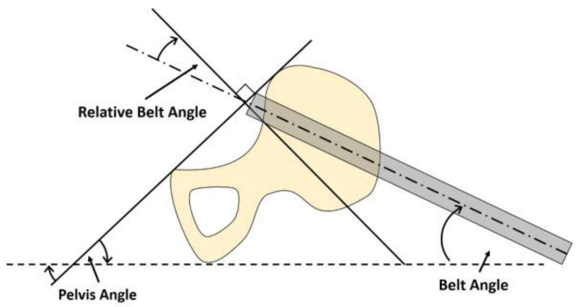

FIGURE 3. Definitions of the pelvis, belt, and relative belt angles.

RESULTS

Twelve sled tests were conducted with twelve PMHS. Three tests were conducted in each of four rear-seat vehicle bucks in a frontal NCAP85 crash condition. The crash pulses were specific to each vehicle and are included in Figure A1 (Appendix A).

Pelvis and sacrum kinematics were measured during each test. In some instances (tests V15-5 and V19-6), pelvis instrumentation was lost during a test and the sacrum kinematics were used instead. Figure B1 (Appendix B) provides a comparison between the pelvis block and sacrum block kinematics. The X and Z-direction acceleration and Y-axis angular speed of the pelvis are provided for each test in Figure B2 through Figure B5. Pelvis and sacrum acceleration were lost due to instrumentation failure in test V14-7 (Figure B3). Pelvis kinematics for all three PMHS tests in vehicle V13 are provided in Figure B6. Pelvis speed for the PMHS and THOR in vehicles V13 and V15 are provided in Figure B7. Time histories of the PMHS and THOR-50M pelvis angles for each vehicle are provided in Figure 5 through Figure 8. Lap belt angles are plotted with pelvis angles in Figure 5 through Figure 8. The relative belt angles over time were calculated for each test and are provided by vehicle (Figure 9) and by restraint and surrogate type (Figure 10).

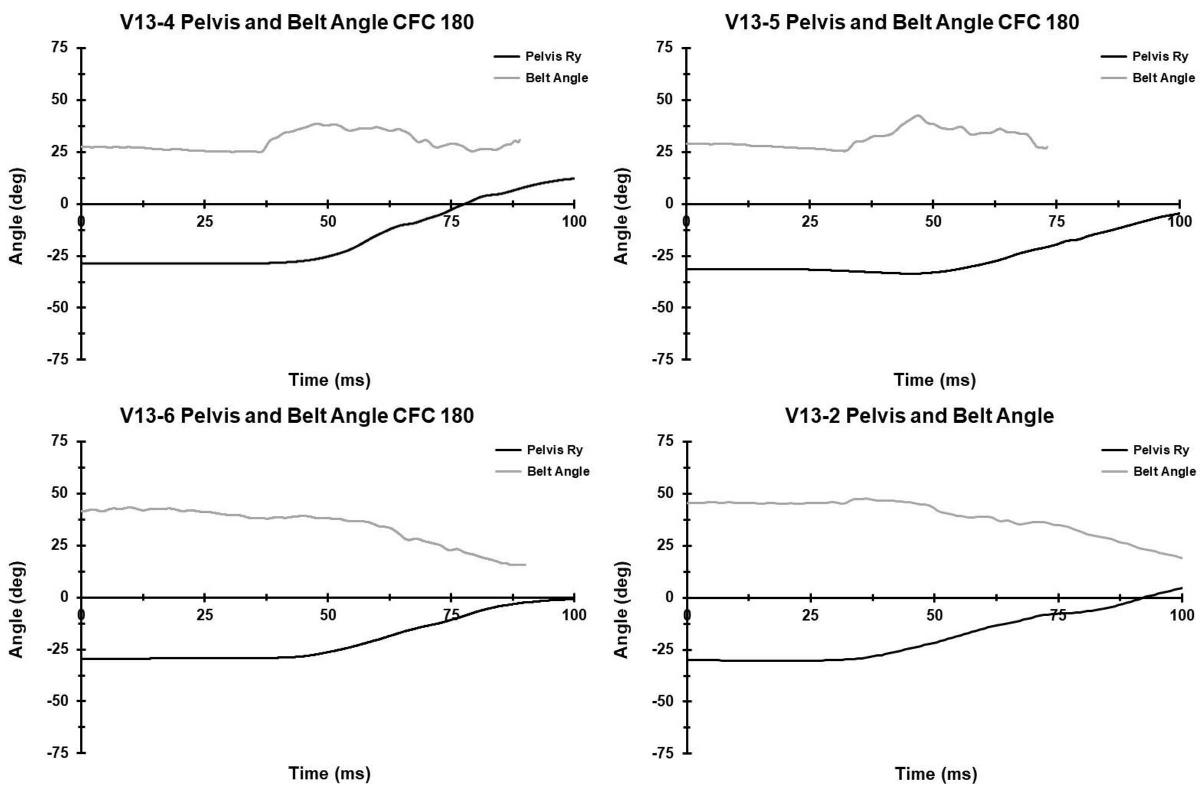

FIGURE 4. Pelvis and belt angle for the PMHS and THOR (bottom right) in vehicle V13.

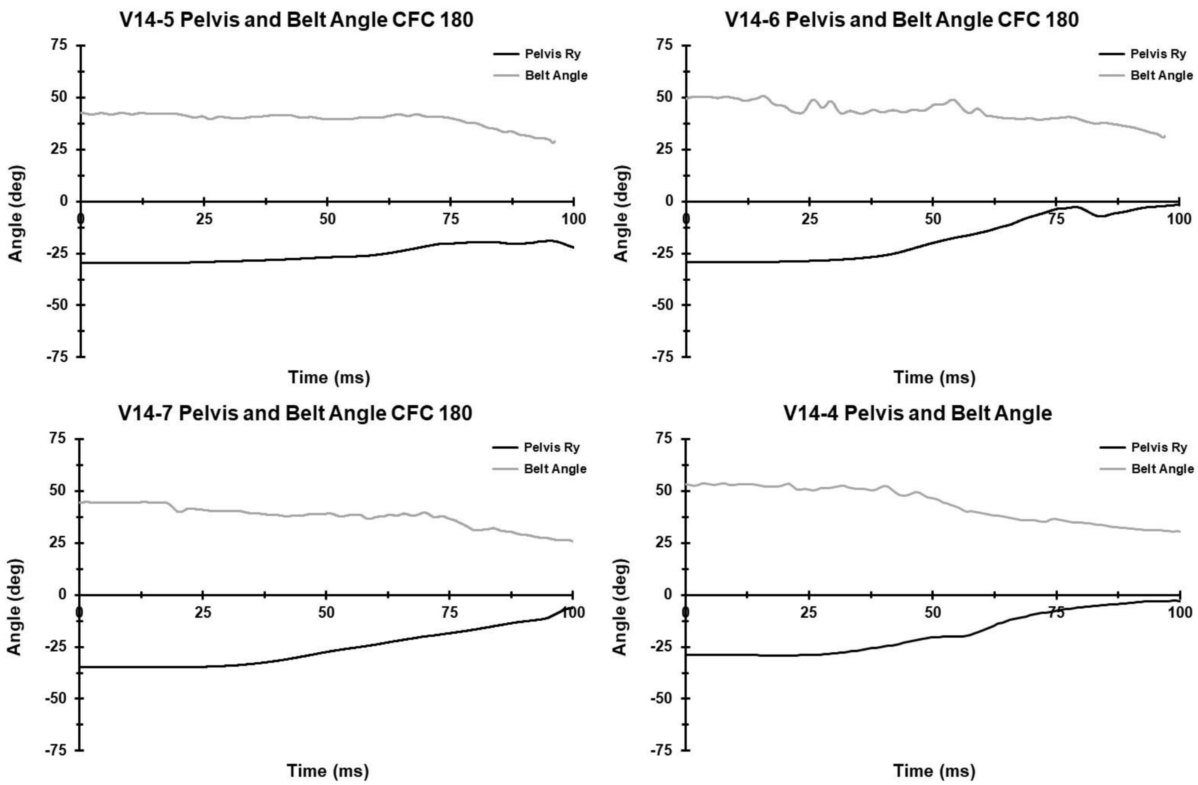

FIGURE 5. Pelvis and belt angle for the PMHS and THOR (bottom right) in vehicle V14.

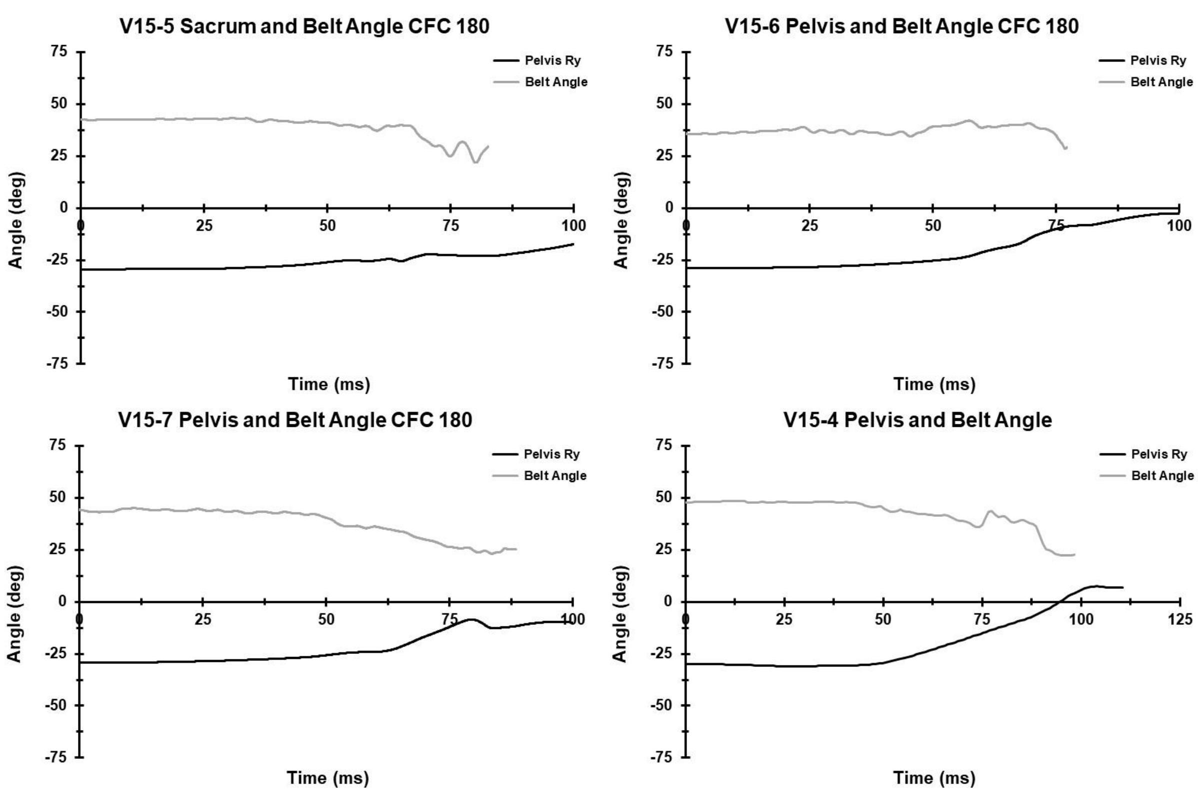

FIGURE 6. Pelvis and belt angle for the PMHS and THOR (bottom right) in vehicle V15.

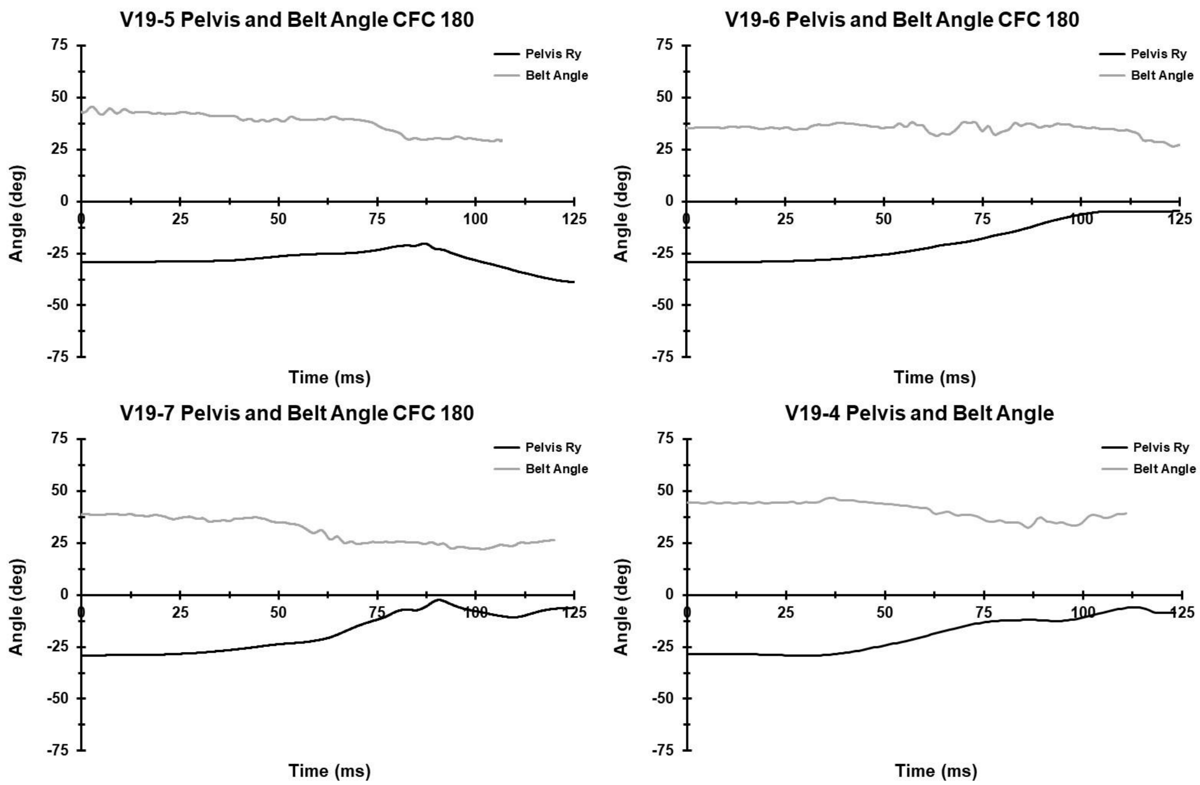

FIGURE 7. Pelvis and belt angle for the PMHS and THOR (bottom right) in vehicle V19.

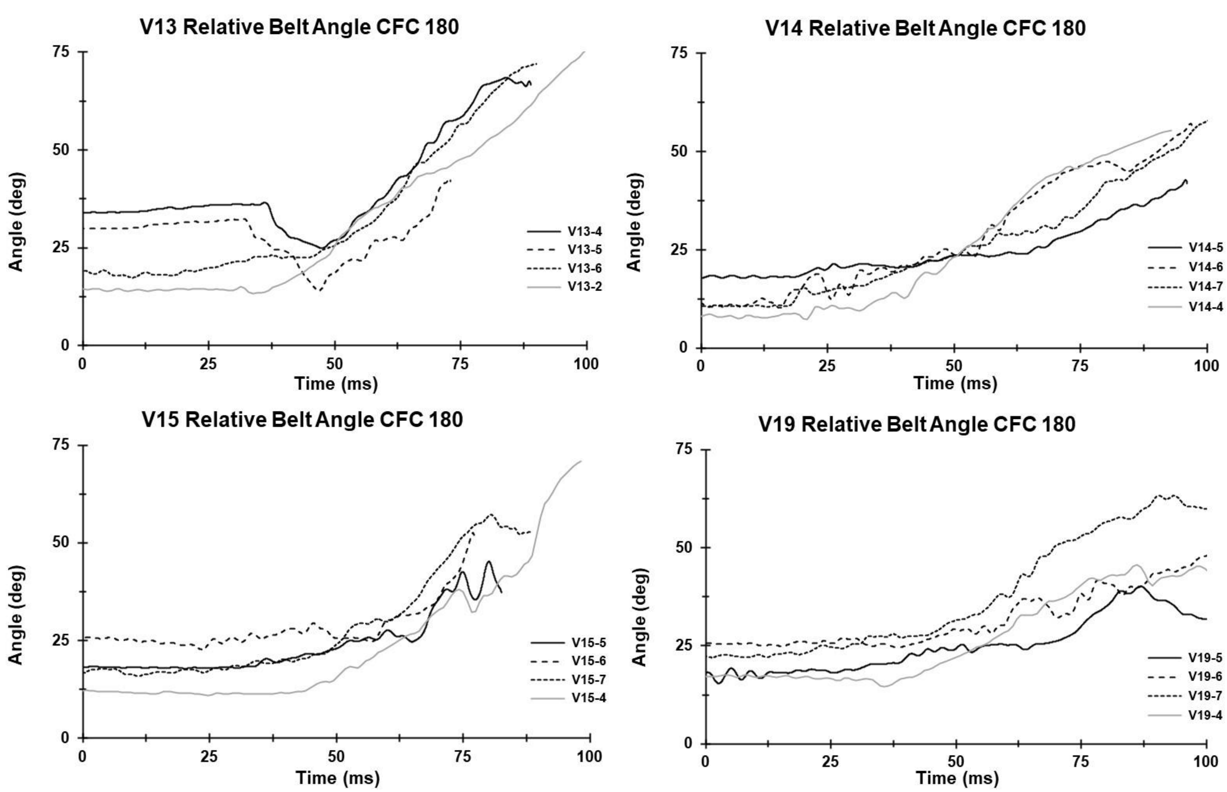

FIGURE 8. Relative belt angles of the PMHS and THOR (bottom right) by vehicle.

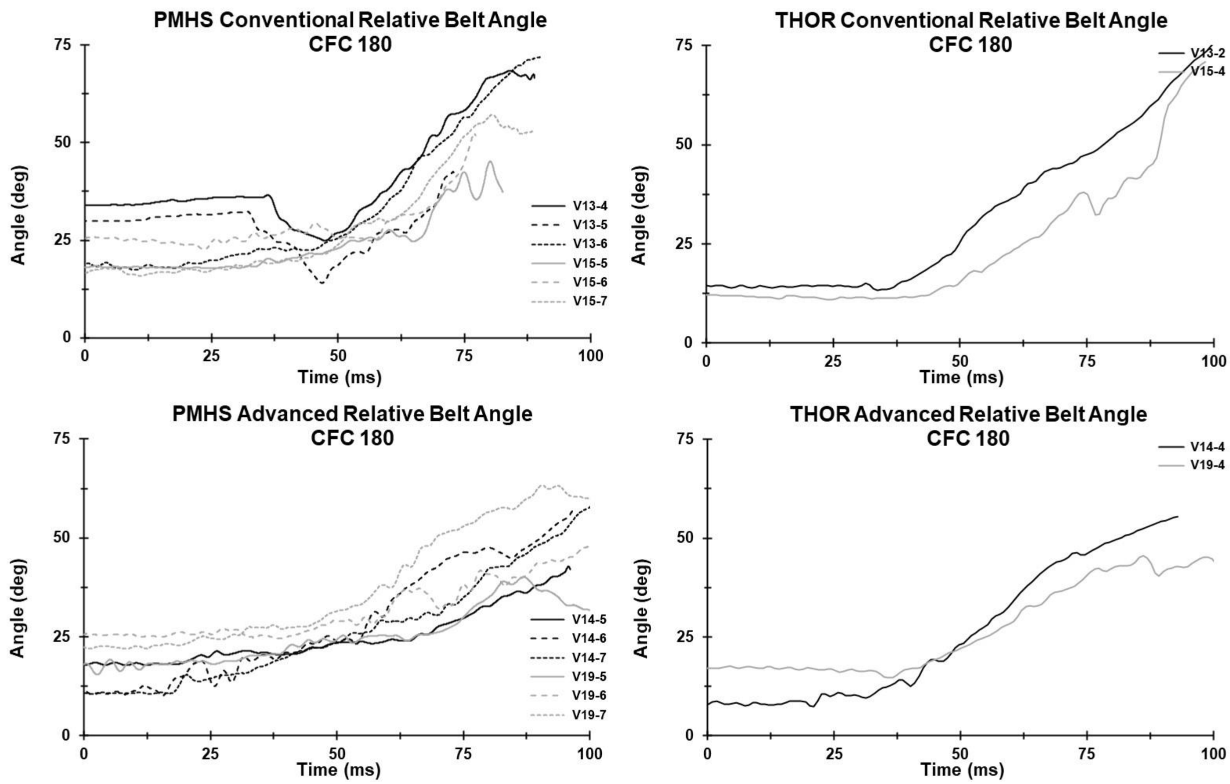

FIGURE 9. Relative belt angle by restraint type and surrogate type.

Belt loads measured at the retractor, above the buckle, and at the anchor and are provided for the PMHS and the THOR-50M reference tests in Figure C1 through Figure C4 (Appendix C). Belt loads plotted by location and vehicle are provided in Figure C5 and Figure C6. Peak belt loads are cataloged in Table 3. Time histories of the PMHS abdominal pressures are presented with the THOR-50M ABISUP pressures in Figure C7 through Figure C10. Peak abdominal and ABISUP pressures are cataloged in Table 4.

Five PMHS submarined (Table 5) in two of the vehicles. All PMHS underwent severe submarining in vehicle V13 while two PMHS underwent moderate submarining in vehicle V14. For all tests, including the THOR-50M tests, the time of submarining was estimated. The submarining time is the average of the estimated submarining time from all data sources listed in Table 5.

Four of the PMHS that did not undergo submarining sustained pelvis fractures (Table 6). In tests V14-5, V15-5, and V19-5, the PMHS sustained bilateral pelvis fractures in the iliac wings, and in test V15-7 the PMHS had a fracture in the left ilium. Fracture times were estimated from belt load and resultant acceleration time histories and averaged (Table 6). In some instances, sign of pelvis fracture could be found in angular speed or abdominal pressures, which were used as confirmation when possible.

TABLE 3. Peak belt loads.

Buck	Test No.	Surrogate	Retractor (kN)	Buckle (kN)	Anchor (kN)
V13	4§	SM129	7.4	5.2	5.8
	5§	SM155	9.8	6.3	8.5
	6§	SM161	8.4	6.0	7.6
	2§	THOR	8.9	6.0	n/a
V14*	5Δ	SM156	6.1	4.8	7.4
	6§	SM157	6.0	4.7	5.2
	7§	SM160	6.8	5.2	4.5
	4	THOR	6.4	4.6	6.8
V15	5 Δ	SM152	10.9	8.8	8.6
	6	SM153	8.6	6.4	7.6
	7 Δ	SM165	11.5	8.6	9.0
	4§	THOR	9.5	6.9	6.6
V19*	5 Δ	SM154	5.6	5.2	7.6
	6	SM095	4.2	4.9	5.5
	7	SM159	4.8	5.9	7.3
	4§	THOR	4.7	4.5	6.5

Advanced Restraints: *, Submarining: §, Pelvis Fracture: Δ

TABLE 4. Peak abdominal pressures with peak THOR ABISUP pressures.

Buck	Test No.	PMHS ID	Vena Cava (kPa)	Aorta (kPa)	Left ASIS (kPa)	Right ASIS (kPa)	Left ABISUP (kPa)	Right ABISUP (kPa)
V13	4§	SM129	100	149	127	227	n/a	n/a
	5§	SM155	134	126	635	286	n/a	n/a
	6§	SM161	119	479	220	200	n/a	n/a
	2§	THOR	n/a	n/a	n/a	n/a	352	294
V14*	5$^{\Delta}$	SM156	119	111	74	92	n/a	n/a
	6§	SM157	127	136	156	139	n/a	n/a
	7§	SM160	92	93	173	98	n/a	n/a
	4	THOR	n/a	n/a	n/a	n/a	127	126
V15	5$^{\Delta}$	SM152	120	102	220	254	n/a	n/a
	6	SM153	-	149	217	434	n/a	n/a
	7$^{\Delta}$	SM165	365	-	-	134	n/a	n/a
	4§	THOR	n/a	n/a	n/a	n/a	366	326
V19*	5$^{\Delta}$	SM154	107	99	106	136	n/a	n/a
	6	SM095	127	118	229	423	n/a	n/a
	7	SM159	111	133	341	183	n/a	n/a
	4§	THOR	n/a	n/a	n/a	n/a	428	449

Advanced Restraints: *. Submarining: §, Pelvis Fracture: Δ

TABLE 5. Submarining results for the PMHS tests with the results of the THOR in each vehicle for comparison.

Buck	Test No.	PMHS	Submarining Severity	Submarining Time (ms)	Belt Loads (ms)	Pressure (ms)	Video (ms)	Resultant Acceleration (ms)	ASIS Fx (ms)	Belt Angle (ms)
V13	4	SM129	Severe	54.65	53.0	57.3	53.7	59.65		
	5	SM155	Severe	56.15	55.75	56.45	56.25	66.75		
	6	SM161	Severe	59.4	59.1	61.7	58.25	58.55		
	2	THOR	Severe	62.39	60.45	63.05	66.15		60.55	61.75
V14*	5	SM156	None	-	-	-	-	-		
	6	SM157	Moderate	64.65	63.4	66.3	64.3	64.5		
	7	SM160	Moderate	70.3	70.6	70.05	70.2	NA		
	4	THOR	None	-	-	-	-		-	-
V15	5	SM152	None	-	-	-	-	-		
	6	SM153	None	-	-	-	-	-		
	7	SM165	None	-	-	-	-			
	4	THOR	Moderate	75.35	75.35	76.95	75.45		74.75	74.25
V19*	5	SM154	None	-	-	-	-	-		
	6	SM095	None	-	-	-	-	-		
	7	SM159	None	-	-	-	-	-		
	4	THOR	Moderate	86.3	85.2	88.6	86.7		84.9	86.1

Advanced Restraints: *

TABLE 6. Pelvis fracture results and timing for the PMHS tests. In all but test V15-7, fractures were bilateral.

Buck	Test No.	PMHS	Fracture Time (ms)	Belt Loads (ms)	Resultant Acceleration (ms)	Angular Speed (ms)	Abdominal Pressures (ms)
V13	4	SM129	-	-	-	-	-
	5	SM155	-	-	-	-	-
	6	SM161	-	-	-	-	-
V14*	5	SM156	80.7	80.7	80.7	N/A	N/A
	6	SM157	-	-	-	-	-
	7	SM160	-	-	-	-	-
V15	5	SM152	69.6	70.1	69.2	70.1	69.1
	6	SM153	-	-	-	-	-
	7	SM165	58.6	58.6	57.7	59.55	NA
V19*	5	SM154	85.2	85.8	84.6	83.6	85.6
	6	SM095	-	-	-	-	-
	7	SM159	-	-	-	-	-

Advanced Restraints: *

In Figure 11, the relative belt angles are plotted by surrogate, by whether or not the PMHS submarined or sustained a pelvis fracture and by whether or not the THOR-50M submarined. In the submarining and pelvis fracture plots, a vertical line designates the time the event occurred. The belt, pelvis, and relative belt angles, as well as the anchor loads at the time of fracture or submarining are provided in Table 7

TABLE 7. Submarining and fracture times and the pelvis, belt, and relative belt angles at that time.

Buck	Test No.	Surrogate	Mass (kg)	Submarining/ Fracture	Sub/Fx Time (ms)	Anchor (kN)	Pelvis Angle (deg)	Belt Angle (deg)	Relative Belt Angle (deg)
V13	4	SM129	63	Submarining	54.65	2.9	-21.8	35.2	33.0
	5	SM155	85	Submarining	56.15	3.4	-30.9	36.4	22.7
	6	SM161	81	Submarining	59.40	3.6	-20.8	35.1	34.1
	2	THOR	77	Submarining	62.39	n/a	-13.4	37.5	39.1
V14*	5	SM156	89	Fracture	80.7	7.3	-20.0	37.0	33.0
	6	SM157	68	Submarining	64.65	4.0	-11.8	40.0	38.1
	7	SM160	79	Submarining	70.3	3.9	-19.9	39.4	30.7
	4	THOR	77	-	-	-	-	-	-
V15	5	SM152	81	Fracture	69.6	8.6	-23.0	33.0	35.0
	6	SM153	64	-	-	-	-	-	-
	7	SM165	89	Fracture	77.3	8.9	-10.0	26.0	55.0
	4	THOR	77	Submarining	75.35	5.8	-14.9	37.1	37.4
V19*	5	SM154	89	Fracture	85.2	7.6	-21.0	30.0	39.0
	6	SM095	64	-	-	-	-	-	-
	7	SM159	73	-	-	-	-	-	-
	4	THOR	77	Submarining	86.3	5.6	-12.0	32.3	45.6

Advanced Restraints: *

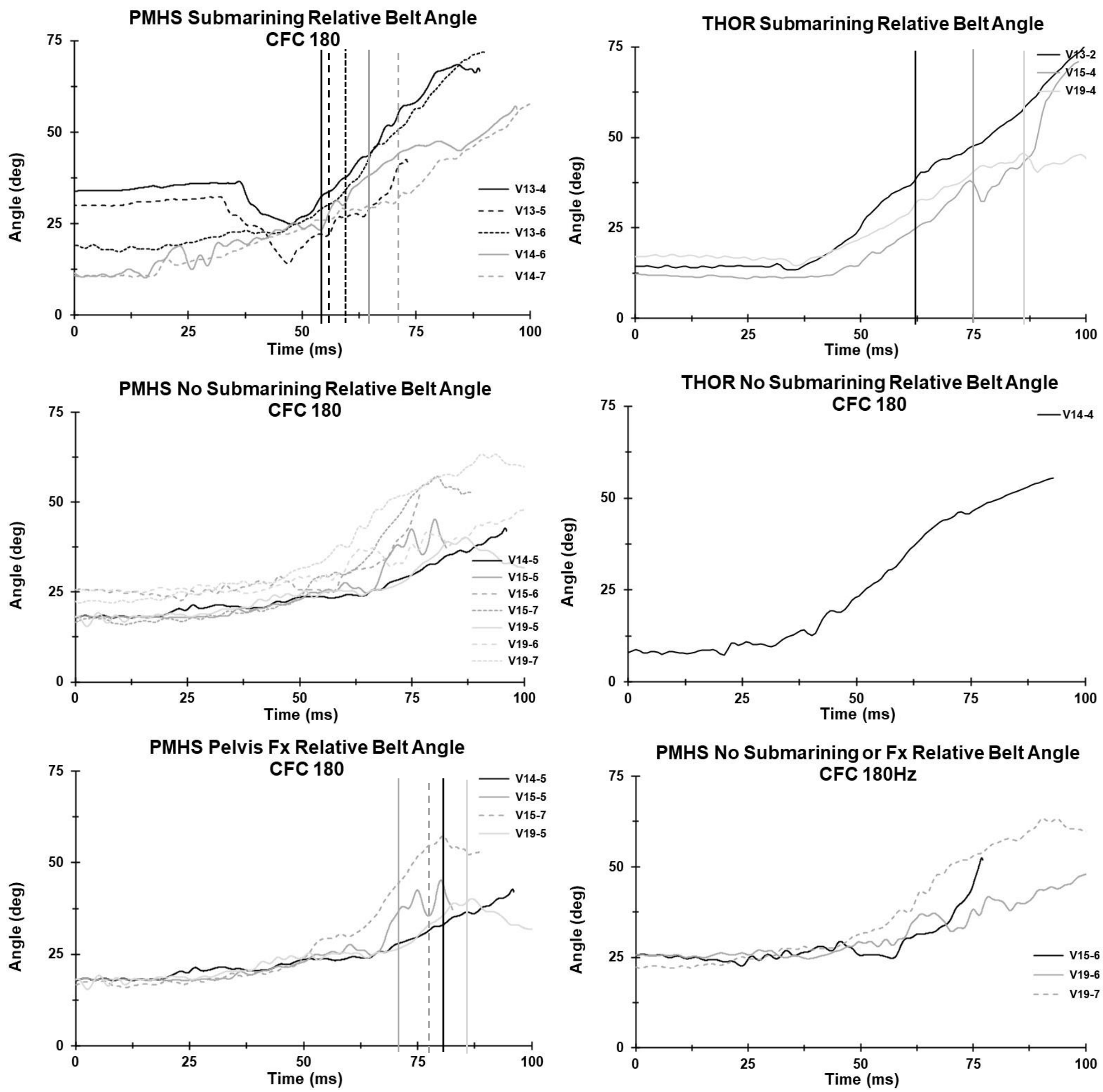

FIGURE 10. Relative belt angles by event type and surrogate type. In submarining or pelvis fracture plots, a vertical line designates the time of the event for the test with the matching line type.

The PMHS and ATD kinematics are summarized using lateral onboard high-speed video frames provided in Appendix D. The frames showing initial position of each surrogate are provided, as well as frames showing the position at the time of submarining or pelvis fracture. For tests not involving submarining or pelvis fracture, a frame representing the approximate time of half-peak X-direction pelvis excursion is provided. The third still frame provided for each test represents peak X-direction pelvis excursion.

In addition to pelvis fractures, damage to the abdominal viscera and lumbar spine was generated in these tests. Table 8 summarizes damage to the abdominal viscera, lumbar spine, and pelvis of each PMHS. Damage to the abdominal viscera occurred regardless of the incidence of submarining. Detailed descriptions and images of the damage to the abdomen, lumbar spine, and pelvis are provided in Appendix E. For discussion purposes, the THOR T12 X and Z-direction loads and Y-axis moments, as well as the ASIS X-direction load and Y-axis moment are provided in Appendix F.

TABLE 8. Summary of damage to PMHS with peak intravascular pressures.

PMHS	Mass (kg)	FRS Test	Submarining Degree	Peak Aorta Pressure (kPa)	Peak Vena Cava Pressure (kPa)	Pelvis Fracture	Lumbar Fracture	Liver	Spleen	Bowel	Mesentery	Peritoneum	Diaphragm
SM129	63	V13-4	Severe	149	100		*			Y	Y		Y
SM155	85	V13-5	Severe	126	134		L2	Y	Y	Y	Y		
SM161	81	V13-6	Severe	479	119		L5/S1	Y		Y	Y	Y	Y
SM156	89	V14-5		111	119	Bilateral		Y			Y	Y	
SM157	68	V14-6	Moderate	136	127			Y			Y		
SM160	79	V14-7	Moderate	93	92		*				Y		
SM152	81	V15-5		102	120	Bilateral		Y		Y			Y
SM153	64	V15-6		149	-			Y		Y	Y		
SM165	89	V15-7		-	365	Left		Y		Y	Y	Y	
SM154	89	V19-5		99	107	Bilateral							
SM095	64	V19-6		118	127						Y		
SM159	73	V19-7		133	111						Y	Y	

*One or more lateral process Fx

DISCUSSION

Pulse Considerations

As seen in Figure A1, there are some differences in the phasing of different test pulses within the same vehicle. There are several factors that produce this appearance of major differences between the tests. First, the sled fires approximately 80 ms after system trigger, however this time can vary slightly. To produce a consistent method for defining the start time of the event (i.e. the start of acceleration), the first time point for which the sled started to move in global negative acceleration was set to 0 ms. In some instances, the sled would stutter before the prescribed pulse would start, leading to a longer time between time zero and the first acceleration peak. Second, there can be variation between the exact pulses produced by the sled despite having the same prescribed acceleration pulse. These differences are often minor and cannot be avoided.

These factors also contribute to the apparent differences in pretensioner firing during the advanced restraint tests (Figure C6). Because it would shift the definition of time zero, a stutter of the sled at the beginning of the acceleration pulse would shift when the pretensioner would fire relative to the defined start of the test.

Factors in Submarining Assessment

As described by Guettler et al. (2022), multiple data sources must be considered in combination to get an accurate determination of submarining. In the current study, lap belt loads, abdominal pressures, pelvis kinematics, high-speed video, and post-test photographs were used to identify submarining and approximate the time at which it occurred. While the lap belt was clearly in the abdomen after each PMHS test with submarining, the instrumentation used in the PMHS tests provided much more subtle indications of the onset of submarining than in the THOR belt, ABISUP, and ASIS load data. For example, in the THOR an indication of submarining is a sharp drop in ASIS load or moment, which is consistent with other ATD studies (Rouhana et al. 1989). Additionally, the magnitude of ABISUP pressure was also related to submarining severity. For the PMHS, the signs of submarining are much more subtle. There is no mechanism for measuring ASIS load, and abdominal pressure measurements are much more localized than in the ABISUP. Slight changes belt loads, pelvis acceleration and abdominal pressures have to be compared to high speed video and the post-test position of the lap belt to make an accurate determination of the onset of submarining in the PMHS. Differences between the anterior contour of the ABISUP and the abdomen of each PMHS contribute to the subtlety of submarining sign in the

PMHS compared to the THOR. In these PMHS tests, the abdomen often extends beyond the anterior-most point of the pelvis, preventing superior motion of the lap belt on the abdomen and concentrating the lap belt load to one area of the abdomen, just above the pelvis. In contrast, the ABISUP abdominal insert in the THOR-50M has a smooth contour that is in line with the anterior pelvis, more readily allowing the lap belt to move from the pelvis to the abdomen.

Submarining by Surrogate

One of the goals of this study was to compare the submarining results of the PMHS to the ATDs in the matched tests in Guettler et al. (2022) to determine which ATD had a more biofidelic response with respect to submarining. In the ATD tests, the Hybrid III did not submarine in any test and the THOR submarined in 16 out of 24 tests, including in three out of the four vehicles in the matched NCAP85 tests. Five PMHS submarined during the current study □ in two out of four vehicles. The results of this study suggest that the Hybrid III is not sensitive enough to predict submarining in the rear-seated PMHS in this study. The inability of the Hybrid III to predict submarining has been highlighted in previous studies (Uriot et al. 2015b). In contrast, the predictive ability of the THOR-50M was more complicated. The THOR-50M accurately predicted severe submarining in vehicle V13, in which all three PMHS underwent severe submarining and sustained substantial damage to the abdominal viscera and lumbar spine. However, the THOR-50M did not predict submarining in vehicle V14, in which two PMHS underwent moderate submarining. Finally, while the THOR-50M underwent moderate submarining in vehicles V15 and V19, none of the PMHS submarined in those vehicles. This result from THOR-50M is somewhat contrary to a previous study in which the THOR accurately predicted both positive and negative submarining results (Uriot et al. 2015b). This contrary result could be related to the specific test configurations of the restraints and seat in the 2015 study. In the configuration where the PMHS and THOR submarined, the surrogates were in “slouched” positions, predisposing them to submarining; in the two configurations in which no surrogates submarined, surrogates were positioned more upright and pretensioners were either at the shoulder retractor (“standard”) or on both sides of the lap belt (“prototype”).

Relative Belt Angle

The initial relative belt angles varied between tests and surrogates. Because the initial pelvis angle was the same target value for the PMHS and the THOR, this variation is from differences in the initial belt angle. Differences in initial belt angles were due to belt anchor locations in each vehicle, the height of the PMHS thighs and ASIS, or the combination of the two. In tests V13-4 and V13-5 (Figure 5), the belt was initially wrapped around the seat cushion so that the angle of the belt that was above the cushion was smaller. When the PMHS loaded the restraints and the belt straightened, increasing the length of the belt visible for tracking and ultimately increasing the measured belt angle. This phenomenon is what caused the concave upward shape of the relative belt angle curves for these two tests.

In general, the relative belt angles increased more gradually throughout the tests involving advanced restraints compared to conventional restraints (Figure 10). The same is observed for cases without submarining compared to those involving submarining. The greater rate of increase in relative belt angle in submarining cases is more readily apparent after the first 50 ms of the tests (Figure 11). The change in relative belt angle for cases involving pelvis fracture is most similar to that observed for cases without submarining or fracture (Figure 11).

For the PMHS tests involving submarining, the relative belt angle at the time of submarining ranged from 22.7 to 38.7 degrees, averaging 31.7 +/- 5.7 degrees. For the matched THOR-50M tests involving submarining, the relative belt angle at the time of submarining ranged from 37.4 to 45.6 degrees, averaging 40.7 +/- 4.3 degrees. This suggests that a larger relative belt angle is required for THOR-50M to submarine than for PMHS to submarine. For PMHS tests involving pelvis fracture, the relative belt angle ranged from 33.0 to 55.0 degrees at the time of fracture, averaging 40.5 +/- 10.0 degrees, which suggests interaction between the belt and pelvis for a longer duration than for submarining cases, or at least until a greater relative belt angle had taken place. Regardless, it should be noted that there is some overlap in relative belt angles between submarining and fracture cases at the time of each event.

There was a large degree of overlap in the pelvis angle at the time of each event in the PMHS submarining and fracture groups. At the time of submarining, the PMHS pelvis angles ranged from -11.8 to -30.9 degrees and averaged -21.0 +/- 6.8 degrees. The pelvis angles at the time of fracture ranged from -10.0 to -23.0 degrees, averaging -18.5 +/- 5.8 degrees. The lap belt angles between groups had less overlap. The lap belt angles at the time of submarining ranged from 35.1 to 40.0 degrees and averaged 37.2 +/- 2.3 degrees while the lap belt angles at the time of pelvis fracture ranged from 26.0 to 37.0 degrees and averaged 31.5 +/- 4.7 degrees. Overall pelvis fractures occurred at shallower lap belt angles than did submarining.

While the overlap in relative belt angle observed in this study within outcome types might result from use of similar anthropometry across all surrogates, some differences in submarining response are likely related to specimen geometry. For example, for tests V14-6 (SM157) and V14-7 (SM160), PMHS characteristics could have contributed to the occurrence of submarining. SM157 had little distance between the top of the thigh and the superior aspect of each ASIS. Therefore, it was difficult to position the lap belt such that it would fully engage the pelvis during the test, facilitating submarining. The abdomen of SM160 was such that the lap belt could not be positioned directly over the pelvis. Considerable flesh was trapped between the belt and pelvis, and the abdomen had a rounded contour down to the groin. This too could have facilitated slip of the lap belt up and over the pelvis. In both cases, the geometry of each PMHS limited the ability of the lap belt to engage the pelvis and could have led them to submarine in a vehicle in which the THOR did not.

Seat Belt Anchor Load

Of the three seat belt loads measured, load near the outboard anchor point is most closely indicative of the load applied across the pelvis. At the time of submarining for the PMHS, the anchor load ranged from 2.9 to 4.0 kN, averaging 3.6 +/- 0.4 kN. The anchor loads for the THOR at the time of submarining were 5.6 and 5.8 kN in the two tests for which anchor loads were available. At the time of pelvis fracture, the PMHS anchor load ranged from 7.3 to 8.9 kN and averaged 8.1 +/- 0.8 kN. The anchor loads associated with pelvis fracture are twice those associated with submarining, on average. This is understandable as the load required to fracture the pelvis would not be reached at the time the belt slips off the pelvis during submarining. For tests that did not involve submarining or pelvis fracture, the peak PMHS anchor loads ranged from 5.5 to 7.6 kN, averaging 6.8 +/- 1.1 kN. Overall, pelvis fractures occurred at relatively high loads while submarining occurred at lower loads, and in cases where neither event occurred, the peak anchor load fell between these two ranges.

Surrogate Mass

While the PMHS selected for this study were approximately 50th percentile, a range of mass was used (Table 2 and Table 7). The PMHS were distributed across the vehicle bucks so that each buck would be tested using a relatively lighter (64.8 +/- 2.2 kg) and heavier PMHS (88.0 +/- 2.0 kg), and one that was very close to 50th percentile (78.5 +/- 3.8 kg). For V13, all PMHS submarined regardless of mass. There were no pelvis fractures observed for this buck. This buck was identified as the poorest performing in terms of submarining by Guettler et al. (2022), which agrees with the PMHS results. For the other three vehicles, it was always the heavy PMHS that sustained pelvis fracture (87.0 +/- 4.0 kg) in the absence of submarining. For all submarining cases, the average PMHS mass was 73.2 +/- 9.3 kg. For cases not involving pelvis fracture or submarining, the average PMHS mass was 67.0 +/- 5.2 kg. This strongly suggests that in the absence of submarining, heavier occupants are at higher risk of pelvis fracture. There is a weaker suggestion that lighter PMHS might not be expected to submarine either. In the V14 tests, two PMHS submarined and one, the heaviest, sustained pelvis fractures. Given that both submarining and pelvis fracture occurred in the same buck using the same restraint systems, it is possible that increased mass contributed to the avoidance of submarining at the expense of pelvis fracture. However, there are too few tests with too many variables to draw firm conclusions.

Vehicle Package Characteristics

The test bucks in this study were fabricated from vehicles in the US fleet and are of model years 2017 and 2018. The restraints and seat cushions were original parts to each vehicle and the seat pan geometries were not altered. Two vehicles (V13 and V15) have conventional restraints and two vehicles (V14 and V19) have advanced restraints. All three PMHS in vehicle V13 underwent severe submarining and two out of three PMHS underwent moderate submarining in vehicle V14. Therefore, submarining occurred regardless of restraint type, and advanced restraints did not necessarily prevent submarining.

Diagrams of the basic seat pan geometries and seat cushion stiffnesses are provided in Figure 12. Vehicles V13 and V14 had shallow seat pan angles and vehicles V15 and V19 had steep seat pan angles. Vehicle V13 was associated with the most severe submarining and had a nearly flat seat pan, an anti-submarining structure that deformed with each test, and a soft seat bottom cushion (stiffness of 7.3 N/mm). V14 had a gradually sloped seat pan that did not form a pocket, and had the stiffest seat bottom cushion of the vehicles used for PMHS testing (12.3 N/mm). These two vehicles produced all of the submarining in the PMHS study although V13 had conventional restraints and V14 had advanced

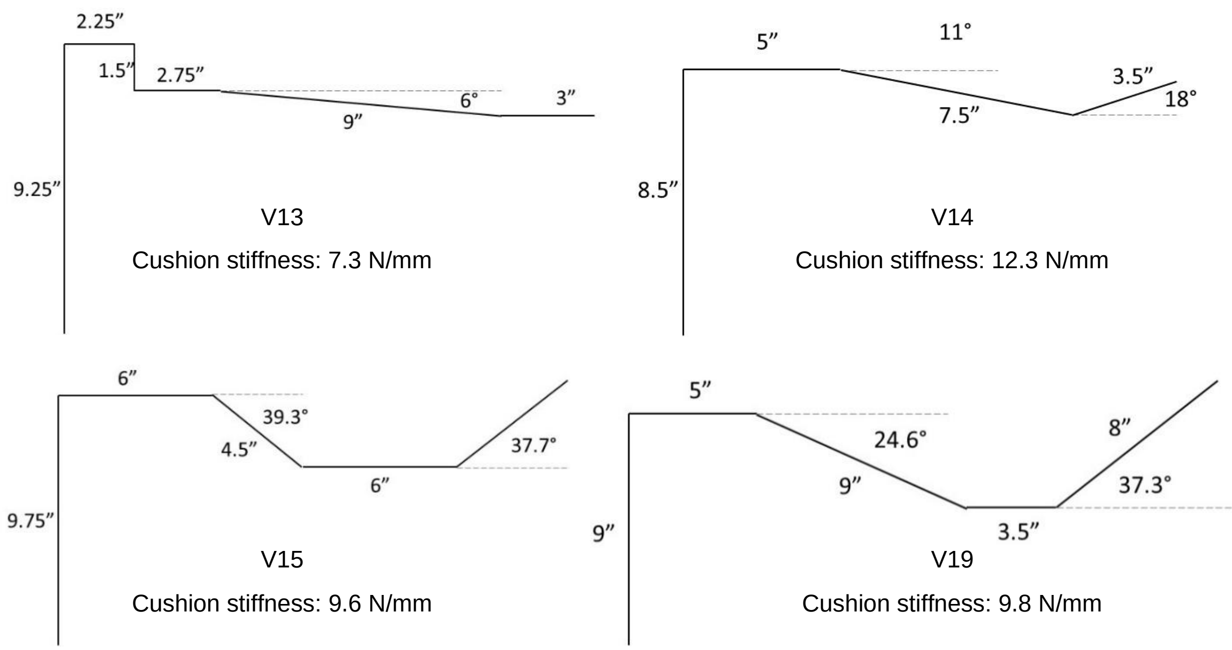

FIGURE 11. Vehicle buck seat pan geometries and bottom cushion stiffnesses.

restraints. Of the vehicles that had steep seat pan angles, one had conventional restraints (V15) and one had advanced restraints (V19). Neither of these vehicles produced submarining in the PMHS. These results suggest that seat pan geometry could be more important than restraint type in reducing submarining in midsized male PMHS in these test conditions.

PMHS Damage Response

In this study, submarining was not an indicator of whether or not damage to the abdominal viscera would occur. Throughout the test series, and in all but one test (V19-5), damage to the abdominal viscera occurred to many different structures and to varying degrees. Pelvis fractures were also produced in this study, in only non-submarining cases, and lumbar spine fractures were produced in only the most severe submarining cases.

Lumbar spine fracture and spleen damage were associated only with the most severe cases of submarining. In the two tests that produced lumbar spine fractures (V13-5 and V13-6), the PMHS slid off of the seat and the butt contacted the floorboards while the lumbar spine was in extreme extension over the riser. The lap belt directly loaded the spine while the restraints arrested downward excursion of the torso. Similarly, during the matched ATD test (V13-2) for this vehicle, the THOR-50M T12 moment (Figure F2) transitioned to extension as the pelvis moved toward the edge of the seat and then over the riser as the pelvis contacted the floorboards.

Vehicle V19 produced the smallest amount of damage to the abdominal viscera. In one test (V19-5) no damage to the abdominal viscera was sustained, but the PMHS sustained bilateral pelvis fractures. In the other two V19 tests, damage only occurred to the mesentery and peritoneum. Damage to the liver and diaphragm was most common in the vehicles with conventional restraints, and was associated with damage to the thoracic cage or interaction with the shoulder belt in the absence of submarining. Interaction with broken ribs produced all damage to the diaphragm and some liver damage. Finally, damage occurred in vehicles with both types of restraints, but damage to the bowels was only produced in vehicles with conventional restraints, again likely due to substantial interaction with the shoulder belt.

No case of submarining involved pelvis fracture. PMHS SM165 (Test V15-7) sustained pelvis fracture on the left side. This was the only incidence of unilateral fracture. It was one of the heaviest PMHS (89 kg) and registered the largest belt anchor load (8.9 kN) among all tests at the time of fracture. This PMHS was the second-to-youngest at death (51 years old), which could indicate bone condition better than most of the PMHS, and could have contributed to the unilateral fracture occurring at the highest load. Bilateral pelvis fractures without submarining are not common in the literature. In a study by Luet et al. (2012), five PMHS sustained pelvis fractures; all of which submarined. In that study, only two PMHS submarined without pelvis fractures. Additionally, the majority of the fractures in the study were unilateral, occurring either to the right or left sides of the pelvis (Luet et al. 2012). Lap belt loads were also lower, ranging from 4-6 kN at the time of fracture. However, these tests were conducted on a rigid seat pan of which the angle ranged from 0-5 degrees depending on the test configuration. Additionally, to reduce variability in lap belt loading caused by shoulder belt lift, the shoulder and lap belts were separated, each anchored independently at two points: the lap belt with retractors at either end and the shoulder belt with a retractor at the upper shoulder only. These conditions are substantively different from the manufacturer seats and restraints used in the current study.

In a later study, a similar setup was used to compare submarining kinematics of midsized male PMHS in front and rear seat conditions (Uriot et al. 2015a). For this study, the rigid seat pan was replaced with a semi-rigid seat pan which allowed for control of the seat angle, included an anti-submarining ramp, and allowed for deformation of the seat bottom during the test. Seat pan angle and angular stiffness as well as anchor locations were changed to represent the front and rear seat conditions. No PMHS sustained pelvis fractures in the front seat configuration, but every PMHS in the rear seat configuration sustained pelvis fractures despite the 5 kN load limit on the inboard and outboard lap belt anchors. The study identified submarining in all rear seat tests, but noted that it was difficult to isolate a potential submarining event from the iliac wing fractures. As with the 2012 study, the seat and restraint characteristics in the 2015 study produce a very different interaction between the seat, PMHS pelvis, and restraints. These differences could lead to the lower belt loads required to produce pelvis fracture and the combined fracture and submarining event that was not seen in the current study.

Abdominal Pressure

The peak intravascular abdominal pressures demonstrate potential trends with damage to the abdominal viscera. In the vena cava, the peak pressure associated with any abdominal damage ranged from 92 to 365 kPa and the peak pressure in test V19-5, in which no abdominal damage occurred, was 107 kPa. The peak pressure in the aorta for test V19-5 was 99 kPa, while peak pressure associated with visceral damage in the abdomen ranged from 93 to 479 kPa. For both the vena cava and aorta pressures, the non-damaging test produced peak pressures in the lower end of the abdominal damage range. It is important to note that while there was no damage to the abdominal viscera in test V19-5, SM154 did sustain bilateral pelvis fractures, which could have led to increased abdominal pressure caused by the lap belt.

In a previous study, the lowest peak aorta pressure associated with abdominal damage was 89 kPa, and the highest aorta pressure related to a non-injurious event was 103 kPa (Foster et al. 2006). In the current study, the lowest peak aorta pressure in a damaging test was 93 kPa and the peak pressure in the non-damaging test was 99 kPa, both values are within the range determined by Foster et al. Another study found the threshold for abdominal damage to be 57 kPa with moderate to severe abdominal damage being associated with peak aorta pressures between 74 and 97 kPa (Ramachandra et al. 2016). Foster et al. also stated that pressure in the abdominal aorta could potentially be used as an indicator for liver injury. In the current study, vena cava pressure (measured near the liver) reflects some indication of a trend for damage to the liver, with damage pressures ranging from 119 to 365 kPa and non-damage pressures ranging from 92 to 127 kPa. Similarly, peak aorta pressure might indicate damage to the mesentery, the non-damage range being on the lower end of the pressure range in this study.

Peak ASIS pressures ranged from 74 to 635 kPa with the highest pressure coming from a submarining test (V13-5) and the next highest peak pressure (434 kPa) occurring during a non-submarining, no pelvis-fracture test (V15-6). Of all the pressure measurements, ASIS pressures varied the most. Part of the variability in ASIS pressures could be related to the positioning of the transducers within the abdomen. The placement relative to other structures achieved during preparation might not be maintained once the specimen is positioned in a seat. It was also not guaranteed that the transducers would be in the line of lap belt loading.

The ABISUP pressures measured in the THOR are not directly comparable to the intravascular and tissue pressures in the PMHS in this study. While the PMHS pressures were not solely determined by submarining occurrence, higher ABISUP pressures were directly related to submarining and could be used in the classification of submarining (Guettler et al., 2022). Some of these differences are likely due to the homogenous nature of the ABISUP insert compared to the highly variable makeup of the human abdomen.

It is important to remember that strict interpretation of abdominal pressure is difficult for these tests given the complex response of the abdomen related to interaction with restraints combined with inertia.

Boundary and loading conditions will affect the pressure responses for different modes of testing. PMHS and ABISUP pressures were likely confounded by loading from the shoulder belt and torso flexion during testing. Additionally, the placement and fixation of the chest bands caused the abdomen of each PMHS to distend more than typical for a PMHS. This distension of the abdomen inhibited slip of the lap belt up the abdomen, changed the mass distribution of the abdominal contents, and could have affected the pressures measured. The forward excursion of the abdomen due to inertial loading also confounded the interpretation of the pressure values. While some trends were described here, there is not enough clear delineation to make any conclusive statements.

Role of Front Seats

The front seats were removed from the vehicle bucks to reduce variability between vehicles, to reduce the number of variables that could not be controlled, and to improve sight lines for high-speed video and the Vicon motion capture system, which were critical for assessing occupant kinematics and submarining. Further, novel seating compartments of the future could consist of forward-facing rear seats and rearward-facing front seats, eliminating rear-seat occupant interaction with the front seats. Finally, the restraint effect of the front seat is dependent on seat-track position, seat back angle, and occupant presence or mass. These conditions would be difficult to match or account for in these tests. The objective of this study was to assess the relative safety performance of different rear seat package characteristics and restraint systems in the absence of confounding factors presented by the front seats. While the complex nature of the problem inhibits inferences about how PMHS response would differ with the front seats present, discussion of the influence of the front seat with respect to submarining kinematics has been previously discussed (Guettler et al. 2022).

Strengths and Limitations

One of the strengths of this study is that the bucks are made from rear-world vehicle seats and have modern rear-seat environments and restraint systems. While this provides invaluable information about the state of rear-occupant safety in modern vehicles, it also makes the analysis and identification of variables affecting submarining and injury protection more difficult. For example, many studies will change one factor at a time, like anchor position or seat cushion stiffness, to determine which conditions will improve submarining protection. In this study, each vehicle has different seat frame and seat pan designs, seat cushion stiffness, restraint anchoring locations, restraint types, and crash pulses.

Due to the severity of the tests and locations of instrumentation, data loss due to instrumentation loss was of concern. For two tests, the data obtained for the sacrum was substituted for the pelvis, due to loss of pelvis data. The pelvic bones and the sacrum are not necessarily fused; so, when possible, kinematics data from the pelvis instrumentation block (left ilium) and the sacrum instrumentation were compared to determine the viability of using sacrum kinematics to describe pelvis motion. As seen in Figure B1, the kinematics measured on the sacrum and pelvis are not vastly different. The sacrum data are often noisier than the pelvis data, likely due to interaction with the seat. Despite this, it was determined that the kinematics of the sacrum could be used as a reasonable replacement for the pelvis kinematics when necessary.

A limitation related to the use of surrogates, whether they are ATDs or PMHS, is that they are not exact representations of a human occupant. While the biofidelity of ATDs is assessed against the response of PMHS, PMHS do not necessarily have the same kinematic or injury response of a human. Two key factors are the lack of blood pressure and muscle tension. Both likely affect loading mechanisms, especially to the viscera, but muscle tension could affect initial occupant position, and therefore overall kinematics, even at these high loading rates. The PMHS in this study were perfused in an attempt to minimize the effects of the lack of circulatory pressure. An effect of greater importance is that the positions of the thoracoabdominal contents are shifted inferiorly in PMHS relative to humans; in several studies, inversion of the PMHS allowed for loading of the thorax and abdomen with the viscera in more accurate position (Hardy et al. 2006; Howes et al. 2012; Howes et al. 2013). The benefits of inverting PMHS are improved interaction of the belt with the abdominal viscera and therefore more accurate description of potential damage, as well as potentially changing mass distribution and improving lap belt-pelvis interaction. Although inversion is not possible in full-body sled tests, valuable information about submarining tendency and potential damage mechanisms can still be observed.

Another limitation for biofidelity of PMHS in this study is related to the effects of the chest band installation on the abdomen characteristics. Two chest bands were applied to each PMHS, which caused distension of the abdomen, which varied in size. In some cases, the shape of the abdomen likely altered the motion of the lap belt and potentially restricted motion of the abdominal viscera during loading. By visual inspection of the high-speed videos and the post-test autopsy damage, it appears that there was inertial loading caused by the restricted abdominal contents, potentially confounding analysis of the damage sustained by the PMHS regardless of submarining in this study.

This study only focuses on the midsized adult male occupant. However, even with this small target demographic, the results of this study highlight the importance on overall occupant size and anthropometry on injury and submarining risk. Even within the range considered a midsized male, differences in mass and surrogate geometry produced different outcomes, emphasizing the importance of studying a wide array of occupants to better represent the protective abilities of the rear-seat environment for the entire population. This is particularly true in light of the fact that the rear seat might soon become the forward-most front-facing seating location.

Finally, this work only addresses submarining and abdominal injury for a rear-seated occupant and does not take into account the entire occupant protection picture. Thoracic loading and injury are critically important to determining the overall effectiveness of occupant protection in these vehicles. There are often tradeoffs in design parameters for given injury risks to different body regions, so the whole-body response must be considered when making those assessments.

CONCLUSION

Twelve NCAP85 frontal crash sled tests were conducted using midsized male PMHS and four vehicle bucks. The results were compared to matched ATD tests conducted by Guettler et al. (2022). The focus of the analyses was on the abdomen and pelvis, with particular attention paid to submarining occurrence. The primary findings include:

- Five out of twelve PMHS underwent submarining, in two out of the four vehicles. While the worst-performing vehicle produced submarining in the THOR-50M and all PMHS, two additional PMHS submarined in the vehicle in which the THOR did not submarine.

- The relative belt angle at the time of submarining averaged 31.7 +/- 5.7 degrees for PMHS submarining cases. For the matched THOR-50M tests involving submarining, the relative belt angle ranged averaged 40.7 +/- 4.3 degrees at the time of submarining.

- At the time of submarining, for the PMHS, the seat belt anchor load averaged 3.6 +/- 0.4 kN. This compares to 5.6 and 5.8 kN at the time of submarining for the two matched tests in which the THOR-50M submarined and for which there are data.

- Restraint type was not indicative of whether or not a PMHS would submarine; due to the complex differences between rear seat environments in this study, individual characteristics that increase submarining risk are difficult to isolate. Neither V15 (conventional restraints) nor V19 (advanced restraints) were associated with submarining. Both V13 (conventional restraints) and V14 (advanced restraints) were associated with submarining, although the V13 cases were severe.

- Seat pan geometry seems to be closely related to the submarining potential for PMHS in this study.

- Four PMHS heavier (87.0 +/- 4.0 kg) than the target midsized male that did not undergo submarining sustained pelvis fractures. This suggests that heavier occupants that do not undergo submarining in the rear seat are at increased risk of pelvis fracture.

- The relative belt angle at the time of fracture averaged 40.5 +/- 10.0 degrees for PMHS pelvis fracture cases.

- At the time of pelvis fracture, the PMHS seat belt anchor load averaged 8.1 +/- 0.8 kN, which is more than twice the average anchor loads observed at the time of submarining for PMHS (3.6 +/- 0.4 kN). For PMHS that did not exhibit pelvis fracture or submarining, the peak seat belt anchor load averaged 6.8 +/- 1.1 kN.

- Pelvis fracture occurred regardless of restraint type, despite the presence of load limiters in the retractors of the advanced restraints.

- Two severe cases of submarining were associated with lumbar spine fractures in the PMHS. In these tests, the butt of the PMHS contacted the floorboards with the lumbar spine in extreme extension over the seat riser, with the lap belt directly loading the spine (AP loading injury).

- While more data are needed, intravascular abdominal pressure might be a useful parameter related to damage to the abdominal viscera.

- Considerable damage to the abdominal viscera was produced regardless of submarining, and specific injury mechanisms are difficult to identify due to many confounding factors related to study design. However, substantial engagement with the shoulder belt in the absence of submarining is likely an important factor.
- Since the Hybrid III 50th-percentile male did not submarine in any of the Guettler et al. (2022) tests, it was found to be insensitive to PMHS submarining risk for the conditions of the matched NCAP85 tests in this study.
- While the THOR-50M submarined under some of the same conditions as did the PMHS, in some conditions it submarined when the PMHS did not, and in some conditions it did not submarine when the PMHS underwent submarining. That is, the THOR-50M was not able to predict submarining for all PMHS in all vehicles in this study.
- Considering only submarining response, comparison between the PMHS and ATD responses suggests the THOR-50M might be more appropriate for use in rear seat occupant protection than the Hybrid III 50th-percentile male ATD.

This study provides further insight regarding submarining and abdominal damage using real-world vehicle and crash characteristics. The occupant responses identified by this study help to fill gaps in occupant protection in the rear seats of modern vehicles, and informs future studies.

ACKNOWLEDGMENTS

This work was funded under NHTSA Contract No., DTNH2214D00328L, Task Order, DTNH2217F00177, and TRC Agreement No., AUCVCN4J of the Research Consortium for Crashworthiness in Automated Driving Systems. The statements in this presentation are those of the authors' and do not necessarily reflect the opinions of the sponsors. The decisions of the donors and their families to contribute to biomechanics research is greatly appreciated.

REFERENCES

Adomeit, D. (1977) Evaluation Methods for the Biomechanical Quality of Restraint Systems During Frontal Impact. Proc. 21st Stapp Car Crash Conference, pp. 3244-3251. Society of Automotive Engineers.

Adomeit, D., and Heger, A. (1975) Motion Sequence Criteria and Design Proposals for Restraint Devices in Order to Avoid Unfavorable Biomechanic Conditions and Submarining. Proc. 19th Stapp Car Crash Conference, pp. 3150-3159.

Bianco, S., Guettler, A. J., Hardy, W. N., Albert, D. L., and Kemper, A. R. (2022) Evaluation and comparison of thoracic injury risk for the Hybrid III and THOR 50th-percentile male anthropomorphic test devices in the rear seat during frontal impacts. *SAE International Journal of Transportation Safety*, 10(2): 403-437.

Bilston, L. E., Du, W., and Brown, J. (2010). A matched-cohort analysis of belted front and rear seat occupants in newer and older model vehicles shows that gains in front occupant safety have outpaced gains for rear seat occupants. *Accident Analysis and Prevention* 42(6): 1974-1977.

Elhagediab, A. M., and Rouhana, S. W. (1998) Patterns of abdominal injury in frontal automotive crashes. Proc. The 16th International Technical Conference on the Enhanced Safety of Vehicles, pp. 327-337, Washington, D.C.

Fedorov, A., Beichel, R., Kalpathy-Cramer, J., Finet, J., Fillion-Robin, J.-C., Pujol, S., Bauer, C., Jennings, D., Fennessy, F., Sonka, M., Buatti, J., Aylward, S., Miller, J.V., Pieper, S., and Kikinis, R. (2012) 3D Slicer as an image computing platform for the Quantitative Imaging Network. *Magnetic Resonance Imaging* 30(9): 1323-1341.

Forman, J., Lopez-Valdes, F. J., Lessley, D., Kindig, M., Kent, R., and Bostrom, O. (2009) The effect of obesity on the restraint of automobile occupants. Proc. 53rd Annals of Advances in Automotive Medicine/Annual Scientific Conference, pp. 25-40. Association for the Advancement of Automotive Medicine, Baltimore, MD.

Forman, J., Lopez-Valdes, F., Lessley, D., Kindig, M., Kent, R., Ridella, S., and Bostrom, O. (2009) Rear seat occupant safety: an investigation of a progressive force-limiting, pretensioning 3-point belt system using adult PMHS in frontal sled tests. *Stapp Car Crash Journal* 53: 49-74.

Foster, C. D., Hardy, W. N., Yang, K. H., King, A. I., and Hashimoto, S. (2006) High-speed seatbelt pretensioner loading of the abdomen. *Stapp Car Crash Journal* 50: 27-51.

Frampton, R., Lenard, J., and Compigne, S. (2012). An in-depth study of abdominal injuries sustained by car occupants in frontal crashes. *Annals of Advances in Automotive Medicine* 56: 137-149.

Guettler, A. J., Bianco, S. T., Kemper, A. R., Albert, D. L., and Hardy, W. N. (2022) Submarining protection for 50th-percentile male anthropomorphic test devices in the rear seat during frontal crash sled tests. *SAE International Journal of Transportation Safety*, 10(2): 439-462.

Hardy, W. N., Shah, C. S., Kopacz, J. M., Yang, K. H., Van Ee, C. A., Morgan, R., and Digges, K. (2006) Study of potential mechanisms of traumatic rupture of the aorta using *insitu* experiments. *Stapp Car Crash Journal 50: 247-266*.

Horsch, J. D., and Hering, W. E. (1989) A kinematic analysis of lap-belt submarining for test dummies. Proc. Stapp Car Crash Conference, pp. 1847-1854. Society of Automotive Engineers.

Howes, M. K., Gregory, T. S., Hardy, W. N., and Beillas, P. D. (2012) Kinematics of the thoracoabdominal contents under various loading scenarios. *Stapp Car Crash Journal* 56: 1-48.

Howes, M. K., Hardy, W. N., and Beillas, P. (2013) The effects of cadaver orientation on the relative position of the abdominal organs. *Annals of Advances in Automotive Medicine* 57: 209-224.

Hu, J., Fischer, K., Lange, P., and Adler, A. (2015) Effects of crash pulse, impact angle, occupant size, front seat location, and restraint system on rear seat occupant protection. SAE Technical Paper. No. 2015-01-1453.

Kent, R., Forman, J., Parent, D., and Kuppa, S. (2007) Rear seat occupant protection in frontal crashes and its feasibility. Proc. 20th International Conference on the Enhanced Safety of Vehicles, pp. 18-21.

Klinich, K. D., Flannagan, C. A. C., Nicholson, K., Schneider, L. W., and Rupp, J. D. (2010) Factors associated with abdominal injury in frontal, farside, and nearside crashes. *Stapp Car Crash Journal* 54: 73-91.

Kuppa, S., Saunders, J., and Fessahaie, O. (2005) Rear seat occupant protection in frontal crashes. Proc. 19th International Conference on the Enhanced Safety of Vehicles, Washington, DC.

Lamielle, S., Cuny, S., Foret-Bruno, J.-Y., Petit, P., Vezin, P., Verriest, J.-P., and Guillemot, H. (2006) Abdominal injury patterns in real frontal crashes: influence of crash conditions, occupant seat and restraint systems. Proc. 50th Annual Proceedings/Association for the Advancement of Automotive Medicine, pp. 109-124.

Lee, J. B., and Yang, K. H. (2002) Abdominal injury patterns in motor vehicle accidents: a survey of the NASS database from 1993 to 1997. *Traffic Injury Prevention*, 3(3): 241-246.

Leung, Y. C., Tarriere, C., Lestrelin, D., Got, C., Guillon, F., Patel, M. M., and Hureau, J. (1982) Submarining injuries of 3-point belted occupants in frontal collisions-description, mechanisms and protection. Proc. 26th Stapp Car Crash Conference, pp. 173-205. Society of Automotive Engineers.

Luet, C., Trosseille, X., Drazétic, P., Potier, P., and Vallancien, G. (2012) Kinematics and Dynamics of the Pelvis in the Process of Submarining using PMHS Sled Tests. *Stapp Car Crash Journal* 56: 411-442.

MacLaughlin, T. F., Sullivan, L. K., & O'Connor, C. S. (1989) Experimental investigation of rear seat submarining. Proc. 12th International Conference on the Experimental Safety of Vehicles, pp. 261–271. Goteborg, Sweden.

Michaelson, J., Forman, J., Kent, R., and Kuppa, S. (2008) Rear seat occupant safety: kinematics and injury of PMHS restrained by a standard 3-point belt in frontal crashes. *Stapp Car Crash Journal* 52: 295-325.

Nie, B., Gan, S., Chen, W., and Zhou, Q. (2020) Seating preferences in highly automated vehicles and occupant safety awareness: A national survey of Chinese perceptions. *Traffic Injury Prevention*, 21(4), 247-253.

Nilson, G., and Håland, Y. (1995) An analytical method to assess the risk of the lap-belt slipping off the pelvis in frontal impacts. Proc. 39th Stapp Car Crash Conference, pp. 2928-2939. Society of Automotive Engineers.

Padgaonkar, A. J., Lawson, S. M., and King, A. I. (1978) Anatomical coordinate systems for human body segments. Proc. 22nd Human

Factors and Ergonomic Society annual meeting, pp. 676-679.

Ramachandra, R., Kang, Y.-S., Bolte, J. H., Hagedorn, A., Herriott, R., Stammen, J. A., and Moorhouse, K. (2016) Biomechanical responses of PMHS subjected to abdominal seatbelt loading. *Stapp Car Crash Journal* 60: 59-87.

Rouhana, S. W., Horsch, J. D., and Kroell, C. K. (1989) Assessment of Lap-Shoulder Belt Restraint Performance in Laboratory Testing. Proc. 33rd Stapp Car Crash Conference, pp. 243-256.

Smith, K. M., and Cummings, P. (2006) Passenger seating position and the risk of passenger death in traffic crashes: a matched cohort study. *Injury Prevention* 12: 83-86.

Society of Automotive Engineers. (2014) SAE J211-1: Instrumentation for Impact Test - Part 1 - Electronic Instrumentation. SAE International.

Tatem, W. M., and Gabler, H. C. (2019) Differential fatality risk between rear and front seat passenger vehicle occupants in frontal crashes. Proc. IRCOBI Annual Conference, pp. 554-560.

Trowbridge, M. J., and Kent, R. (2009) Rear-Seat Motor Vehicle Travel in the U.S.: Using National Data to Define a Population at Risk. *American Journal of Preventive Medicine* 37(4): 321–323.

Uriot, J., Potier, P., Baudrit, P., Trosseille, X., Petit, P., Richard, O., Compigne, S., Masuda, M., and Douard, R. (2015) Reference PMHS sled tests to assess submarining. *Stapp Car Crash Journal* 59: 203-223.

Uriot, J., Potier, P., Baudrit, P., Trosseille, X., Richard, O., and Douard, R. (2015) Comparison of HII, HIII and THOR dummy responses with respect to PMHS sled tests. Proc. IRCOBI Annual Meeting, pp. 435-451.

APPENDIX A

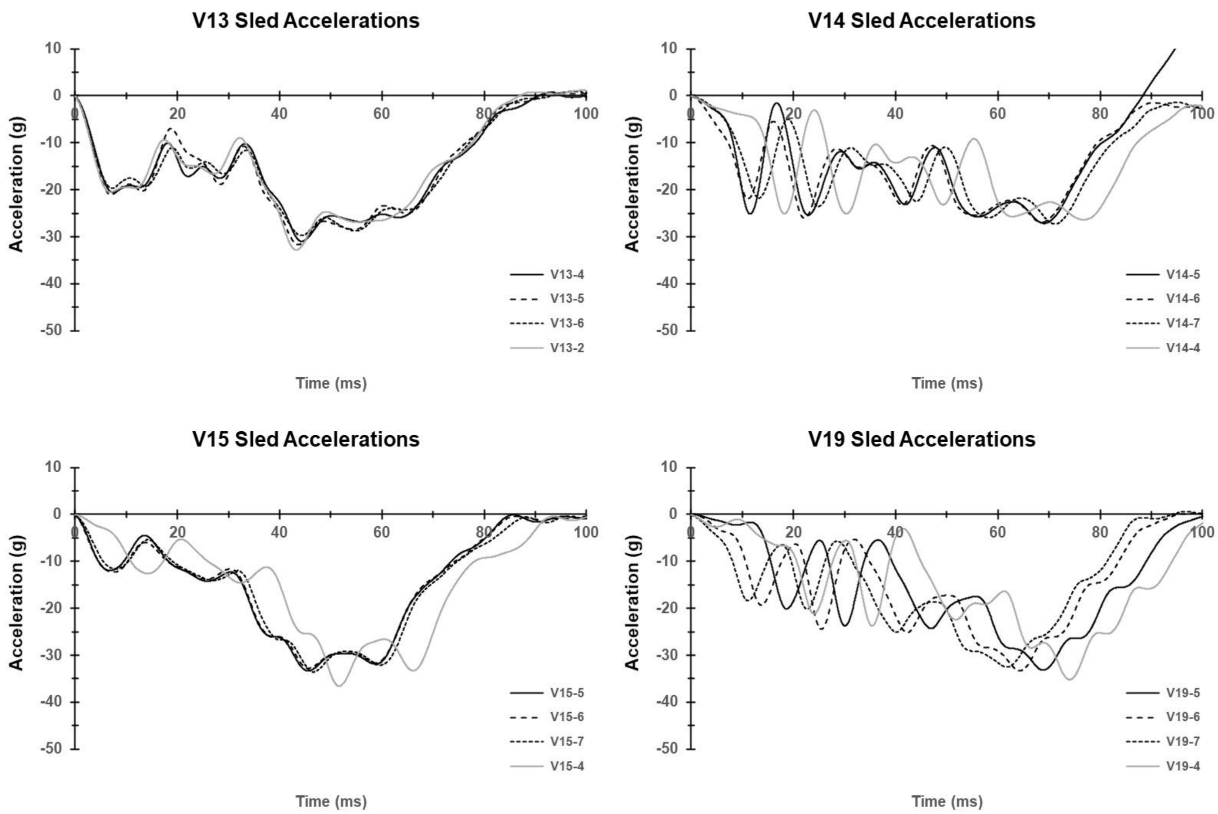

FIGURE A1. Sled accelerations (g) for the PMHS tests and the matched ATD tests

APPENDIX B

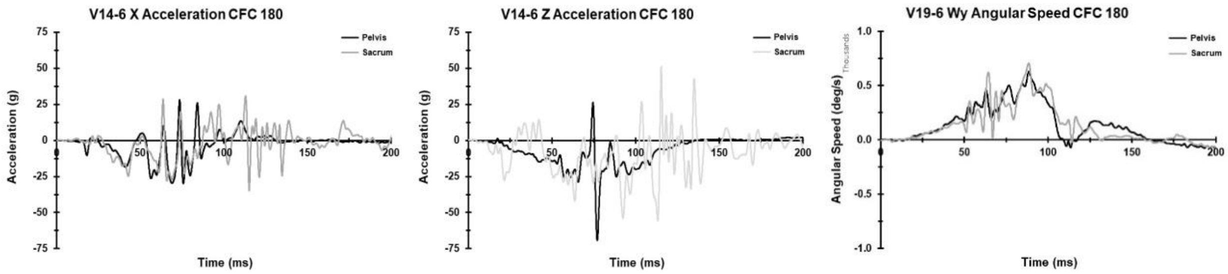

FIGURE B1. Pelvis kinematics as measured with the ilium motion block and the sacrum motion block

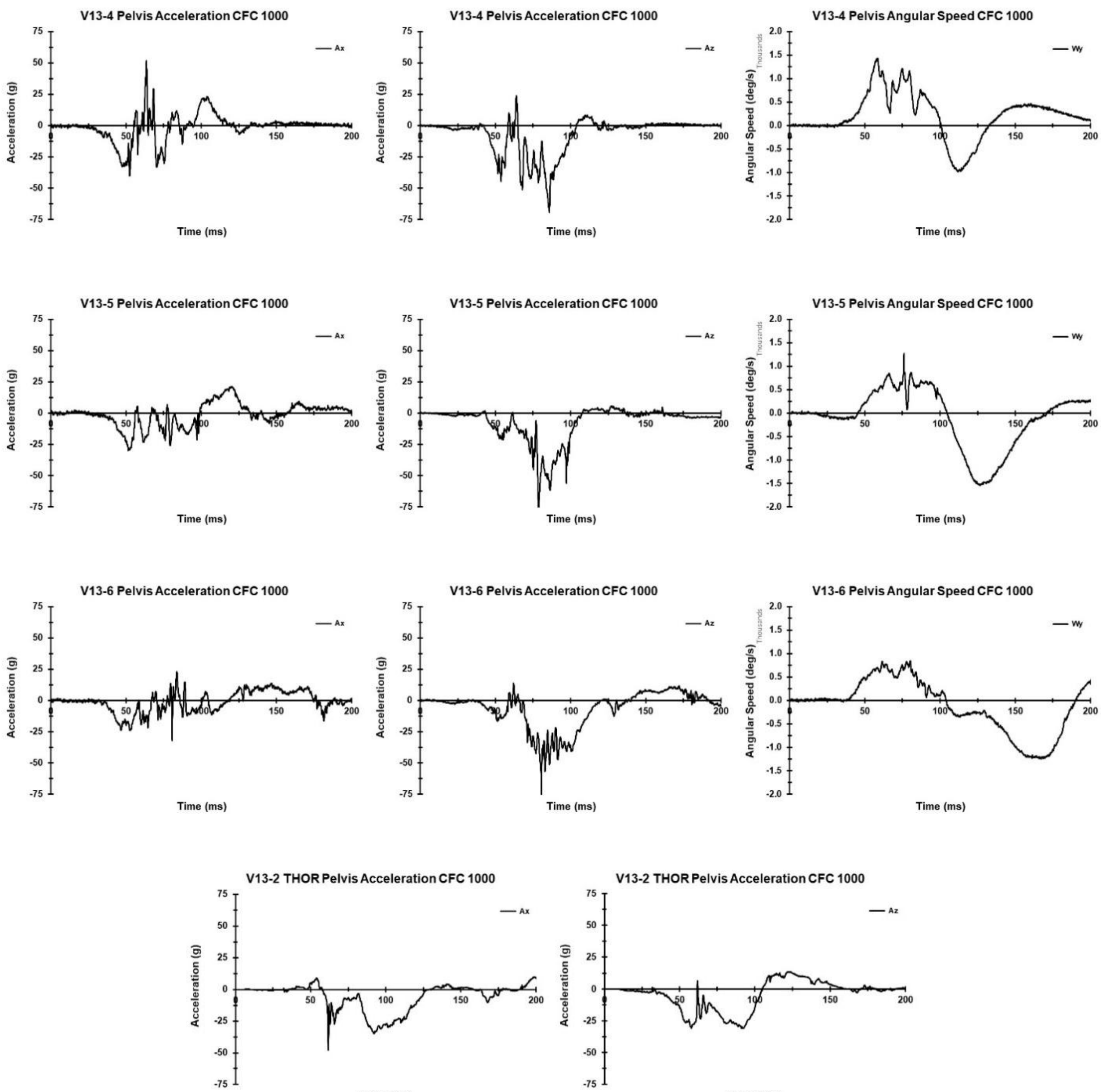

FIGURE B2. PMHS X and Z-direction pelvis acceleration and Y-axis pelvis angular speed for vehicle V13 tests

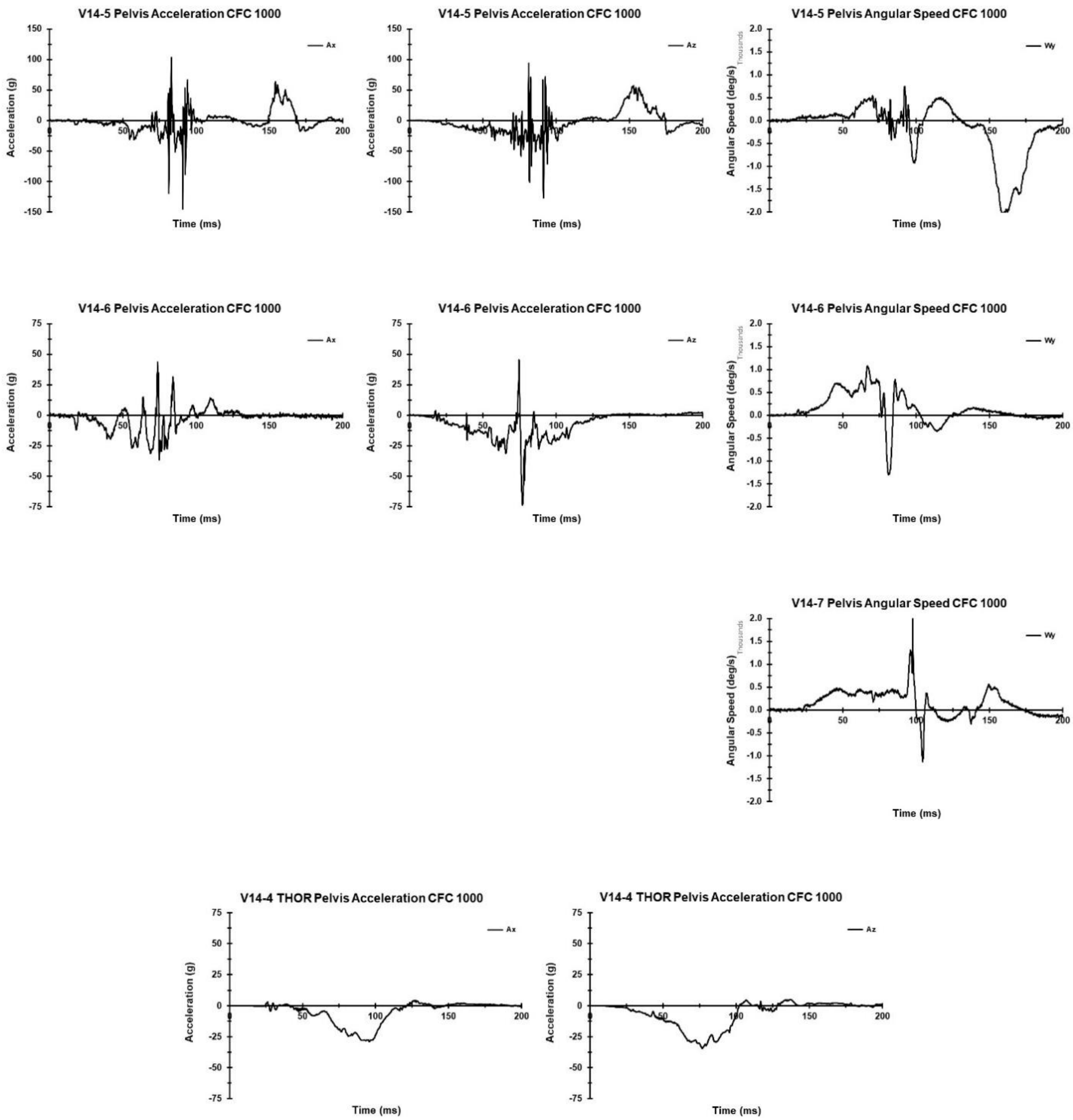

FIGURE B3. PMHS X and Z-direction pelvis acceleration and Y-axis pelvis angular speed for vehicle V14 tests. Pelvis and sacrum accelerations are unusable due to instrumentation loss in V14-7.

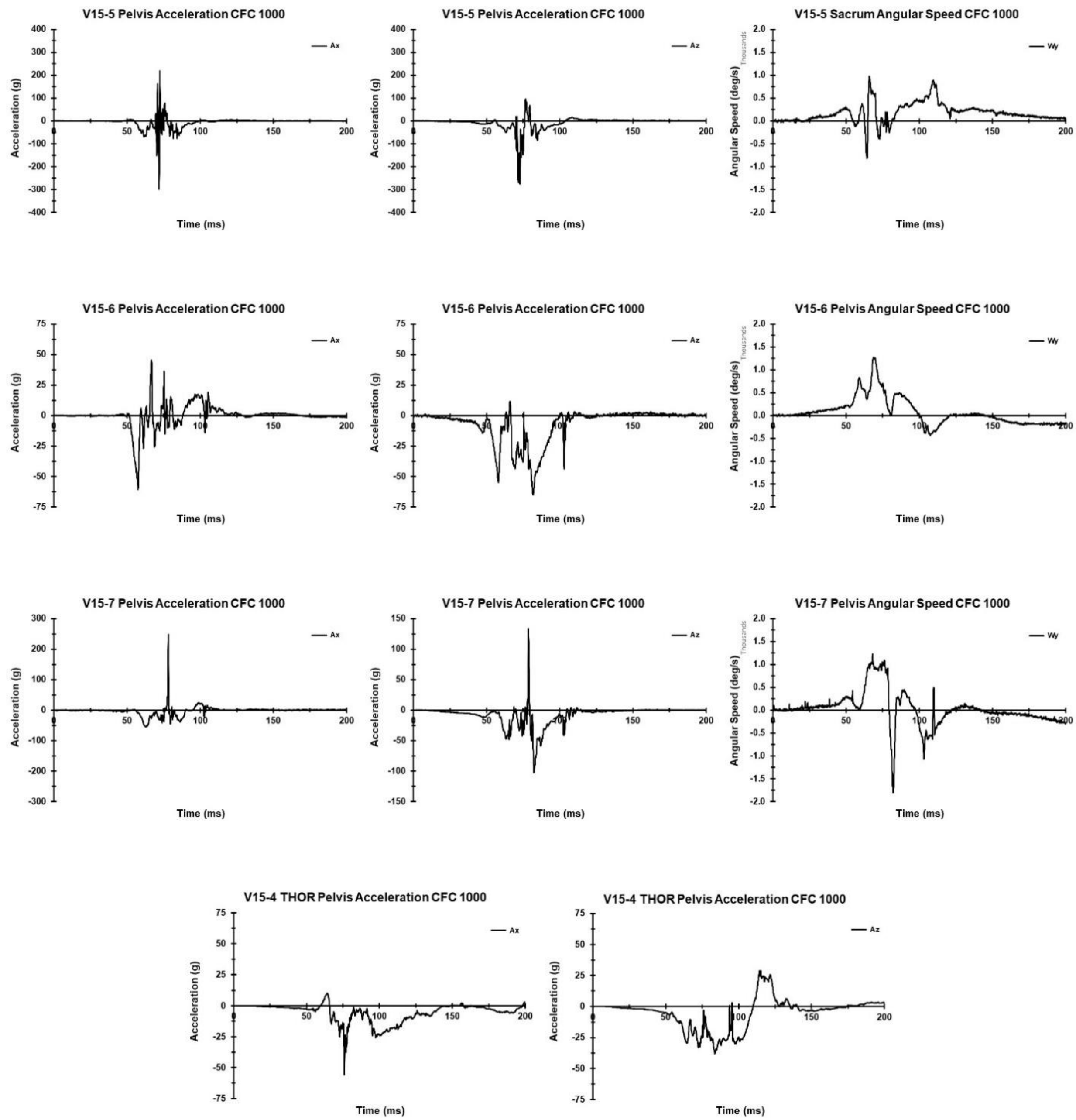

FIGURE B4. PMHS X and Z-direction pelvis acceleration and Y-axis pelvis angular speed for vehicle V15 tests

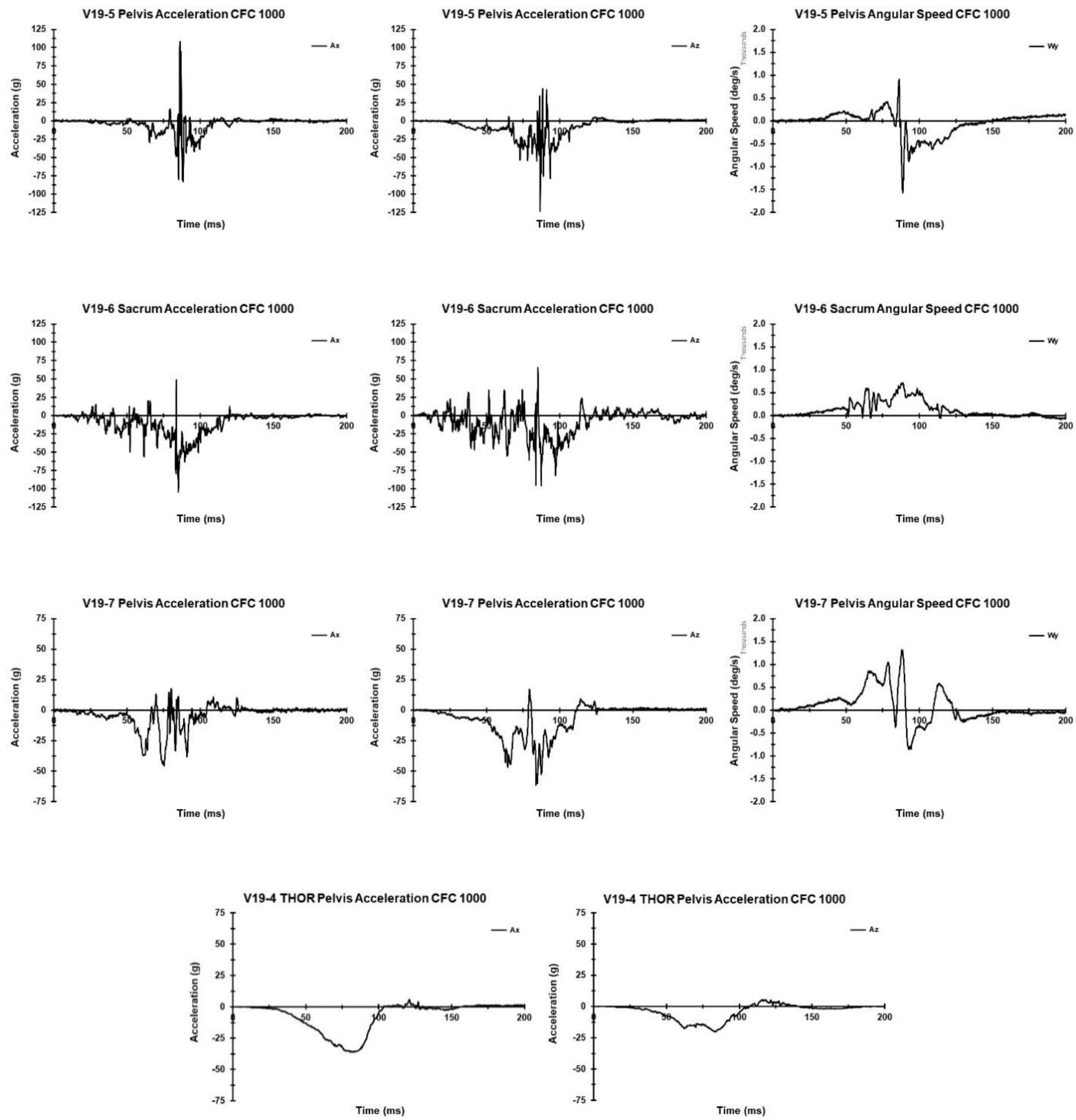

FIGURE B5. PMHS X and Z-direction pelvis acceleration and Y-axis pelvis angular speed for vehicle V19 tests

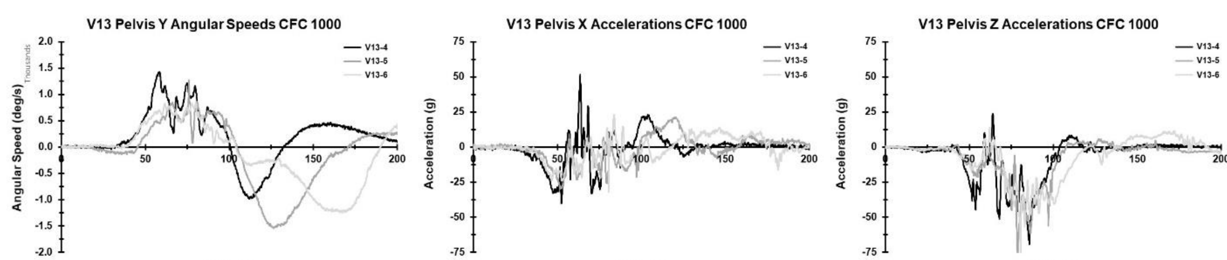

FIGURE B6. Pelvis kinematics for all three PMHS tests in vehicle V13

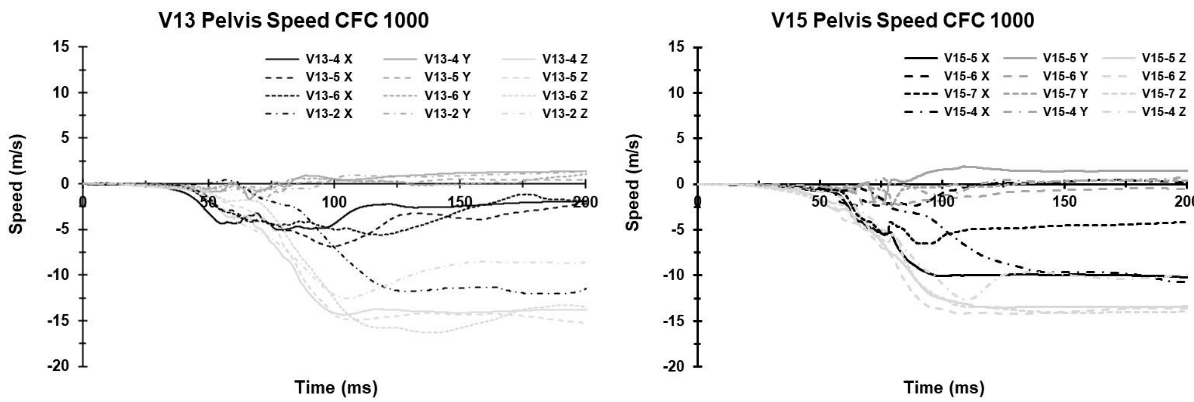

FIGURE B7. Pelvis speeds for all tests in vehicles V13 (left) and V15 (right).

APPENDIX C

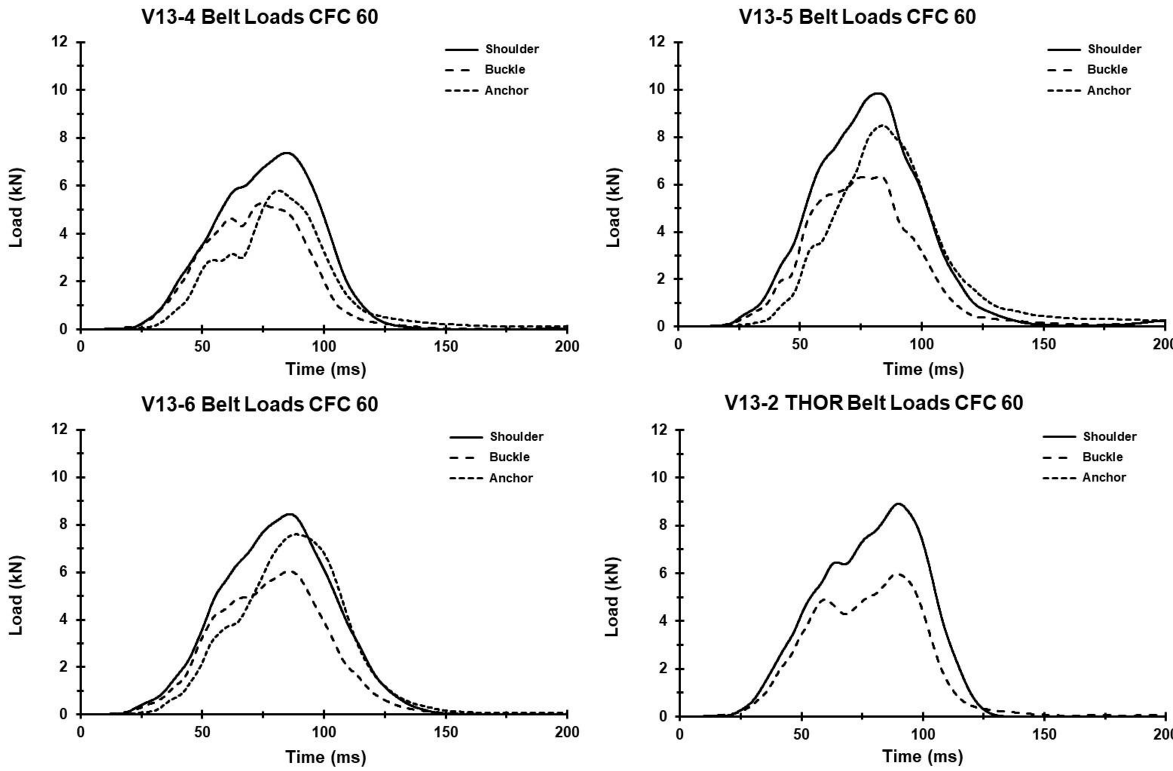

FIGURE C1. Belt loads for vehicle V13 (kN).

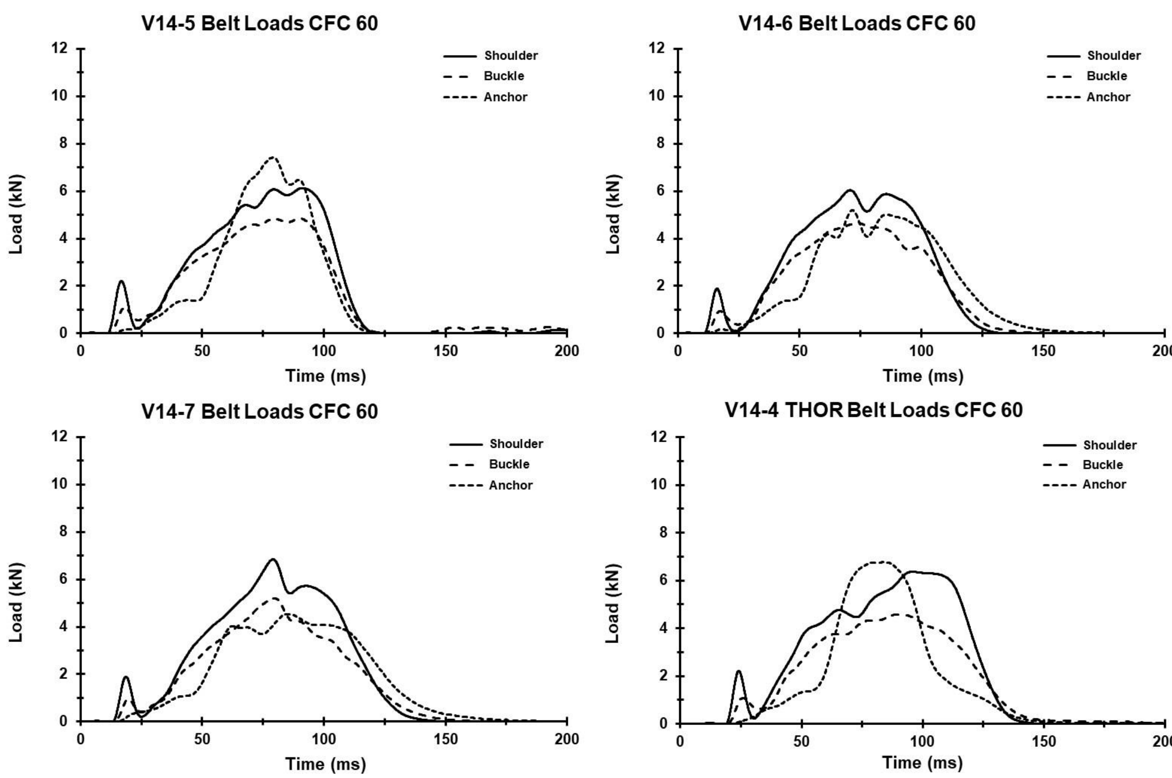

FIGURE C2. Belt loads for vehicle V14 (kN).

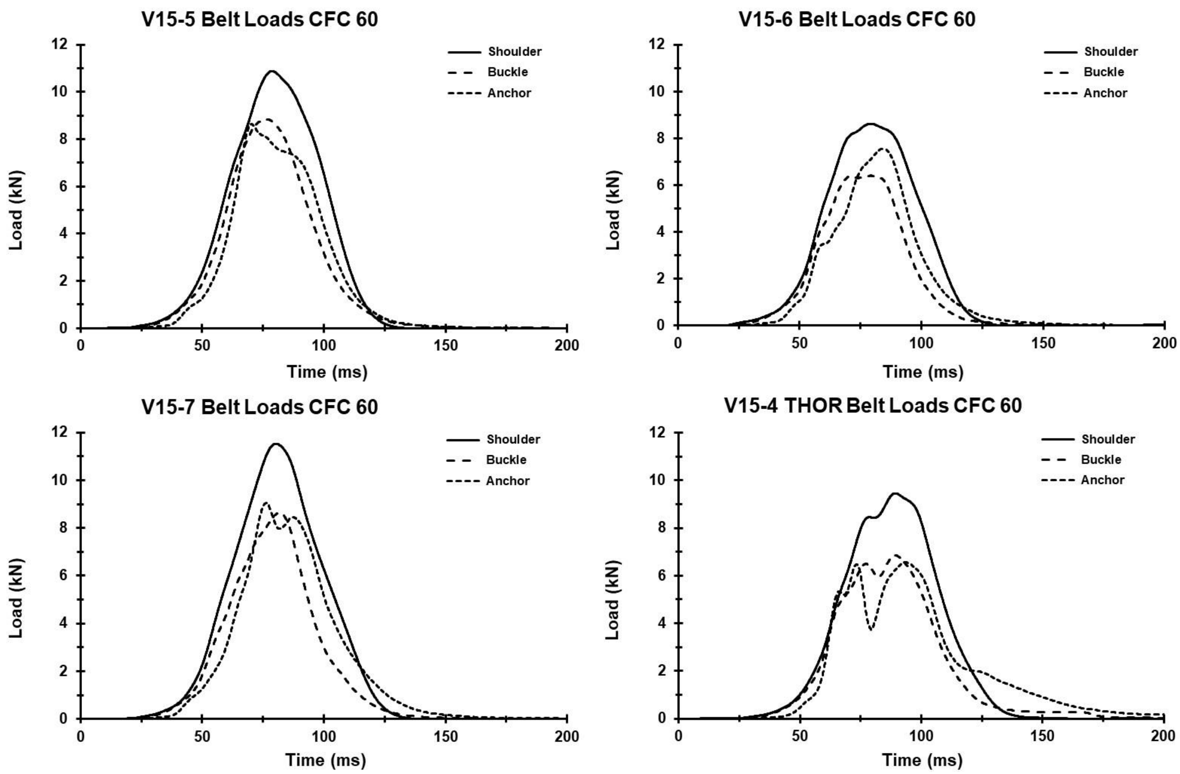

FIGURE C3. Belt loads for vehicle V15 (kN).

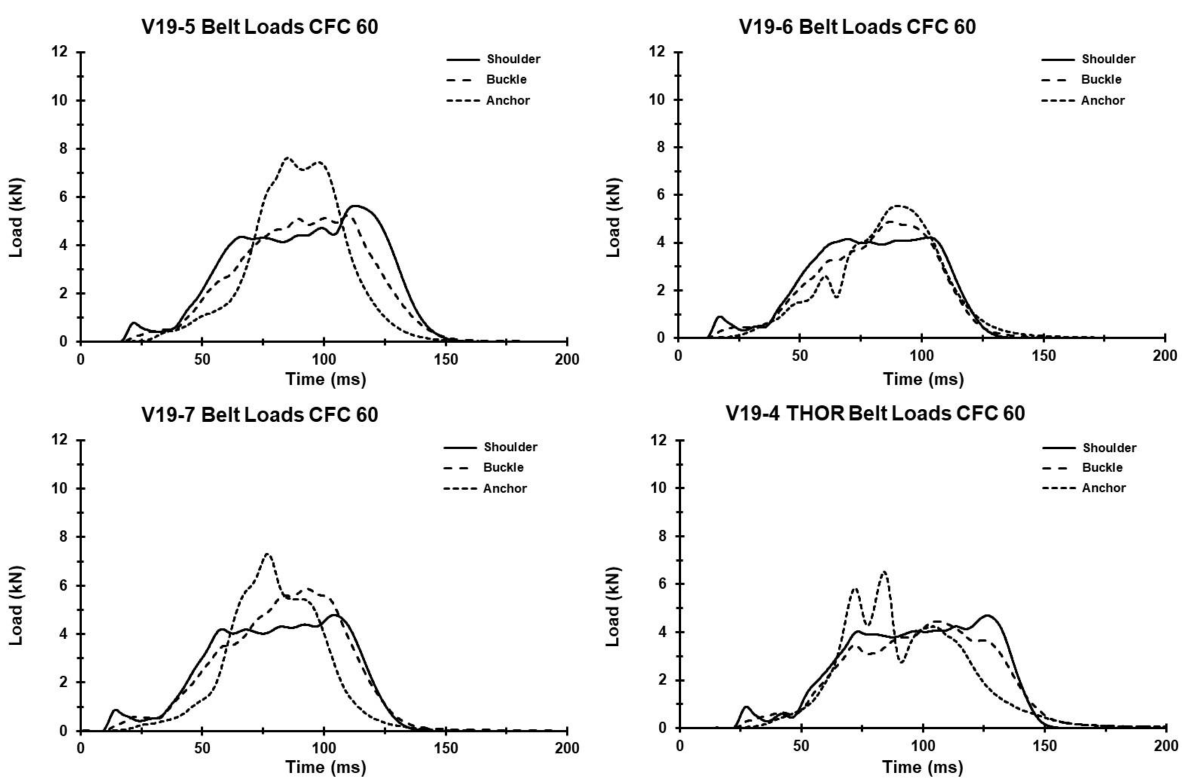

FIGURE C4. Belt loads for vehicle V19 (kN).

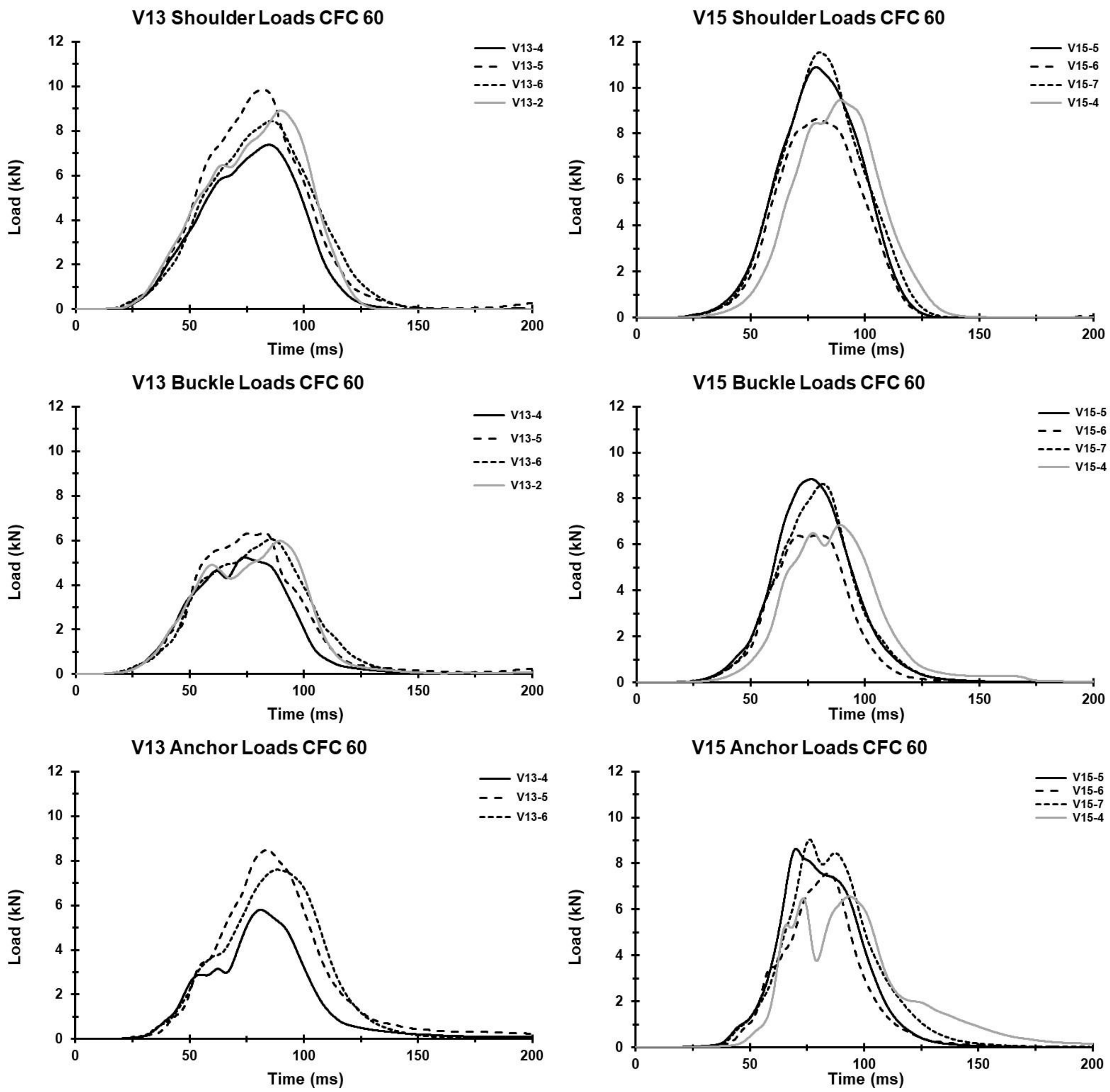

FIGURE C5. Belt loads (kN) by load cell location and vehicle for the vehicles with conventional restraints

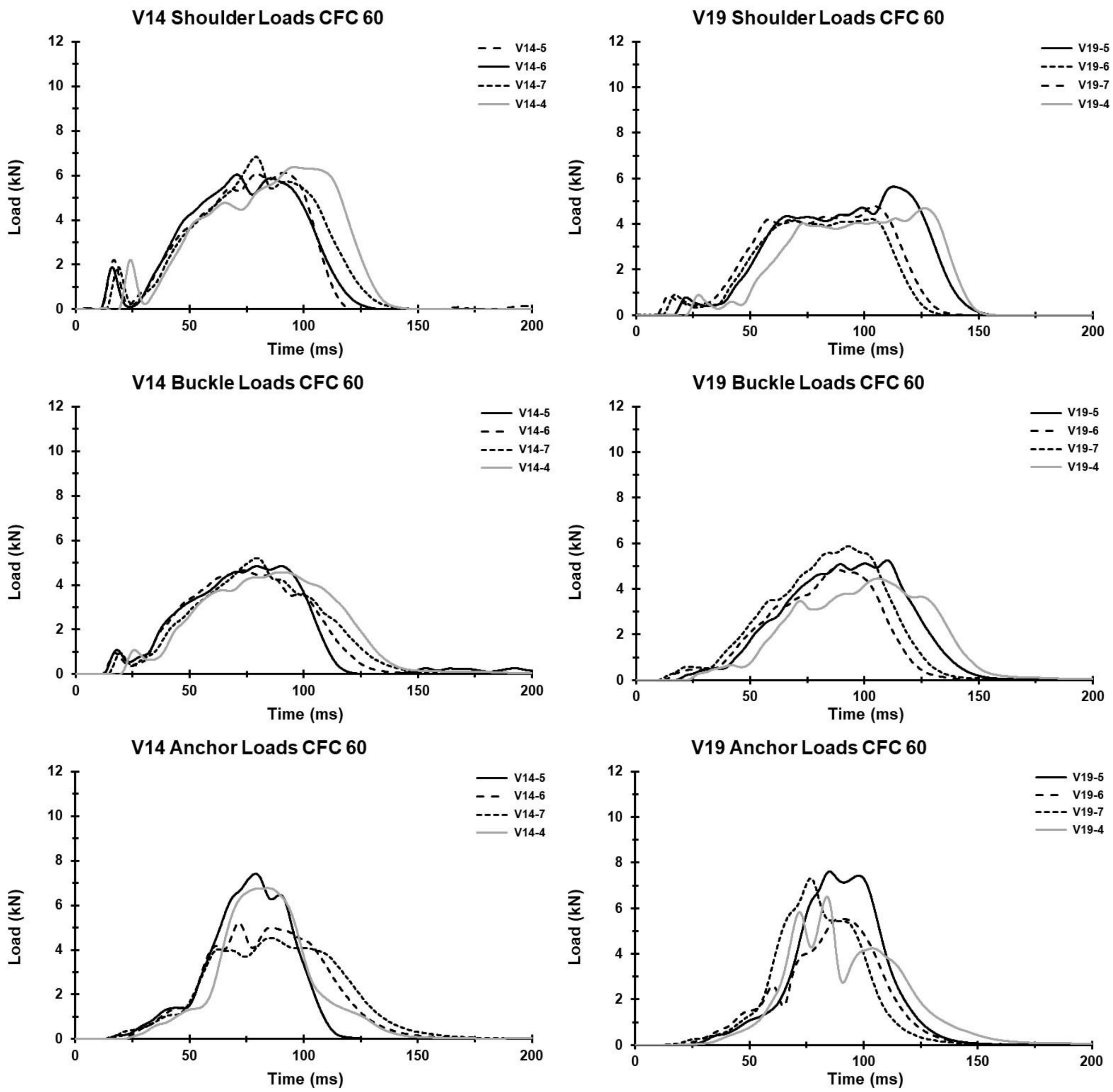

FIGURE C6. Belt loads (kN) by load cell location and vehicle for the vehicles with advanced restraints

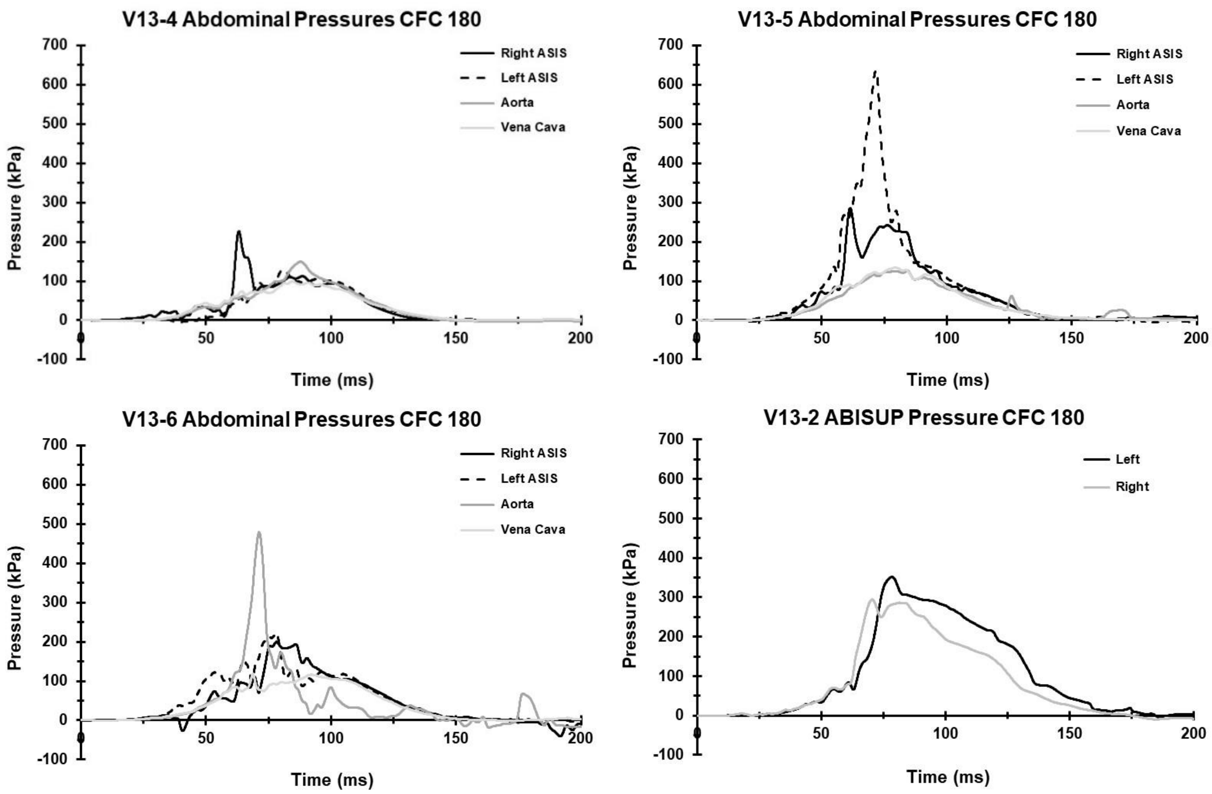

FIGURE C7. Abdominal pressures from vehicle V13 (kPa).

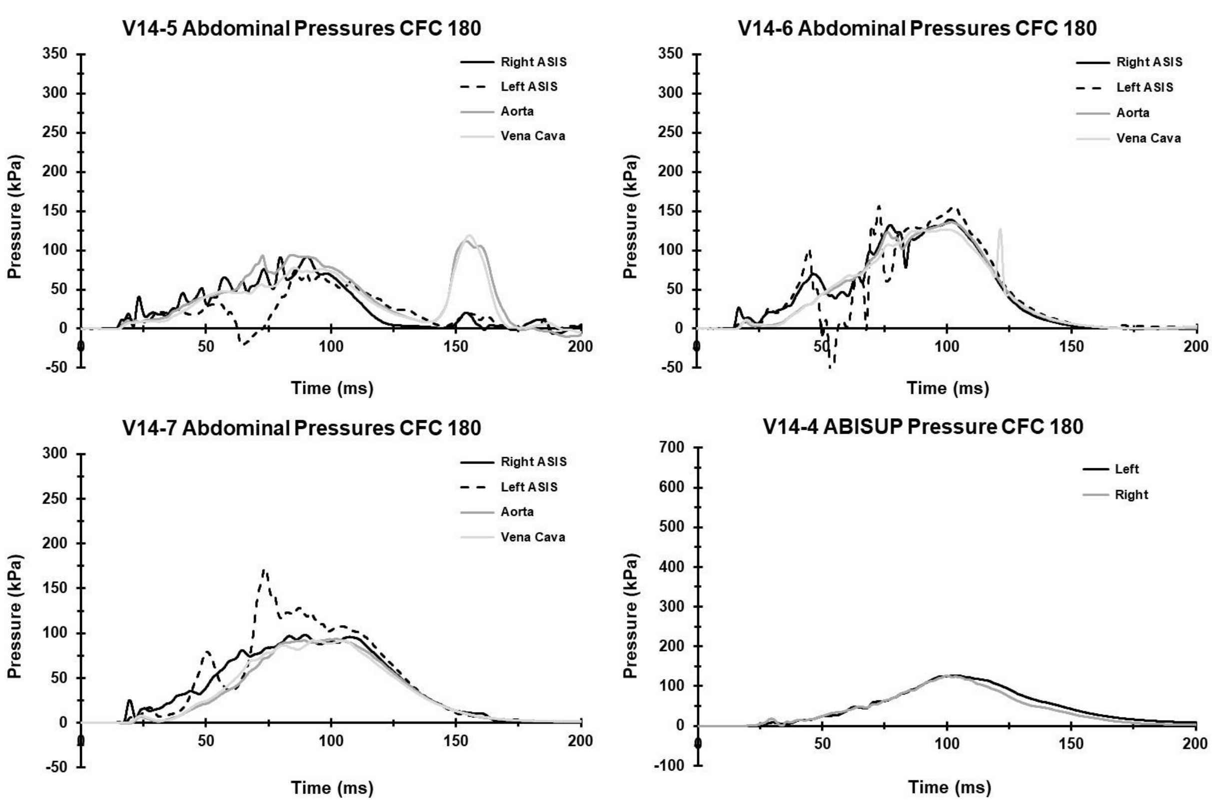

FIGURE C8. Abdominal pressures from vehicle V14 (kPa).

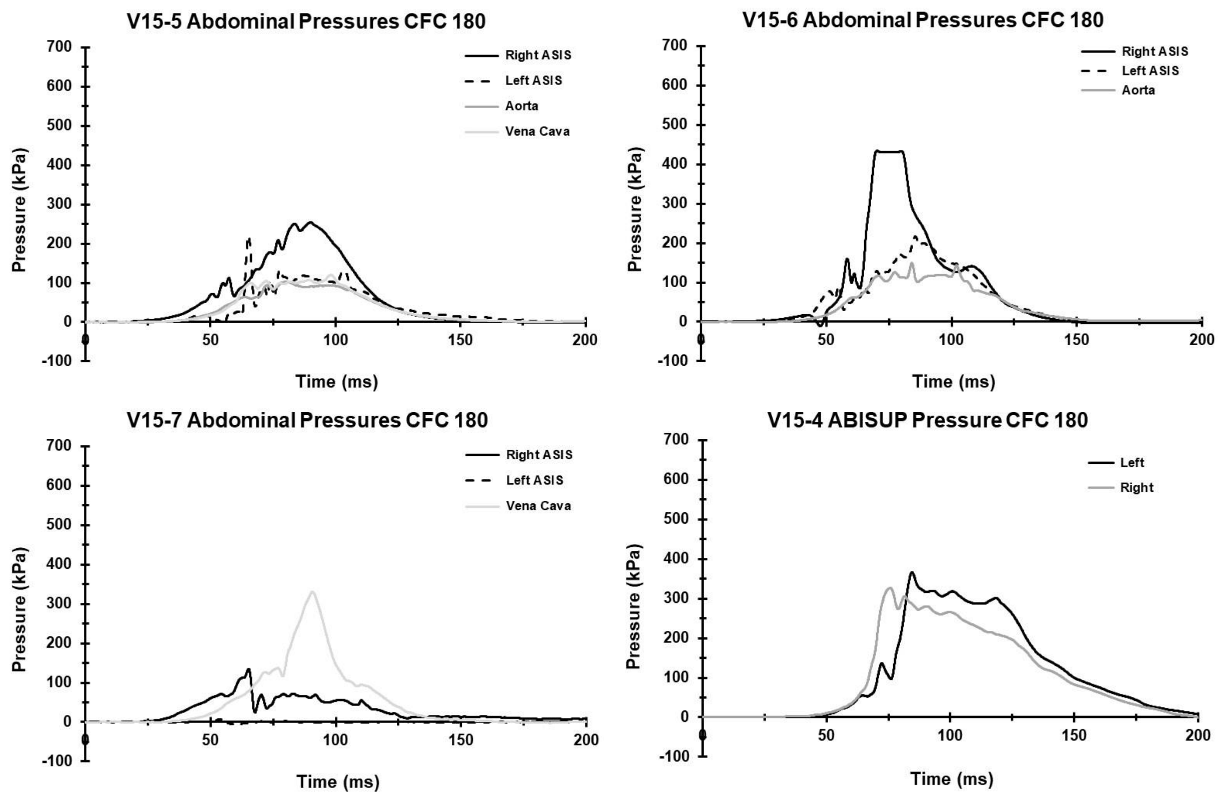

FIGURE C9. Abdominal pressures from vehicle V15 (kPa).

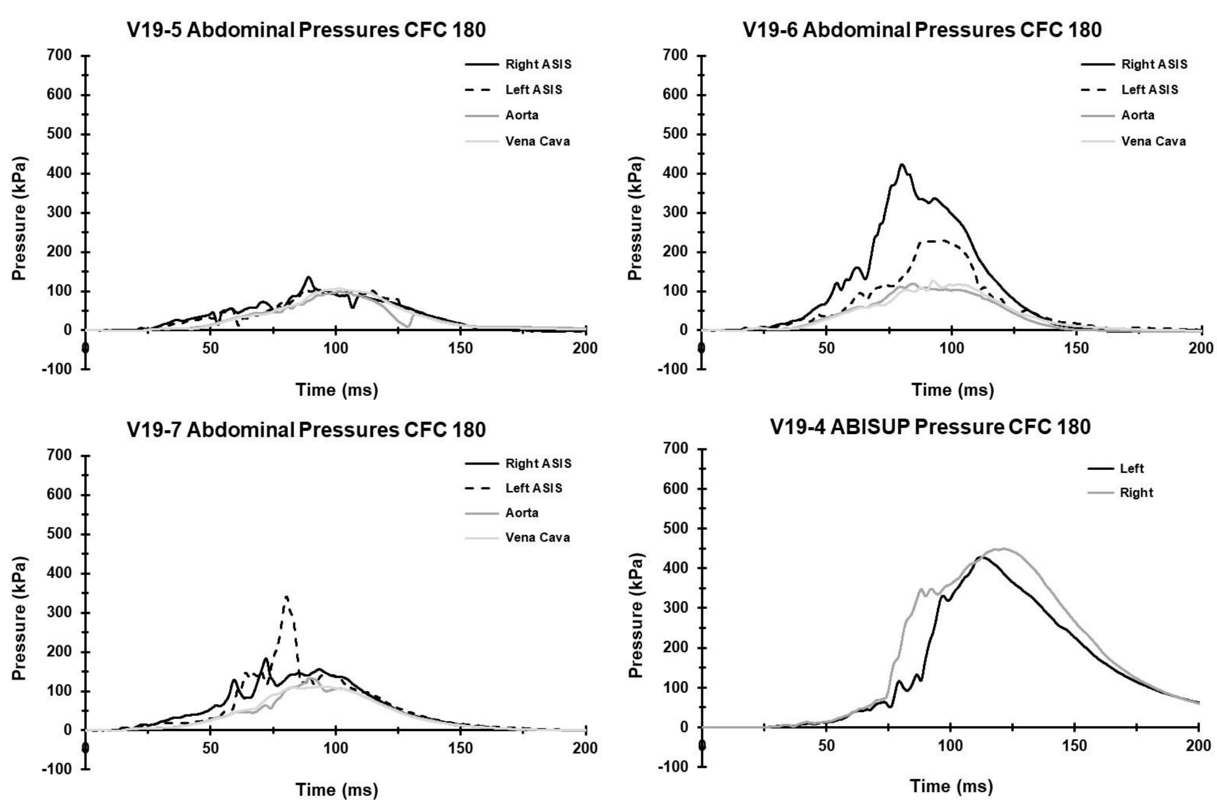

FIGURE C10. Abdominal pressures from vehicle V19 (kPa).

APPENDIX D

FIGURE D1. Images for test V13-2 at the start of the test (left), at time of submarining (middle), and time of peak excursion (right).

FIGURE D2. Images for test V13-4 at the start of the test (left), at time of submarining (middle), and time of peak excursion (right).

FIGURE D3. Images for test V13-5 at the start of the test (left), at time of submarining (middle), and time of peak excursion (right).

FIGURE D4. Images for test V13-6 at the start of the test (left), at time of submarining (middle), and time of peak excursion (right).

FIGURE D5. Images for test V14-4 at the start of the test (left), midpoint of forward excursion (middle), and time of peak excursion (right).

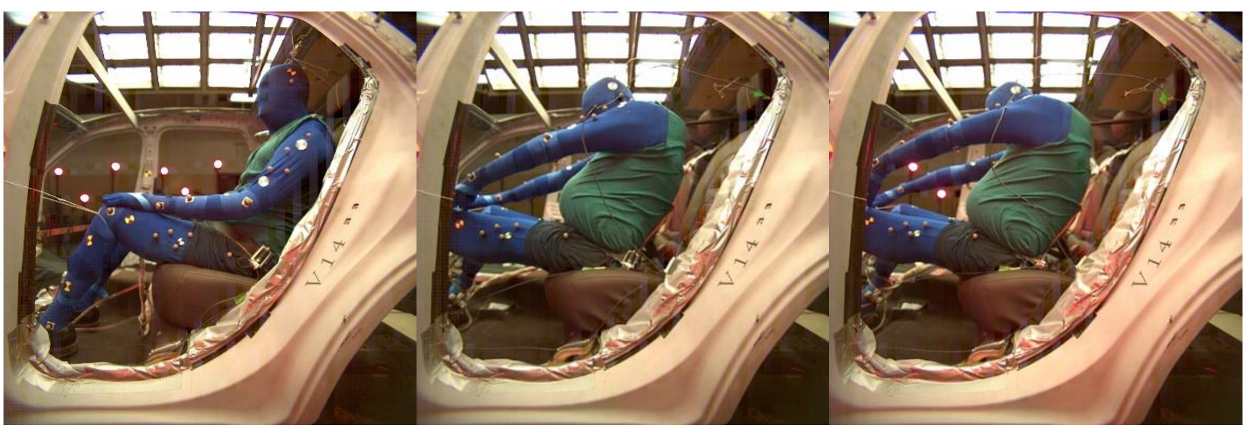

FIGURE D6. Images for test V14-5 at the start of the test (left), at time of pelvis fracture (middle), and time of peak excursion (right).

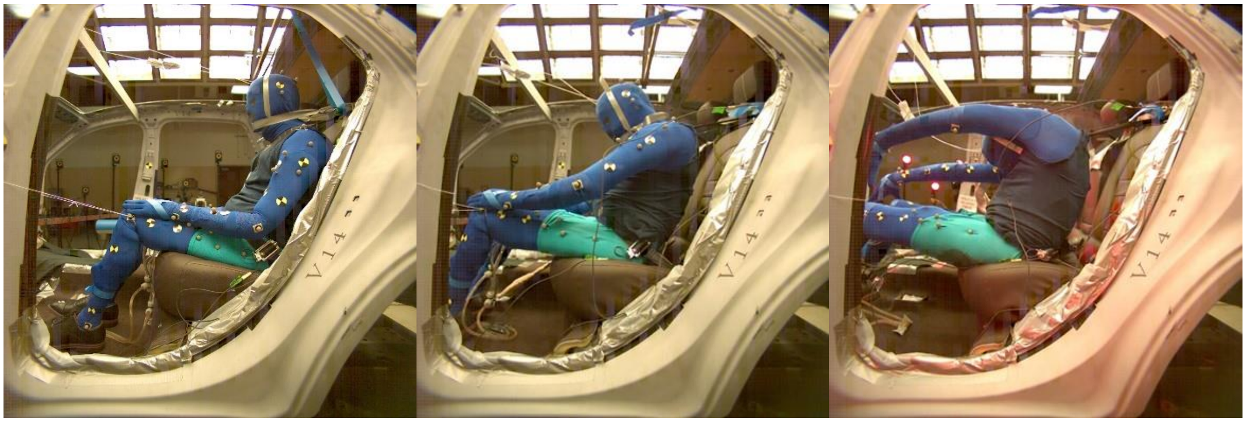

FIGURE D7. Images for test V14-6 at the start of the test (left), at time of submarining (middle), and time of peak excursion (right).

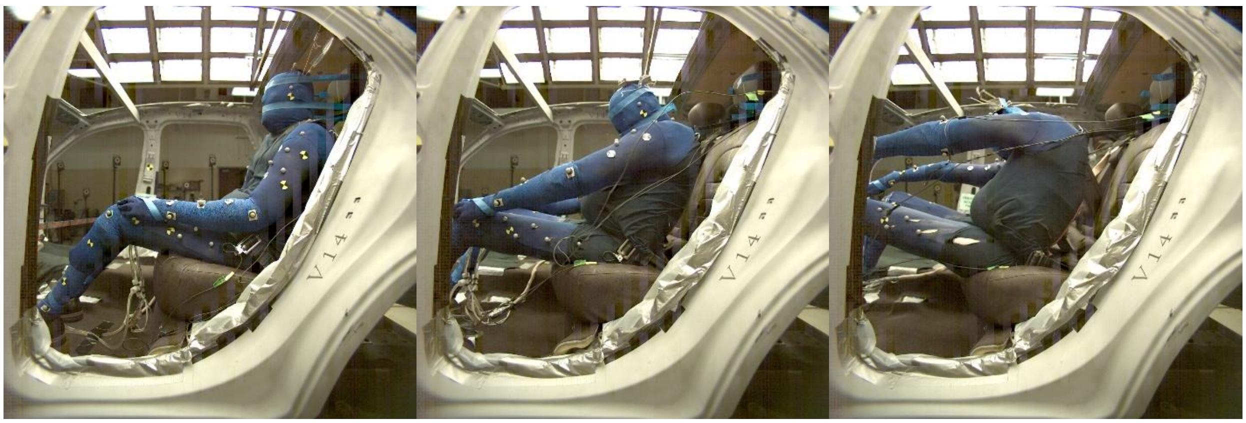

FIGURE D8. Images for test V14-7 at the start of the test (left), at time of submarining (middle), and time of peak excursion (right).

FIGURE D9. Images for test V15-4 at the start of the test (left), at time of submarining (middle), and time of peak excursion (right).

FIGURE D10. Images for test V15-5 at the start of the test (left), at time of pelvis fracture (middle), and time of peak excursion (right).

FIGURE D11. Images for test V15-6 at the start of the test (left), at the midpoint of forward excursion (middle), and time of peak excursion (right).

FIGURE D12. Images for test V15-7 at the start of the test (left), at time of pelvis fracture (middle), and time of peak excursion (right).

FIGURE D13. Images for test V19-4 at the start of the test (left), at time of submarining (middle), and time of peak excursion (right).

FIGURE D14. Images for test V19-5 at the start of the test (left), at time of pelvis fracture (middle), and time of peak excursion (right).

FIGURE D15. Images for test V19-6 at the start of the test (left), at the midpoint of forward excursion (middle), and time of peak excursion (right).

FIGURE D16. Images for test V19-7 at the start of the test (left), at the midpoint of forward excursion (middle), and time of peak excursion (right).

APPENDIX E

PMHS	Sex	Stature (cm)	Mass (kg)	Test	Submarining
SM129	M	178	63	V13-4	Yes
Region	Damage				
1. Peritoneum	• 12 cm wide, 10 cm long tear in the peritoneum to the right of the bifurcation of the abdominal aorta				
2. Mesentery and small intestine	• A. Tear in mesentery (8 cm long) and stretching of the small intestine (3 cm long) 234 cm from the ileocecal junction. (ileum) • B. Tear in mesentery (7 cm long) and transection of the small intestine 264 cm from the ileocecal junction. (ileum)				
3. Mesentery	• Button hole tear (3 cm long) 0.5 cm perpendicular to the intestine, 455 cm from the ileocecal junction (jejunum)				
4. Ileocecal Junction	• Partial tear (serous membrane), 9 cm long				
5. Sigmoid Colon	• Longitudinal tear through wall (3 cm long) about 25 cm from the anus. In the vicinity of the ala of the left pelvic bone				
6. Lumbar vertebrae	• A. Fracture of the tip of the right transverse process of L2 • B. Fracture of the tip of the left transverse process of L4 • C. Fracture of the right transverse process of L4				

PMHS	Sex	Stature (cm)	Mass (kg)	Test	Submarining
SM155	M	168	85	V13-5	Yes
Region	Damage				
1. Liver	• A. Field of multiple surface compromise on the dorsolateral aspect of the diaphragmatic side, 6-to-10cm long, up to 2.5-cm deep • B. Triangular field of disruption/abrasion on the ventrolateral aspect of the diaphragmatic side, with 2 accompanying fractures (1.5 cm x 0.5-cm deep, and 3.0 cm x 1.5-cm deep) • C. Triangular field of disruption/abrasion on the lateral aspect of the visceral side, with an accompanying fracture (3.0 cm x 2.0-cm deep)				
2. Spleen	• A. Capsular tear on the dorsomedial aspect of the diaphragmatic side (3 x 1.5 cm) • B. Capsular tear on the ventromedial aspect of the visceral side (3 x 2cm)				
3. Small Intestine	• Complete transections, forming a segment from 142 cm to 266 cm from the ileocecal junction				
4. Mesentery and large intestine	• Mesentery tear to the root and colon “sleeve” (6 cm long) 99 cm from ileocecal junction				
5. Lumbar vertebrae	• A. L2: cranial and caudal ventral avulsion • B. Fracture of the right transverse processes of L1-L4 • B. Fracture of the left transverse processes of L1-L2				

PMHS	Sex	Stature (cm)	Mass (kg)	Test	Submarining
SM161	M	175	81	V13-6	Yes
Region	Damage				
1. Diaphragm	• Tear/puncture right anterolateral, near fracture of rib 7				
2. Liver	• A. Fracture on diaphragmatic surface near right margin, 0.5 cm deep/6.8 cm long • B. An oblique tear on the posterior aspect of the diaphragmatic surface, 1.3 cm deep and 5 cm long • C. A 2.5 cm long superficial tear on the posterior aspect of the diaphragmatic surface				
3. Kidney and ureters	• A. Tear in left kidney anterior and inferior to the hilum about 1.5 cm long and 0.9 cm deep • B. Complete transection of ureters at level L2/L3 vertebrae				
4. Pancreas	• Complete dissociation, predominantly on the right aspect				
5. Mesentery and large intestine	• A. 2 tears, radial from the root one 37 cm from the ileocecal junction and 12.5 cm long and another 6.5 cm long, 61 cm from the ileocecal junction • B. Cecum: stretching at ileocecal junction • C. Complete transection at transition from descending to sigmoid colon				
6. Peritoneum	• General disruption, anterior and lateral				
7. Vasculature	• Complete transection of the abdominal aorta and inferior vena cava at L2/L3 vertebrae				
8. Lumbar vertebrae	• A. L5/S1 separation, about 6 inches • B. Fracture of the right transverse processes of L1, L2, L5 • B. Fracture of the left transverse processes of L1, L4, L5				

PMHS	Sex	Stature (cm)	Mass (kg)	Test	Submarining
SM156	M	188	89	V14-5	No
Region	Damage				
1. Liver	• Fracture on diaphragmatic surface (4.3 cm long, 1.5 cm deep) within 13 cm from the lateral edge of the visceral surface and 7.5 cm from the posterior edge of the visceral surface				
2. Mesentery	• Small mesenteric tear, 1.7-cm long				
3. Peritoneum	• Tear (6 cm long) at about the level of L5 vertebra				
4. Pelvis	• A. Fracture of the ala of the right ilium • B. Fracture of the ala of the left ilium				

PMHS	Sex	Stature (cm)	Mass (kg)	Test	Submarining
SM157	M	173	68	V14-6	Yes
Region	Damage				
1. Liver	• Superficial disruption 9.5 cm long on diaphragmatic surface, from 2 cm to 8.5 cm from the lateral margin and 5 cm to 2.5 cm from the dorsal margin				
2. Mesentery and small intestine	• A. Mesenteric tear starting 486 cm and ending 540 from the duodenum, having transverse/circumferential length of 17 cm • B. Contused/stretched ileum 271 cm from the ileocecal junction, with mesenteric tear having radial length of 8.5 cm				

PMHS	Sex	Stature (cm)	Mass (kg)	Test	Submarining
SM160	M	178	79	V14-7	Yes
Region	Damage				
1. Colon and mesentery	• A. Medial sigmoid mesenteric tear 10 cm long, starting 3.4 cm from rectum and lateral sigmoid mesenteric tear 21.5 cm long, starting at the rectum • B. Descending colon mesenteric tear with minor disruption at both ends, 13.3 cm long, starting 36 cm from the rectum				
2. Fascia	• General minor tears of fascia at midline of the level of L3 vertebra				
3. Lumbar vertebrae	• Fracture of the left transverse process of L2				

PMHS	Sex	Stature (cm)	Mass (kg)	Test	Submarining
SM152	M	180	81	V15-5	No
Region	Damage				
1. Diaphragm	• A. Lacerations to pleural surface on the right side (multiple) • B. Minor lacerations to pleural surface on the left side (multiple)				
2. Liver	• A. Large laceration/fracture/puncture in diaphragmatic surface of right lobe. 9.5 cm long, 2.3 cm deep; 7.4 cm from anterior visceral margin • B. Fracture on dorsal diaphragmatic surface, 2.1-cm long, 0.8-cm deep; 16.6 cm from anterior visceral margin				
3. Small Intestine	• Ileum contusion 126 cm from ileocecal junction, 10-cm long				
4. Pelvis	• A. Fracture of the ala of the right ilium • B. Fracture of the ala of the left ilium • C. Separation of the sacroiliac joint on the left side				

PMHS	Sex	Stature (cm)	Mass (kg)	Test	Submarining
SM153	M	168	64	V15-6	No
Region	Damage				
1. Liver	• A. Multiple deep fractures of parenchyma on the ventrolateral diaphragmatic surface, some through to visceral surface at ventrolateral margin • B. Multiple superficial disruptions of the dorsolateral aspect of the diaphragmatic surface, 0.2-to-1.2-cm deep				
2. Mesentery	• A. Tear in mesentery, 106 cm from ileocecal junction, 14-cm long, 4-cm wide at small intestine • B. Tear in mesentery, 332 cm from ileocecal junction, 12-cm long (to the root) and 4.6 cm wide at small intestine • C. Tear in mesentery to root, 9.5 cm from rectum, 23 cm along the sigmoid colon				
3. Large Intestine	• Transection of the descending colon, 38 cm from the rectum				

PMHS	Sex	Stature (cm)	Mass (kg)	Test	Submarining
SM165	M	175	89	V15-7	No
Region	Damage				
1. Liver	• Superficial tear, 1.5 cm long, anterolateral aspect of diaphragmatic surface				
2. Small Intestine and mesentery	• A. Stretch of ileum 6.7-cm long, 99 cm from ileocecal junction • B. Transection 16.3 cm from stretch with associated mesenteric tear • C. General disruption of mesentery superior to bladder				
3. Pelvis	• Fracture of the ala of the left ilium				

PMHS	Sex	Stature (cm)	Mass (kg)	Test	Submarining
SM154	M	178	89	V19-5	No
Region	Damage				
1. Pelvis	• A. Fracture of the ala of the right ilium • B. Fracture of the ala of the left ilium				

PMHS	Sex	Stature (cm)	Mass (kg)	Test	Submarining
SM95	M	170	64	V19-6	No
Region	Damage				
1. Mesentery	• Tear (53-cm long) parallel to the longitudinal direction of the small intestine starting 239 cm and ending 292 cm from the ileocecal junction				

PMHS	Sex	Stature (cm)	Mass (kg)	Test	Submarining
SM159	M	163	73	V19-7	No
Region	Damage				
1. Mesentery and peritoneum	• Disruption/tears in mesentery and peritoneum at the distal sigmoid colon				

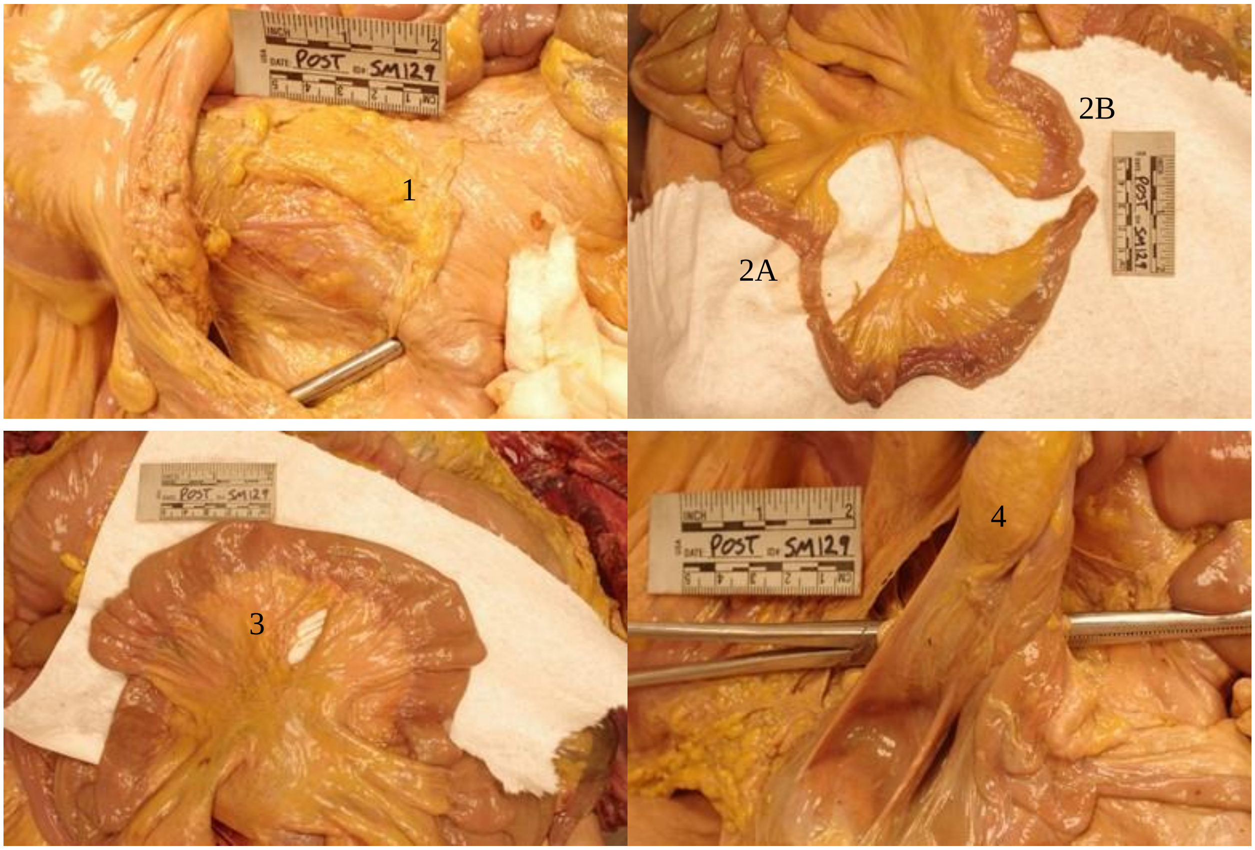

FIGURE E1. Select autopsy images for SM129 (test V13-4) including: peritoneal tear (1), mesenteric tears and associated stretching (2A) and transection (2B) of the small intestine, button hole tear of mesentery (3), and partial tear of the bowel at the ileocecal junction (4).

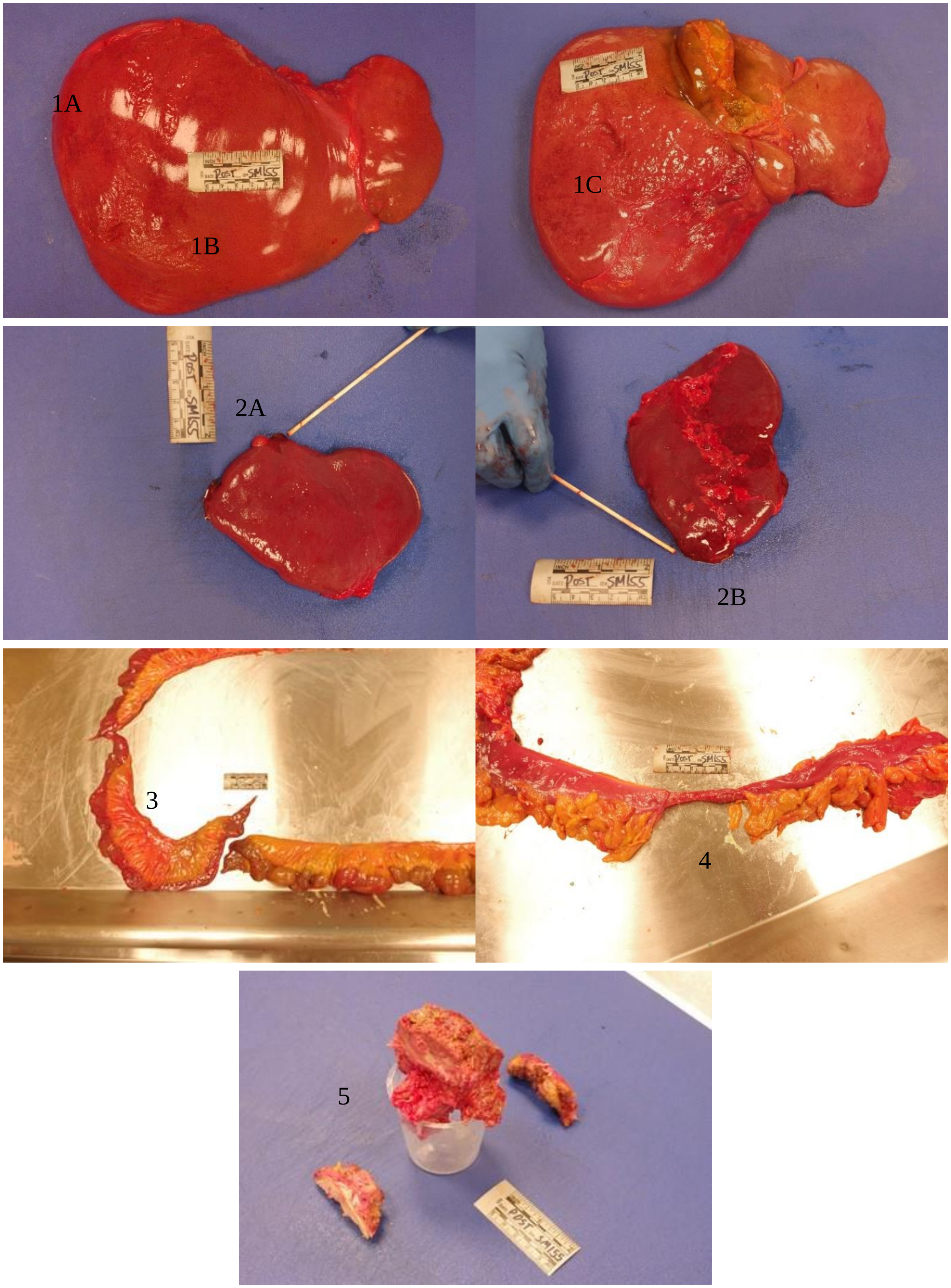

FIGURE E2. Select autopsy images for SM155 (test V13-5) including: damage to the liver (1A-C), capsular tears on the spleen (2A&B), two complete transections of the small intestine (3), stretching of the colon (4), and cranial and caudal ventral avulsions of the L2 vertebra (5).

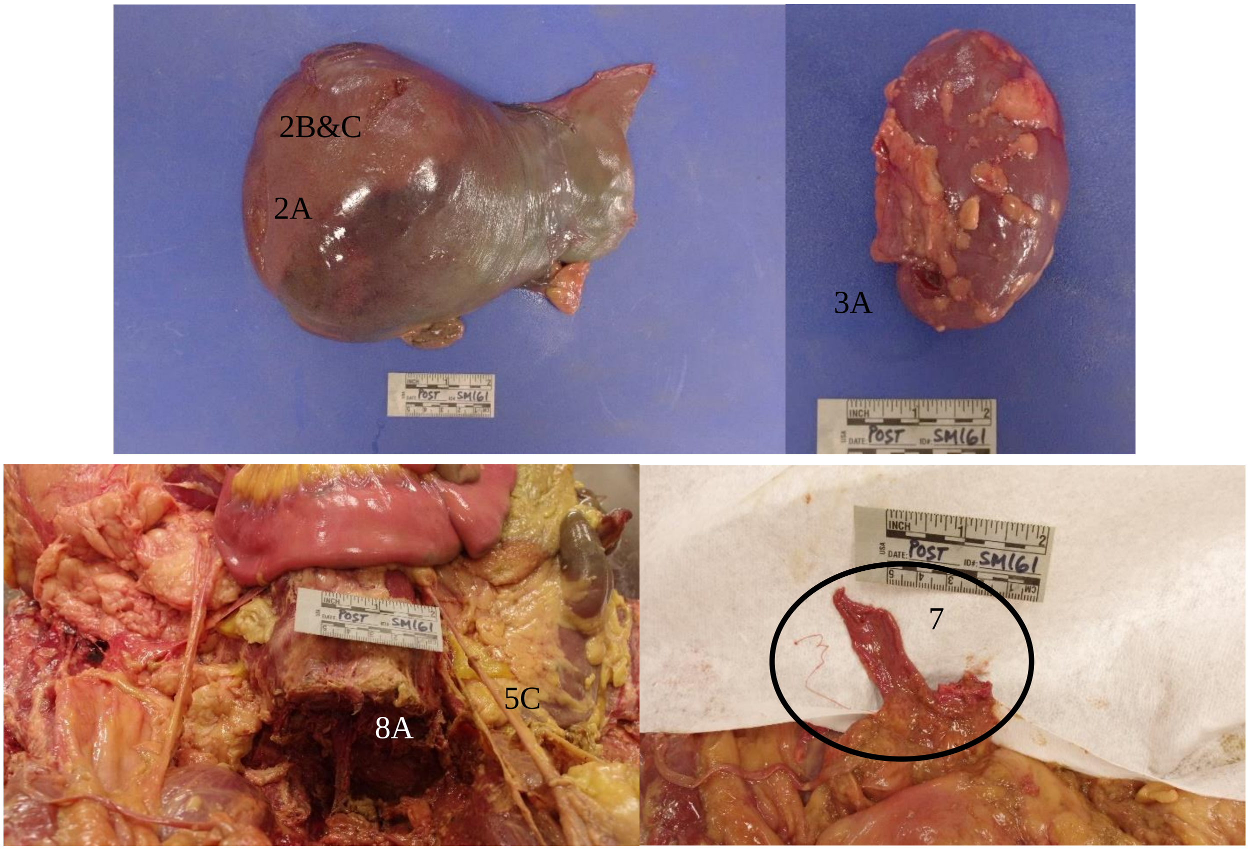

FIGURE E3. Select autopsy results for SM161 (test V13-6) including: fracture of the liver (2A), tears of the liver (2B&C), tear in the left kidney (3A), complete transection of the descending colon (5C), complete transection of the inferior vena cava and abdominal aorta (7), and separation of the spine at L5/S1 (8A).

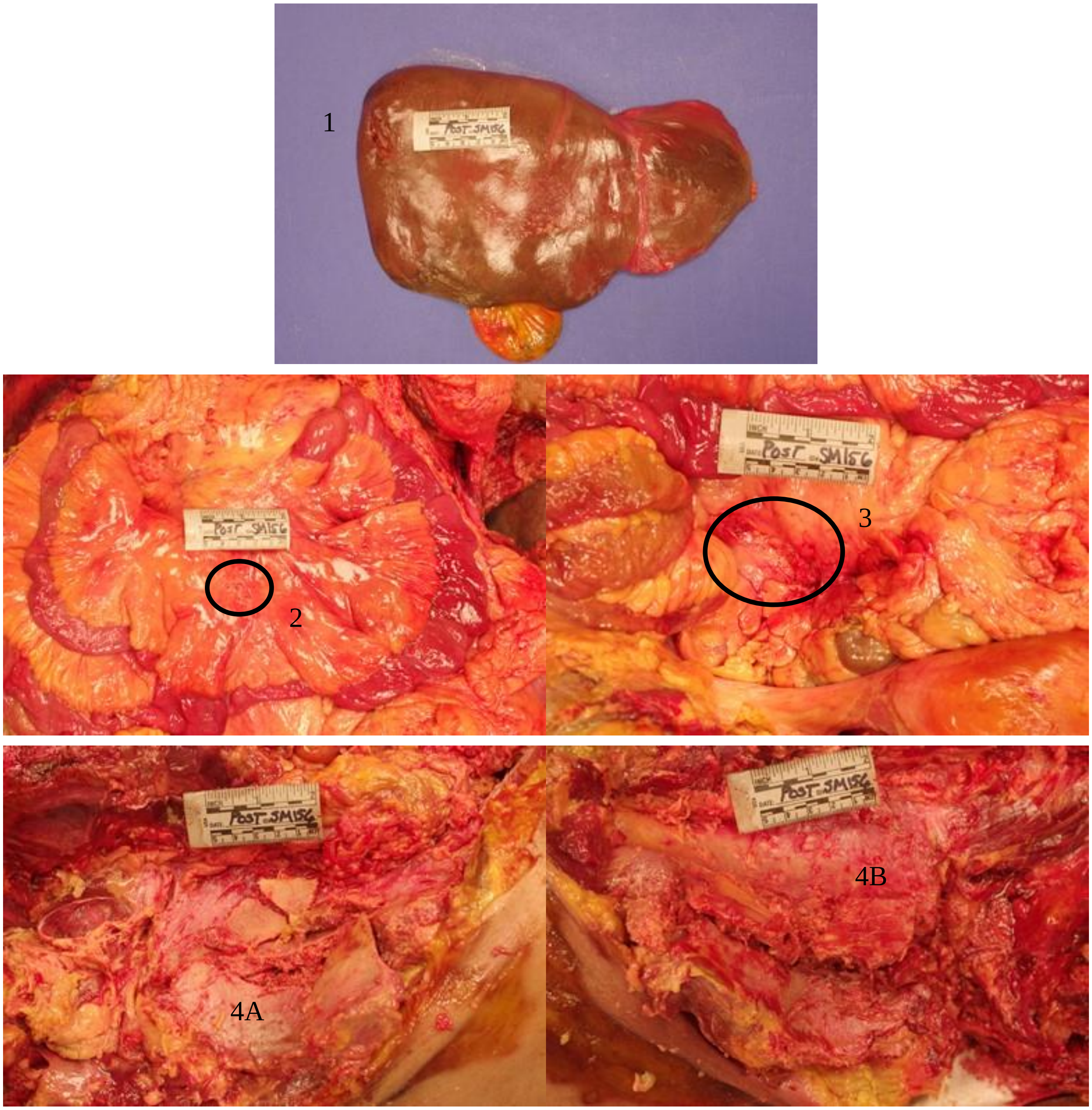

FIGURE E 4. Select autopsy images from SM156 (test V14-5) including: fracture of liver (1), small mesenteric tear (2), peritoneal tear (3), fractures of the right (4A) and left (4B) ilium.

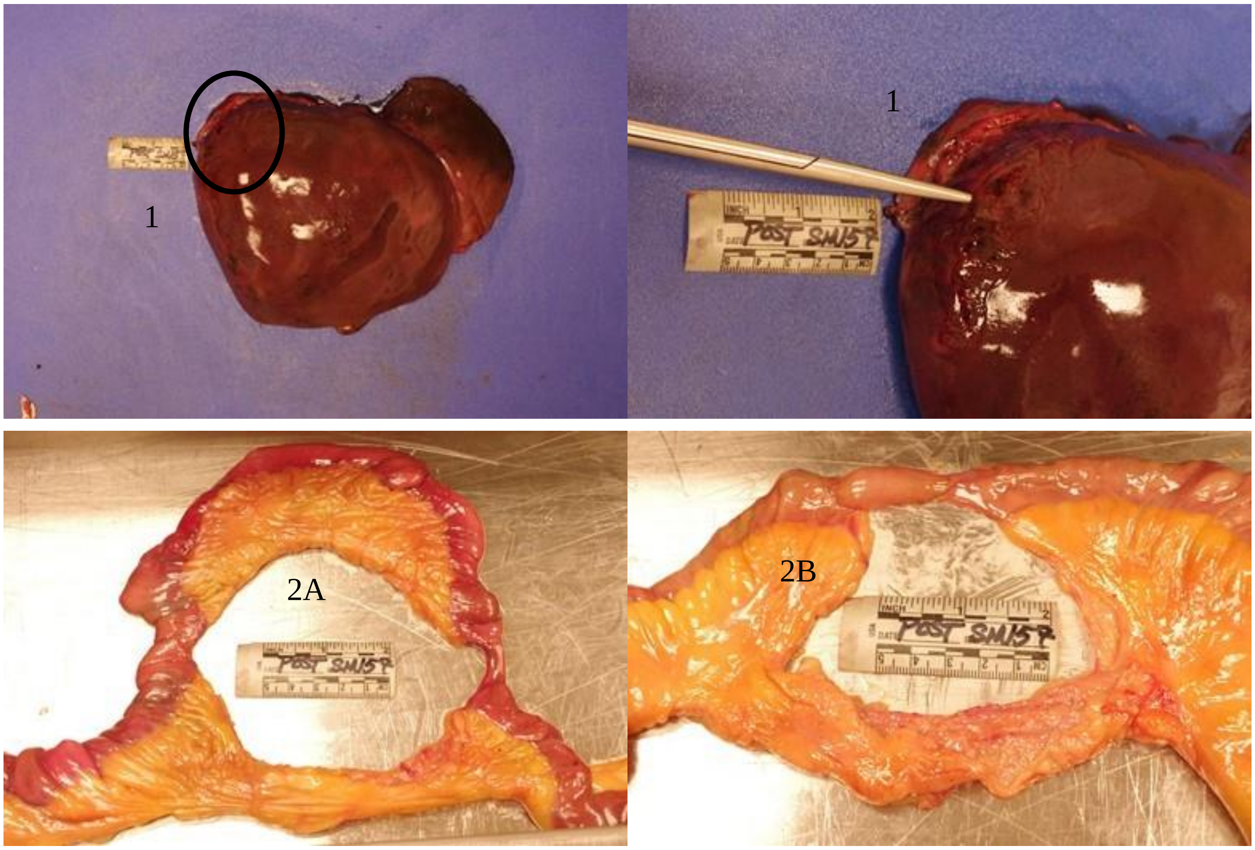

FIGURE E5. Autopsy images from SM157 (test V14-6) including: superficial disruption of the surface of the liver (1), mesenteric tear (2A), and contused/stretched ileum with associated mesenteric tear (2B).

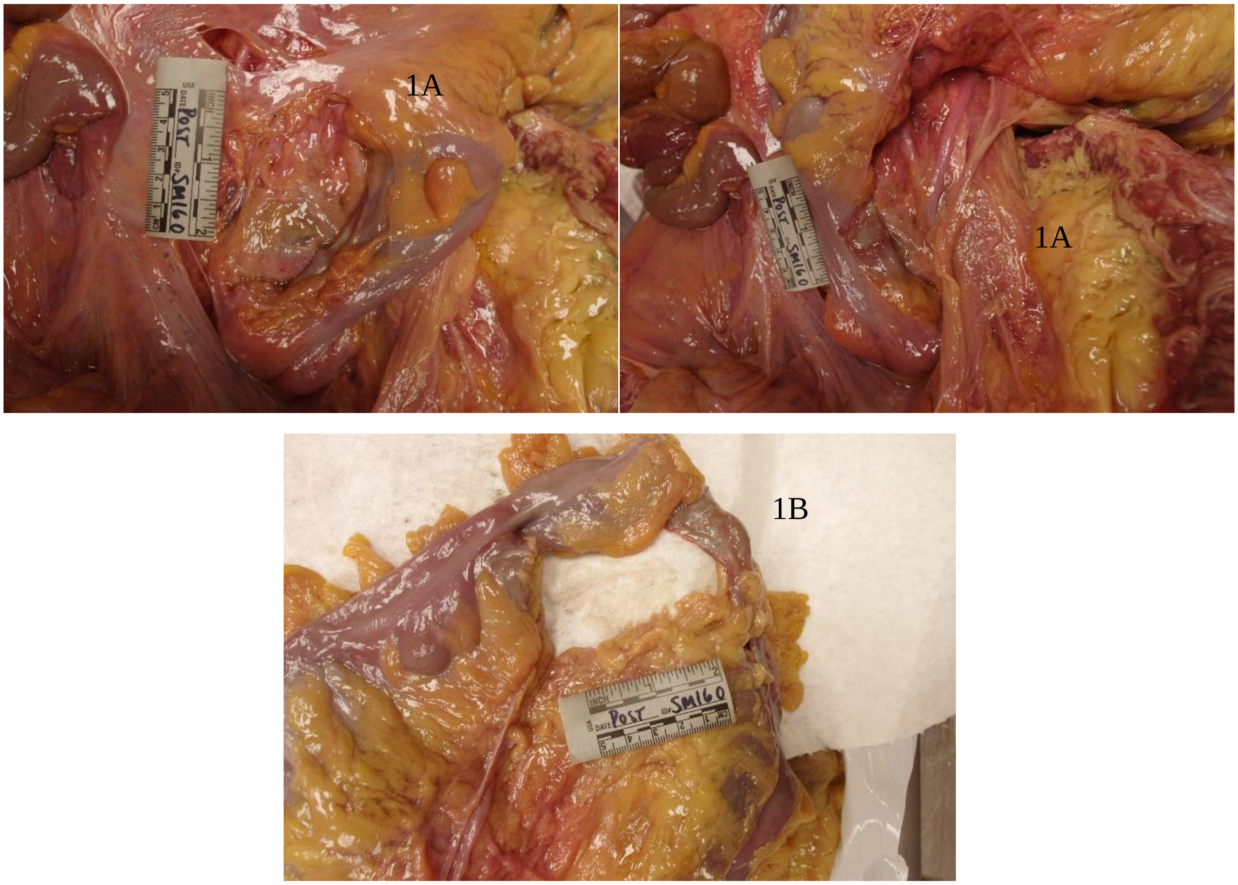

FIGURE E6. Select autopsy images from SM160 (test V14-7) including: mesenteric tear along the sigmoid colon (1A), mesenteric tear and minor disruption of descending colon on both ends of tear (1B).

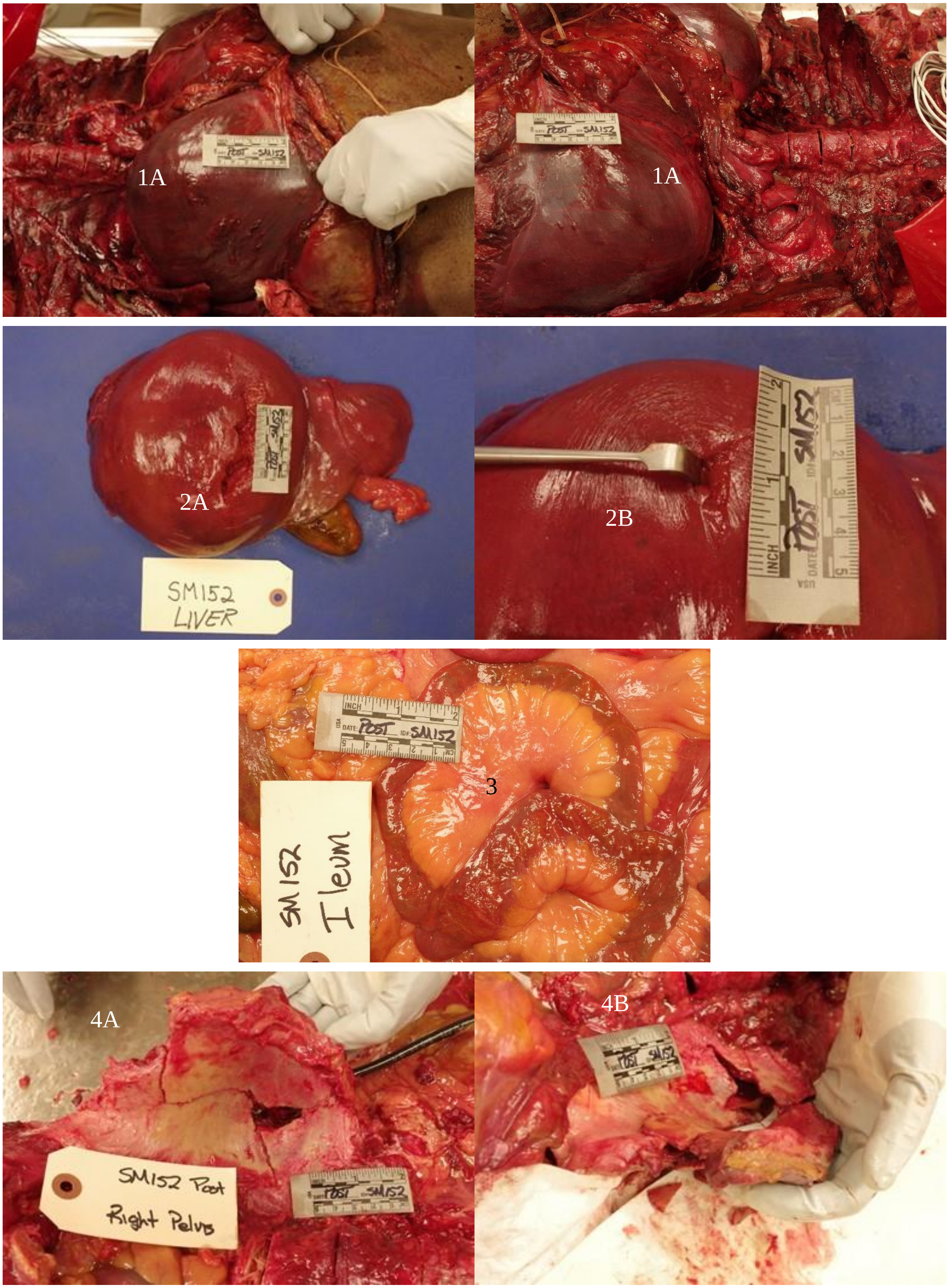
1A
1A
2A
SM152
LIVER
2B
3
SM152
Ileum
4A
SM152 Post
Right Pelvis
4B

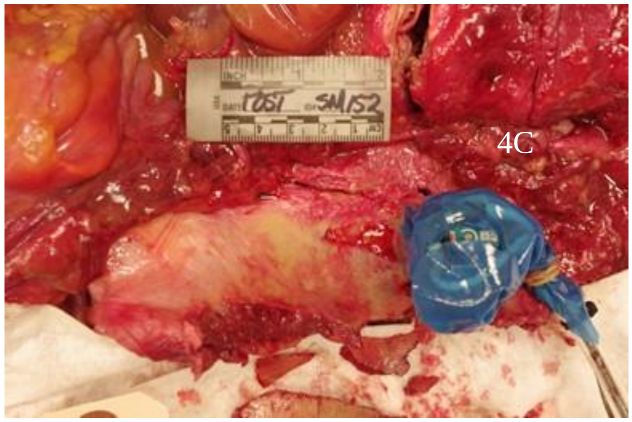

FIGURE E7. Select autopsy images from SM152 (test V15-5) including: lacerations to the pleural surface of the diaphragm (1A&B), fractures of the liver (2A&B), contusion of the ileum (3), fracture of the ala of the right ilium (4A) and left ilium (4B), and separation of the left sacroiliac joint (4C).

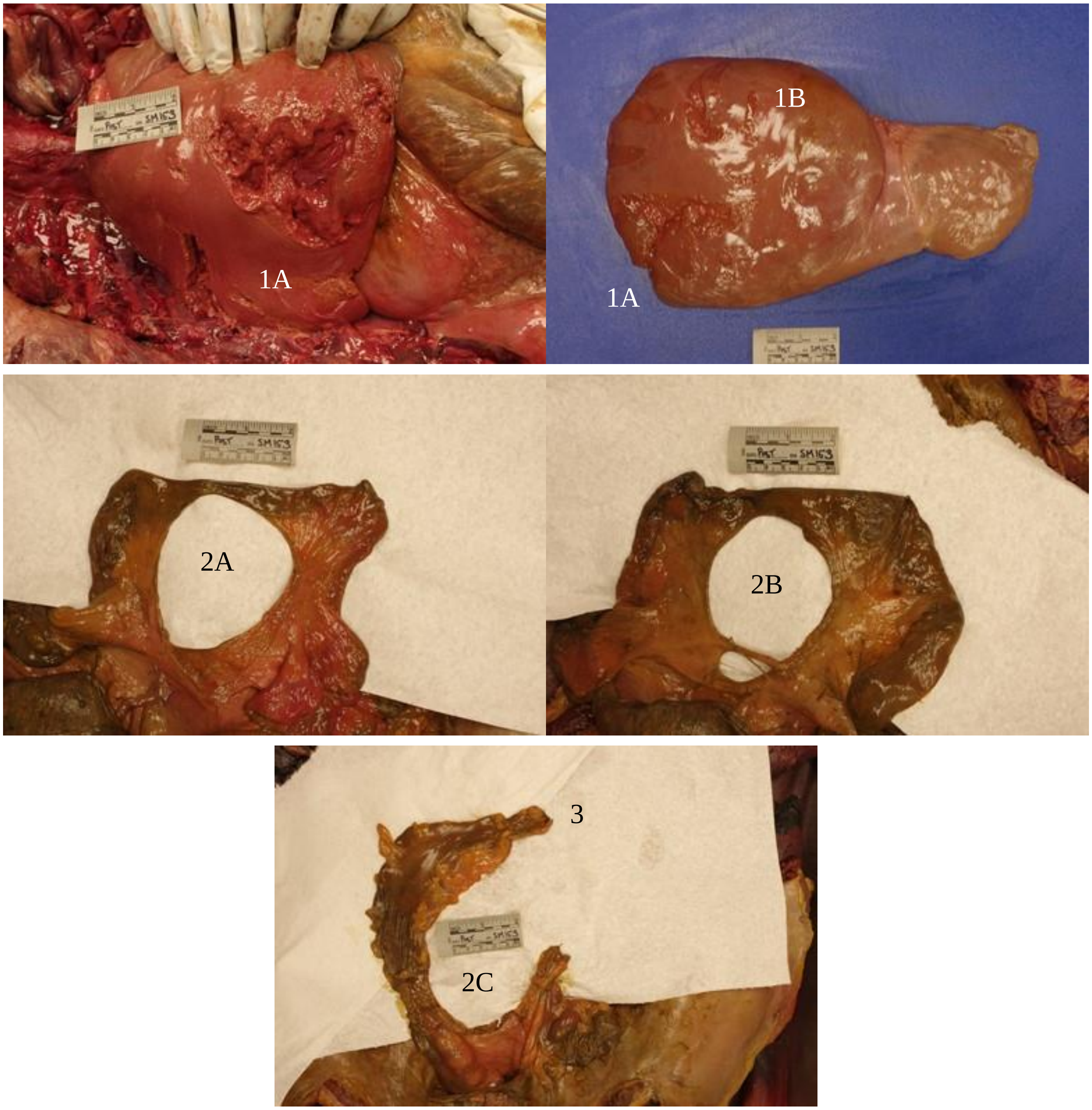

FIGURE E8. Select autopsy images from SM153 (test V15-6) including: deep fractures of the liver parenchyma (1A), superficial disruptions of the diaphragmatic surface of the liver (1B), tears of the mesentery (2A-C), and transection of the descending colon (3).

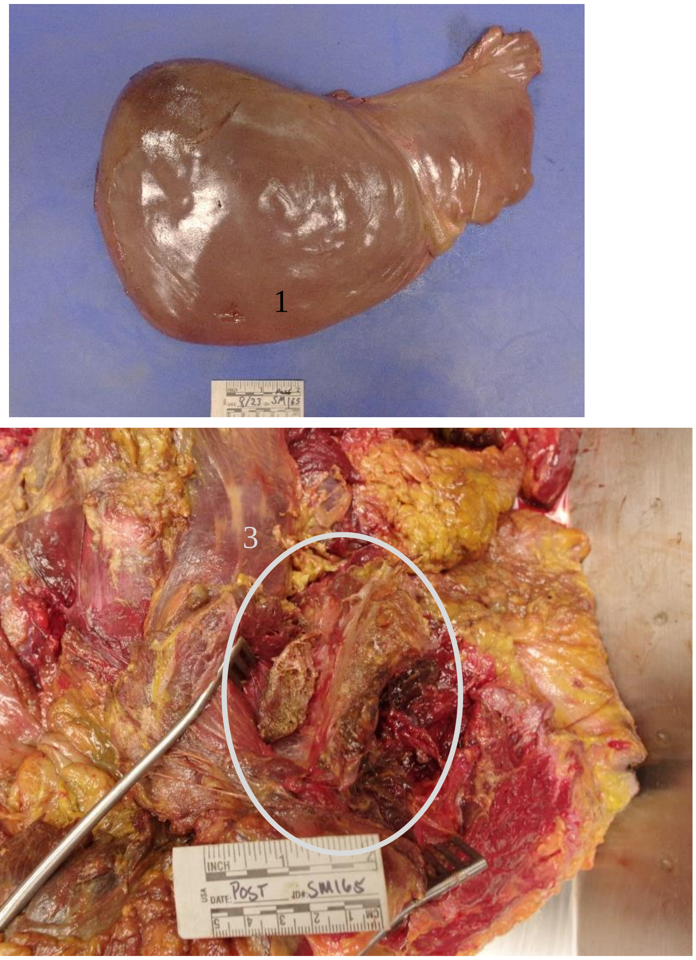

FIGURE E9. Select autopsy images from SM165 (test V15-7) including: superficial tear of the diaphragmatic surface of the liver (1) and fracture of the ala of the left ilium (3).

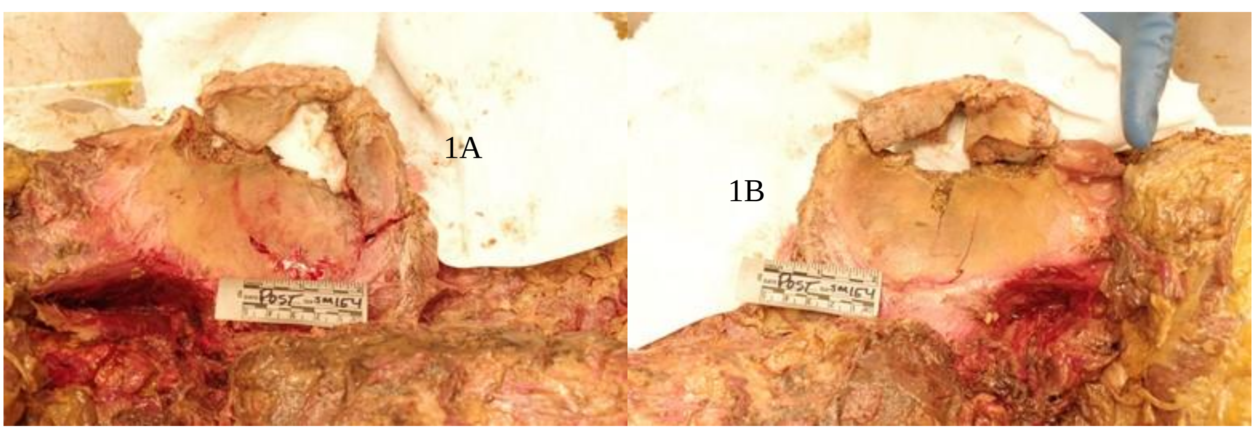

FIGURE E10. Autopsy images from SM154 (test V19-5): fracture of the ala of the right ilium (1A) and left ilium (1B).

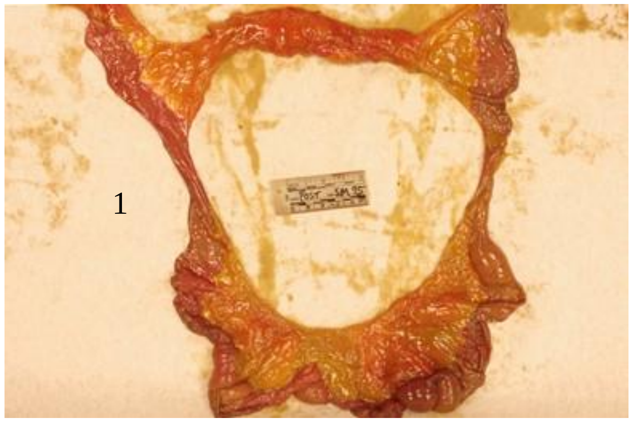

FIGURE E11. Autopsy image from SM95 (test V19-6) of the mesenteric tear along the small intestine (1).

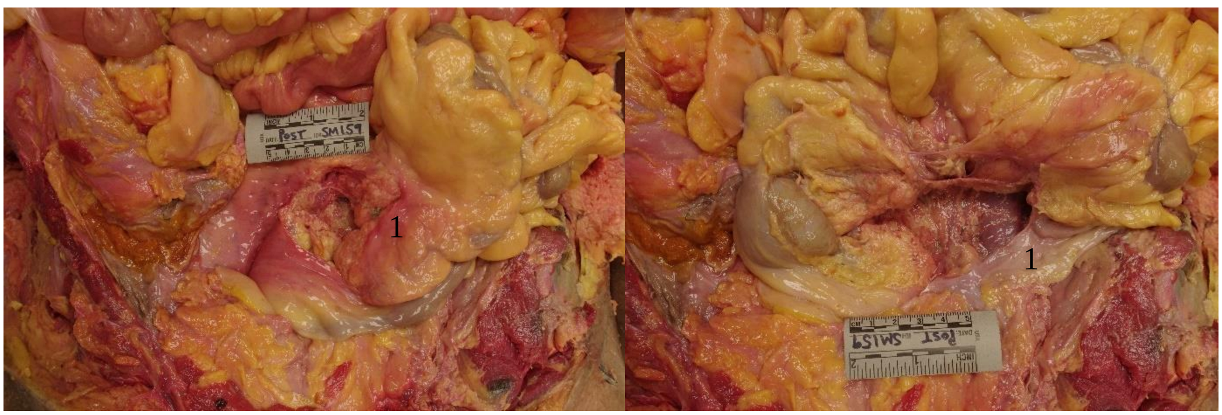

FIGURE E12. Autopsy images from SM159 (test V19-7) of the tears in the mesentery and peritoneum at the distal colon (1).

APPENDIX F

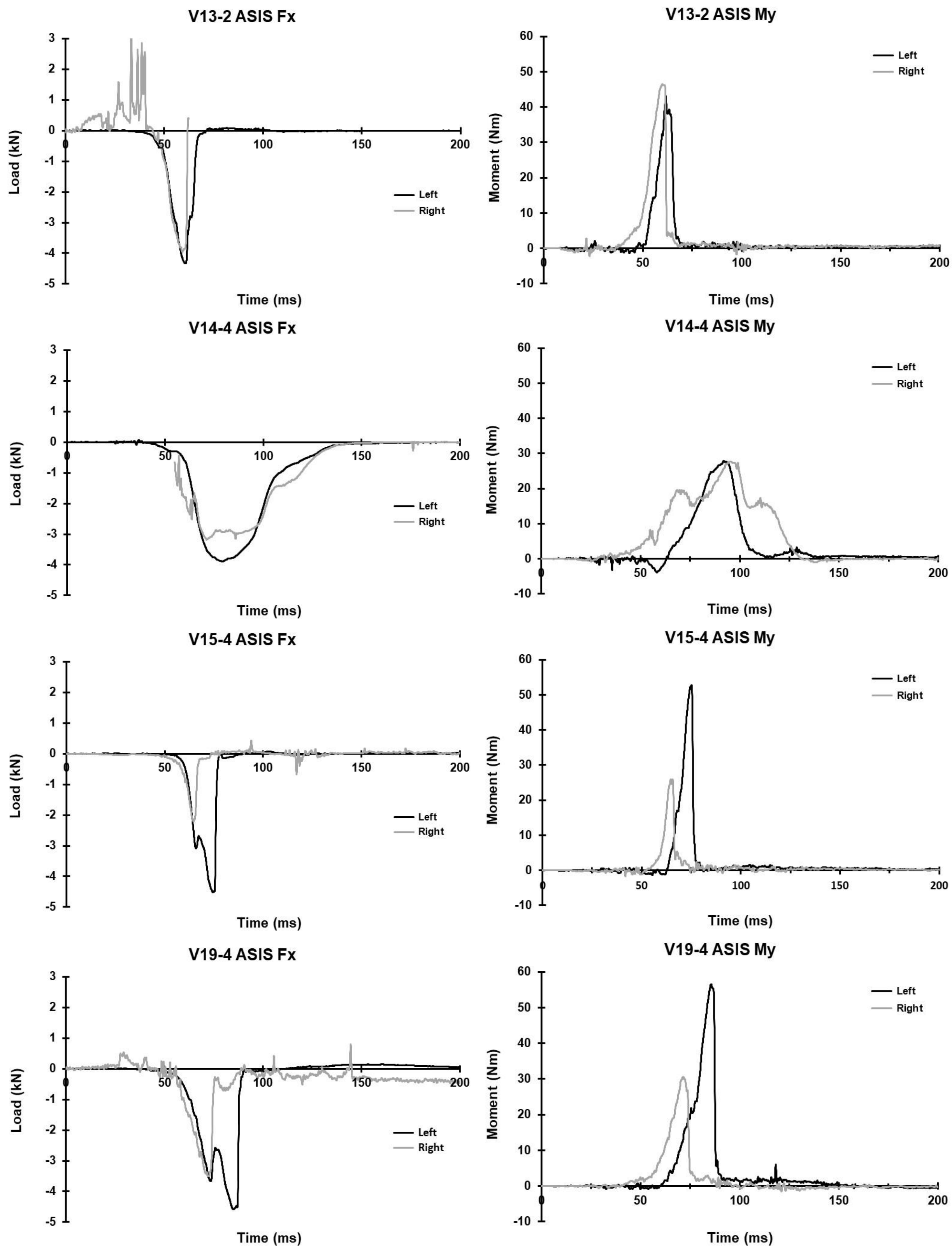

FIGURE F1. THOR ASIS loads (kN) and moments (Nm)

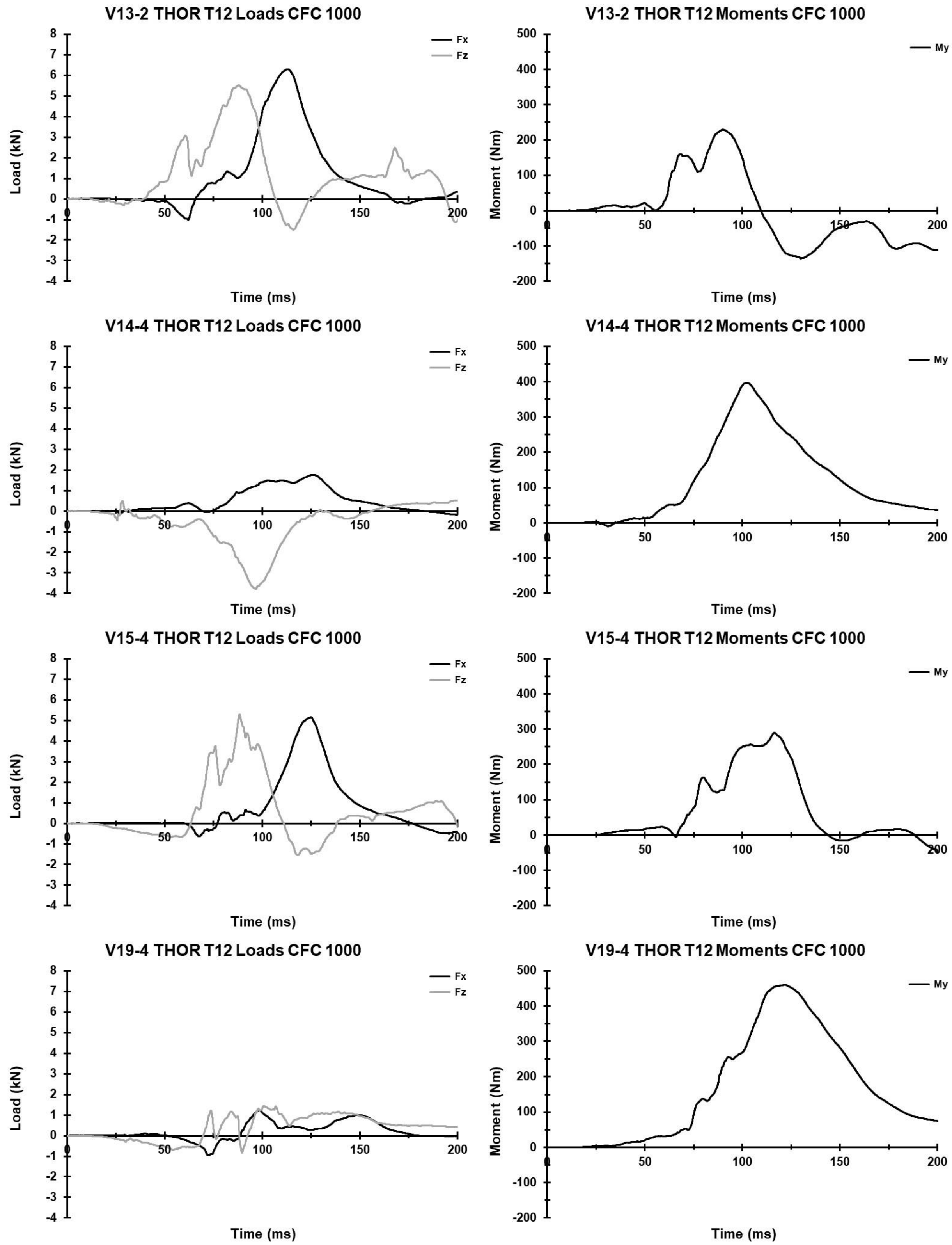

FIGURE F2. THOR T12 loads (kN) and moments (Nm)